2D material-based nanofluidic devices and their applications

Yangjun Cui[1], Long Gao[1], Cuifeng Ying[2]*, Jianguo Tian[1]*, Zhibo Liu[1,3]*

[1] *The Key Laboratory of Weak Light Nonlinear Photonics, Ministry of Education, School of Physics and Teda Applied Physics Institute, Renewable Energy Conversion and Storage Center, State Key Laboratory of Photovoltaic Materials and Cells, Nankai University, Tianjin 300071, China*

[2] *Advanced Optics & Photonics Laboratory, Department of Engineering, School of Science & Technology, Nottingham Trent University, Nottingham NG11 8NS, UK*

[3] *The collaborative Innovation Center of Extreme Optics, Shanxi University, Taiyuan, Shanxi 030006, China*

*To whom correspondence should be addressed: E-mail, liuzb@nankai.edu.cn, jjtian@nankai.edu.cn, cuifeng.ying@ntu.ac.uk

ABSTRACT

Nanofluidics is an interdisciplinary field of study that bridges hydrodynamics, statistical physics, chemistry, materials science, biology, and other fields to investigate the transport of fluids and ions at the nanometric scale. The progress in this field, however, has been constrained by challenges in fabricating nanofluidic devices suitable for systematic investigations. Recent advances in two dimensional (2D) materials have revolutionized the development of nanofluids. Their ultra-thin structure and photo-thermo-electric response make it possible to achieve the scale control, friction limitation and regulatory response, all of which are challenging to achieve with traditional solid materials. In this review, we provide a comprehensive overview of the preparation methods and corresponding structures of three types of 2D material-based nanofluidic devices, including nanopores, nanochannels and membranes. We highlight their applications and recent advances in exploring physical mechanisms, detecting biomolecules (DNA, protein), iontronics devices, ion/gas selectivity and osmotic energy generation. We discuss the challenges facing 2D material-based nanofluidic devices and the prospects for future advancement in this field.

Keywords: nanofluidics, 2D material-based nanofluidic devices, nanopores, nanochannels, membranes, biomolecules, iontronics devices, ion/gas selectivity, osmotic energy generation.

1. INTRODUCTION

Nanofluidics is a multidisciplinary field that investigates the fluid dynamics and heat transfer phenomena occurring at the nanoscale. Its ability of precise control of fluids within nanometer-sized channel opens the possibilities to study the physical, chemical and biological characteristics of liquids, gases and other fluids at this scale, offering potential to explore the practical applications of nanofluids across various industries.[1, 2] Nanofluids are invaluable research tools, essential for addressing fundamental challenges in physics, materials science, energy, biology, environmental science, and medicine.

Originating from microfluidic devices, nanofluidic devices has a history of several decades, closely linked to the development of micro-and nano-processing technologies and materials science.[3] The progress of semiconductor and micro-filtration processes has significantly improved the accessibility and efficiency of nanofluidic devices, leading to devices such as nanopores, nanochannels, and membranes with nanogaps. Additionally, nanofabrication techniques have significantly reduced the scale of nanofluids, from tens of nanometers to the sub-nanometer, achieving single-molecule level. The nanopore DNA sequencing technology, providing single base resolution, marks a major technological progress in this field.[4, 5] Nanofluidic devices have also achieved substantial progresses in ionic electronic devices and bionic ionic devices, highlighting their great potential and bright future.[6]

Nevertheless, this field faces challenges due to material limitations and complexities of nanofabrication. Traditional materials used for nanofluidic devices, such as silicon dioxide (SiO_2),[7, 8] glass,[9] Silicon nitride (SiN_x),[10] Polydimethylsiloxane (PDMS),[11-13] aluminum oxide (Al_2O_3),[14] present difficulty in achieving precise structures. The involved fabrication methods, including focused ion beam (FIB) and acid-based solution corrosion, often result in high surface roughness, affecting the fluidic transmission on the surface. Moreover, controlling the thickness of these materials at the nanoscale is challenging, and even the nanoscale suspension films, like SiN_x membranes, are fragile to work with. While laser-assisted pulling of the quartz capillaries can form nanopores for biological monitoring, miniaturization and integration of these devices remain challenging.[15, 16]

The emergence of 2D materials, such as graphene, molybdenum disulfide (MoS_2), black phosphorus (BP), boron nitride (h-BN) and others, offer a new avenue for the advancement of nanofluidics.[17-20] Their layered lattice structure, atomic-scale thickness, ease of processing, and abundant surface properties (charge, flatness, hydrophilicity, etc.) make 2D materials ideal for constructing nanoconfined structures and exploring nanofluidics. 2D materials show strong responsiveness to photothermal and photoelectric, providing additional modulation capabilities for nanofluidic devices.[21, 22] The integration of nanofluids and 2D materials has expanded the research scope in this field, enabling studies of mass transfer within accurate sub-nanometer confined structures,[23, 24] a scale beyond the range of traditional nanofluids (1-100 nm). Under sub-nanometer spatial confinement, the influence of van der Waals forces, Coulomb forces, and space hydration forces, altering the physical and chemical properties of ions. This difference challenges classical concepts of molecular-ion interactions and leads to discoveries in 2D material confinement systems that go beyond traditional understanding, bringing new prospects for applications and technologies.

This review provides a comprehensive overview of 2D material-based nanofluidic devices, including nanopores, nanochannels, and lamina membranes, and their fabrication methods. It highlights their wide-ranging applications in fundamental physics, biosensing, iontronics device, ion selective separation, blue energy and gas separation. The review also discusses the current challenges and potential future advancements in this field.

2. CLASSIFICATION AND FABRICATION OF 2D MATERIAL-BASED NANOFLUIDIC DEVICES

Nanofluidic devices made of 2D materials are mainly divided into three categories: nanopores, nanochannels and lamina membranes (Figure 1). The fabrication usually begins with one of the following approaches: mechanically exfoliating a thin layer of 2D materials from the bulk phase, transferring the chemical-vapor-deposited (CVD) 2D materials to a target substrate, or forming a dispersion by liquid phase exfoliation, followed by self-assembling to form 2D material nanosheets. To create nanopores, the thin layer of 2D material must be carefully transferred to the target substrate for drilling. 2D material nanochannels are formed by transferring and assembling layer by layer. The 2D material membranes are prepared by layer by layer deposition of the dispersion liquid of nanosheets.[18] This chapter will provide a comprehensive overview of the classification and preparation methods for these three structures.

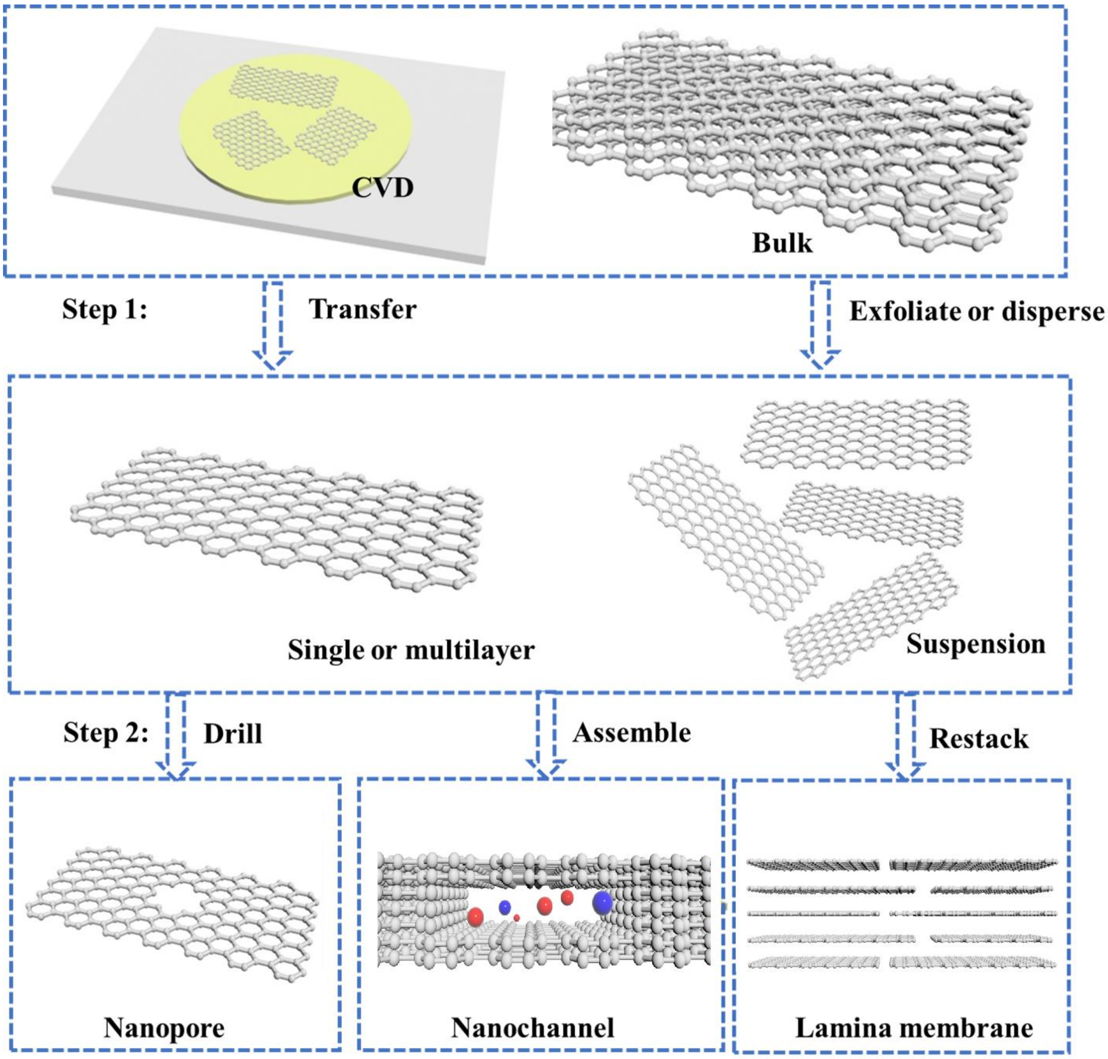

Figure 1. Three main types of 2D material-based nanofluidic devices.

2.1 2D material nanopores

2.1.1 Types of 2D material nanopores

2D materials used for creating nanopores must possess sufficient mechanical strength and stability to endure prolonged exposure to solution or electrical measurements. Some 2D materials show specific pore structures, such as the hexagonal honeycomb arrangement of atoms in single layer graphene and h-BN, in which each hexagonal lattice can be regarded as a sub-nano pore. These pores allow only protons to pass through, resulting in a strong shielding effect on the fluid.[25] By exerting external forces to destroy the bonds, just like carbon-carbon (C-C) bonds in graphene, atoms can be released from their fixed lattice positions, which can enlarge the pore size and allow ions and molecules to pass through.[26-28]

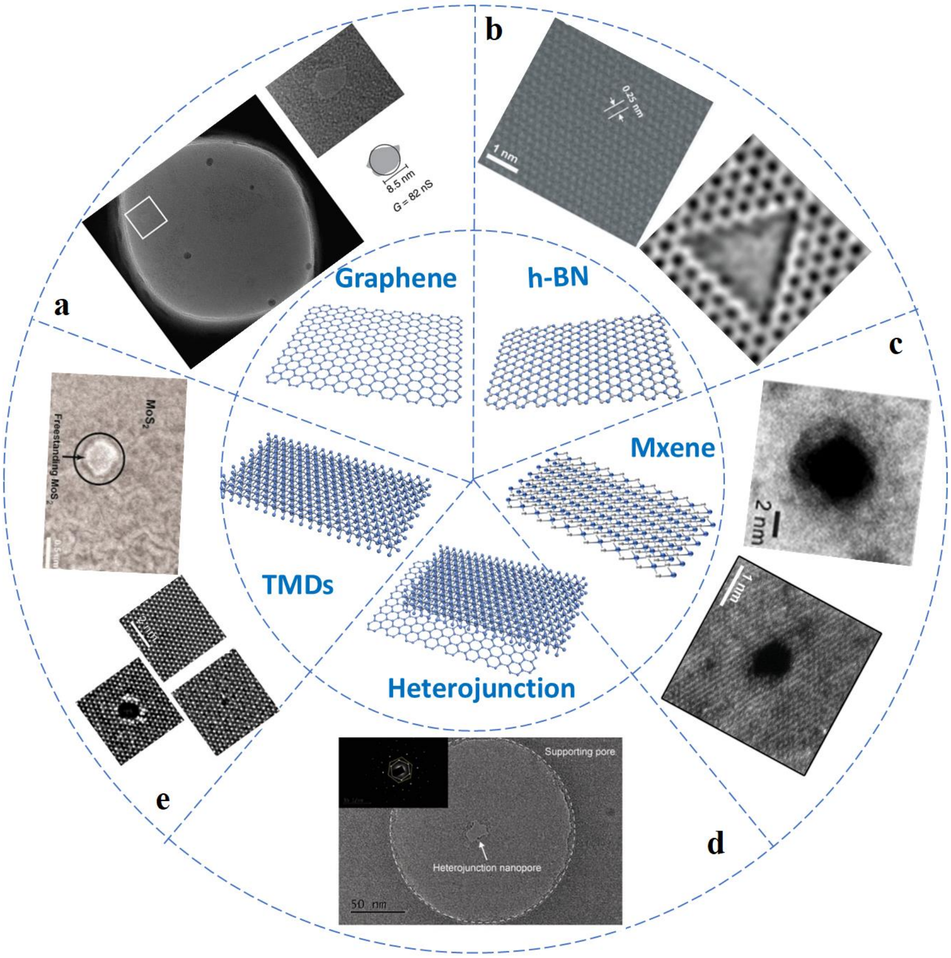

Figure 2. The main types of 2D material nanopores and its structure. a) graphene nanopore. Reproduced with permission under a Creative Commons CC BY License from ref 29. Copyright 2016 Springer Nature. b) h-BN nanopore. Reproduced with permission from ref 30. Copyright 2023 John Wiley and Sons. Reproduced with permission from ref 31. Copyright 2017 American Chemical Society. c) MXene nanopore. Reproduced with permission from ref 32. Copyright 2019 American Chemical Society. Reproduced with permission from ref 33. Copyright 2022 John Wiley and Sons. d) Heterojunction nanopore. Reproduced with permission from ref 34. Copyright 2023 American Chemical Society. e) TMDs nanopore. Reproduced with permission from ref 35. Copyright 2014 American Chemical Society. Reproduced with permission from ref 36. Copyright 2017 American Chemical Society.

Graphene is the first 2D material used to prepare nanopores (Figure 2a). A single layer of graphene is only one atomic layer thick (0.34 nm), so it can be made into the thinnest nanopore.[29, 37-39] The lattice structure of h-BN is similar to graphene, showing inherent chemical inertness, excellent stability and corrosion resistance in highly acidic and alkaline solutions, so is an excellent candidate material for nanopore manufacturing (Figure 2b).[30, 31] Transition metal disulfide (TMDs), such as MoS_2 and tungsten disulfide (WS_2), can be used for electrical and optical modulation of nanopores due to their remarkable photoelectric response (Figure 2e).[36, 40, 41] Compared with graphene, single layer MoS_2 with a thickness of 0.67 nm shows better signal/noise intensity, while maintaining its monolayer property.[28] Its low base attachment also provides an opportunity for DNA sequencing.[42] In the field of biosensor, MoS_2 nanopore is more commonly used than graphene nanopore.[43-45] 2D transition metal carbides and nitrides, namely MXene, represent an emerging class of 2D materials whose metal carbide core layers and their surface -O, -OH, and -F functional groups give them metal-conductive and functionalized surfaces (Figure 2c).[32, 33] Its hydrophilicity and conductivity can be widely used in the field of biosensing. Nanopores constructed from 2D materials with functional surfaces and electronic conductivity have various potential applications in biosensing, including electric gating and lateral reading through DNA sensing. In addition to single-material nanopores, there has been a growing focus on heterojunction nanopores formed by the superposition of two distinct 2D materials, like graphene/MoS_2, MoS_2/WS_2 (Figure 2d).[34, 46, 47] This assembly not only integrates the different characteristics of the two materials, but also adjusts the transport of ions or biomolecules by using the response of the heterostructure.

Some materials, such as metal-organic frameworks (MOFs), covalent organic frameworks (COFs), zeolitic imidazolate frameworks (ZIFs). carbon nitride (g-C3N4), contain porous lattice structures and can be synthesized in 2D forms similar to graphene.[48-53] Compared to nanoporous structures created through defect engineering, 2D sheets with highly uniform pores offer significantly higher permeability. Due to their structural diversity and precise tunability, these materials can be customized for specific functions or applications.

2.1.2 Transfer methods for 2D materials

The formation of nanopores can be categorized into "top-down" or "bottom-up" methods. In the top-down approach, processing techniques are used to generate nanopores inside the 2D material, while in the bottom-up approach, nanopores appear directly during the synthesis and growth of the 2D material, such as the direct synthesis of 2D COFs. The top-down method is more popular than the bottom-up method because it has better control over the formation of nanopores.[54, 55] 2D material nanopores are typically supported by a suspended SiN_x membrane with a central microhole. The first step is to transfer the 2D material layers to the microhole and completely cover it. The transfer methods can be categorized as wet transfer or dry transfer (Figure 3a).[56] The wet transfer method uses polymethyl methacrylate (PMMA) as a support layer to separate the 2D material from the substrate (silicon wafer or copper foil) by corrosion. The dry transfer process is directly exfoliation the 2D material onto PDMS and selecting the target sample for transfer. Under the microscope, a three-dimensional displacement stage with a clamp holder is used to clamp the support layer containing the 2D material, the target 2D material is aligned with a microhole in a SiN_x membrane (Figure 3b). Subsequently, the clamp holder is lowered to make the target 2D materials contact with the SiN_x surface and cover the microhole. After the 2D material is transferred to the designated position, the supporting layer needs to be eliminated.

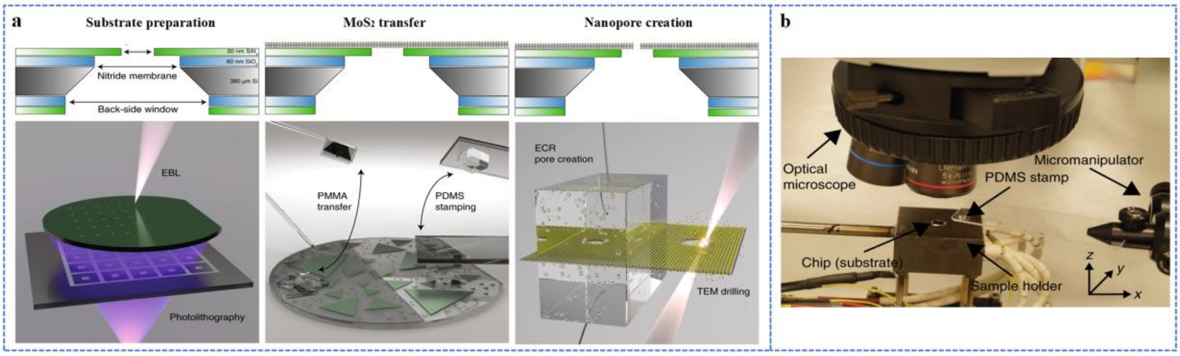

Figure 3. a) Transfer and preparation process of 2D material nanopore. b) 2D material transfer under micromanipulation system. Reproduced with permission from ref 54. Copyright 2019 Springer Nature.

PDMS usually leaves the 2D materials on SiN_x surface after the holder lifting, and do not need additional treatment. Samples with a PMMA as supporting layer need to use organic solvent to dissolve PMMA. After the transfer, the sample needs to be annealed. Mainly for two purposes: first, to improve the surface cleanliness and eliminate organic impurities; Second, enhance the contact between the 2D material and the SiN_x substrate to prevent separation in the subsequent test.

2.1.3 Drilling methods for 2D material-based nanopores

The commonly employed techniques for drilling 2D materials are primarily categorized into high-energy particle beam bombardment, chemical reaction, and other physical and chemical methods. High-energy particle bombardment includes transmission electron microscope (TEM) engraving, FIB irradiation, helium ion microscope (HIM) sculpting and so on.[55] In these technologies, energy is transferred from incoming high-energy particles (such as electrons, ions) to the target material, resulting in the destruction of chemical bonds between the atoms and the creation of vacancies. TEM has become the most widely used method for nanopore manufacturing because of its excellent machining accuracy, even reaching the bombardment accuracy of atom level (Figure 4a).[26, 31, 37] Furthermore, high-resolution real-time observation of the size and shape of nanopores can be realized during the drilling. FIB use gallium or helium ions as bombardment particles. (Figure 4b).[57] However, due to the limitation of the spot size of the focused beam, the fabrication accuracy of the FIB is not as high as TEM. HIM milling demonstrates excellent precision in controlling nanopore size and shape, potentially enabling wafer-scale production (Figure 4c).[38]

Chemical reaction methods are frequently employed for the fabrication of nanopores in 2D materials. Through redox or electrochemical reaction, defects are intentionally introduced on the surfaces to produce nanoporous structures. Commonly used technologies include electrical pulse (EP) method, electrochemical reaction (ECR) method and oxygen ion etching (OIE) method. The EP method involves the application of ultra-short high-voltage pulses to 2D materials (Figure 4d).[29, 58] When an electric field passes through a dielectric, electrons pass through a charge trap (defect) in it, creating a leakage current. As the voltage continues to be applied, these defects form a permeation path, which leads to the peak of current. When an electric field is applied through the electrolyte solution, an electrochemical reaction occurs at the membrane-electrolyte interface, and charge is injected and released. These electrochemical reactions may limit the leakage current across the membrane, thus affecting the breakdown dynamics.[59] When applying high voltage electric pulses, transmembrane ion current is used to monitor the state of nanopore. At first, the leakage current is very small, indicating that there are no defects in the 2D materials. Subsequently, with the formation of pores, the current increases. The expansion of nanopores is promoted by voltage pulses, and measuring the pore conductivity at a low bias between each pulse to feedback the pore size.

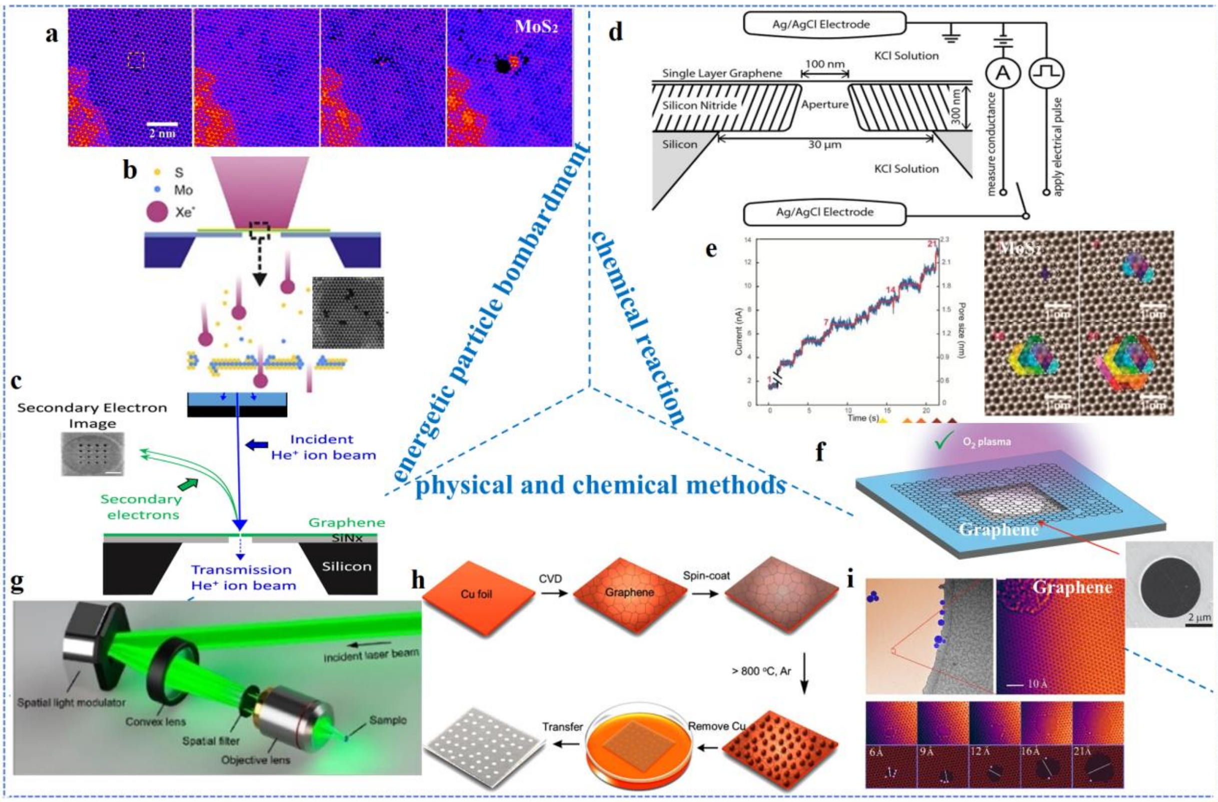

Figure 4. Drilling method of 2D material-based nanopore. High-energy particle beam bombardment. a) TEM. Reproduced with permission from ref 26. Copyright 2017 RSC Pub. b) FIB. Reproduced with permission from ref 57. Copyright 2022 American Chemical Society. c) HIM. Reproduced with permission from ref 38. Copyright 2017 IOP Publishing. Electrochemical reaction. d) EP. Reproduced with permission from ref 58. Copyright 2015 AIP Publishing. e) ECR. Reproduced with permission from ref 60. Copyright 2015 American Chemical Society. f) OIE. Reproduced with permission from ref 61. Copyright 2015 Springer Nature. Other physical and chemical methods. g) laser irradiation. Reproduced with permission from ref 62. Copyright 2023 American Chemical Society. h) nanoparticle etching. Reproduced with permission from ref 63. Copyright 2017 American Chemical Society. i) single atom catalysis. Reproduced with permission from ref 64. Copyright 2014 American Chemical Society.

The ECR method is often used to prepare MoS_2 nanopores.[54, 60] During the process of pore formation, a gradually increasing transmembrane voltage is applied in small increments. Upon reaching a sufficient voltage level, a surge in current signifies nanopore formation. Subsequently, the voltage is kept at breakdown levels to gradually enlarge the nanopore until measured current exceeds the predetermined threshold, and then the breakdown voltage is reduced to 0. The formation of nanopores begins at the defect of the membrane, and then the exposed atoms are removed by ECR to expand in pore size. By ECR, the oxidation of MoS_2 to MoO_3, and then MoO_3 diffuses into solution.[28] A stepwise increase in current indicating its capability to selectively remove individual atoms from the lattice (Figure 4e).[60] EP and ECR methods have the advantage of continuous formation and testing of nanopores, which allows continuous testing of nanopores with different pore sizes by continuously applying reaming voltage and monitoring pore sizes.[29] However, the aperture monitoring may not be able to accurately capture the exact shape of nanopores, especially if the aperture is very small (less than 1 nm).

The OIE method utilizes oxidation reactions to induce the formation of defects and pores on the surface of 2D materials (Figure 4f).[61, 65, 66] This method cannot control the number and shape of pores. There is a linear relationship between pore density, etching time and power. The introduction of oxygen ions leads to the incorporation of numerous oxygen-containing groups at the edges of pores and on the surface of 2D materials, significantly increasing surface charge density. In addition to the ionized gas participating in the oxidation reaction to directly generate pores, Huang et al. found that exposing graphene to the strongly oxidizing gas O_3 can directly epoxide the reaction at room temperature, introducing epoxidation groups on the graphene lattice.[67] The epoxide group is heated at high temperature, and the group vaporizes into sub-nanometer pores. The pore density increases exponentially with epoxidation temperature. With the increase of heating temperature, the pore size distribution shifted to larger pores. This decoupling of cluster nucleation and pore formation provides a new way to control pore size and density. The drawback of the chemical reaction approach lies in the inability to control the placement of the nanopore, as it is determined by a random occurrence of the chemical reaction.

Table 1. Fabrication methods of nanopores in 2D materials.

Method	Materials	Single/Multiple	Diameter(nm)	Application	Ref.
TEM	MoS_2	Single	0.6-20	DNA translocation, osmotic power	31, 35, 68
	Graphene	Single	5-25	DNA translocation	39, 69
	h-BN	Single	0.5-12	DNA translocation, osmotic power	30, 31, 70, 71
	WS_2	Single	>0.3	DNA translocation	36
	Mxene	Single	<10	DNA translocation	32, 33
	MoS_2/WS_2	Single	13-55	Transport of ions and molecules	47

	G/MoS_2	Single	2−20	DNA or proteins translocation, osmotic power	34, 46
EP	Graphene	Single	8.5	Ion Selectivity	29
ECR	MoS_2	Single	>0.5	Amino acids or DNA translocation	45, 60, 72, 73
He^+ ion irradiation	Graphene	Single	5−12	DNA translocation	38
Au ion bombardment	Graphene	Multiple	0.8±0.16	Ion selectivity	74
Xe^- ion irradiation	MoS_2	Multiple	1		57
Ga+ ion irradiation	MoS_2	Multiple	0.5−1		75
O_2 plasma	Graphene	Multiple	0.6−0.69	Water evaporation or desalination	61, 76
O_3 epoxidation	Graphene	Multiple	Å-scale	Gas separation	67
O_3/O_2 reaction	Graphene	Multiple	<0.85	Ion Selectivity	77
Ar+O_2 plasma	Graphene	Multiple		Ion Selectivity	78
Nanoparticle etching	Graphene	Multiple	~50	Water evaporation	63
local heating	Graphene	Single	20−80		79
Femtosecond laser irradiation	Graphene	Multiple	<100		62
Tip-controlled local breakdown	h-BN	Single	4−16	Osmotic power	80
Single-atom catalyst	Graphene	Single	>0.6		64

Other techniques, such as laser irradiation (Figure 4g),[62] nanoparticle etching (Figure 4h),[63] and single atom catalysis (Figure 4i),[64] et.al, have also been employed for the fabrication of 2D material-based nanopores. Table 1 summarizes the fabrication methods for creating nanopores in different 2D membrane, comparing their pore sizes and applications. Membranes with single nanopores are predominantly used for studying DNA transport, protein sensing, and ion transport mechanisms. TEM is widely employed in fabricating single pores in a wide range of 2D materials, including heterojunctions, due to its precise scale control. However, TEM requires high equipment and operational cost. EP and ERC offer precise control over pore size through current feedback mechanisms, but may introduce defects and redox reactions that alter the surface properties of 2D materials, such as increasing the surface charge. Despite of these challenges, EP and ERC are cost-effective and convenient methods for drilling pores, particularly for MoS_2, achieving accuracy comparable to TEM. Additionally, techniques such as ion beam bombardment, oxidation reactions, and plasma treatment can generate high-density nano- or sub-nanopores on the material surface. Oxidation reactions and plasma treatment also introduce surface charges, which are critical for modulating ion selectivity and enhancing osmotic energy performance.[66]

2.2 2D material-based nanochannels

2.2.1 Advantages of 2D materials for nanochannel preparation

There are two types of structures for 2D material-based nanochannels. One is using the 2D material as the channel framework, which is assembled layer by layer. The other type is covering the 2D material onto the surface of the channel. Using 2D materials to make nanochannels has obvious advantages. First, it can accurately control the channel height. 2D materials have layered crystal structure, such as graphene, exhibiting a minimum single layer height of 0.34 nm. Mechanical exfoliation can achieve graphene with various layers, enabling production of nanochannel with different heights through etching. This eliminates the need of strict machining parameters to control the etching depth, as required for traditional solid materials. Since Geim et al. first made the smallest artificial nanochannel (0.34 nm) from graphene for the first time, 2D material-based nanochannels have attracted considerable attention.[81-83] Mass transfer at nano and sub-nano scales has gone beyond the traditional classical fluids field, which needs new mechanisms and formulas to explain. Additionally, graphene is composed of layers of carbon atoms arranged in a 2D structure. Theoretically, the surface roughness of mechanically exfoliated graphene should be at the atomic level, while other 2D materials, although not as flat as single-layer graphene, still exhibit less roughness compared to channels prepared by pulsed. The high flatness reduces the limitation of transmission and the possibility of channel blockage. When the silicon-based channel is covered with a 2D material, it shields the friction between the fluid and the rough surface, enhancing the internal fluid transport.[84-86] Using micro-and nano-processing platforms, 2D materials can be easily assembled layer by layer by van der Waals forces, forming stable contact after annealing without additional fixation or bonding.

2.2.2 Fabrication of 2D material nanochannels by layer assembly

The layer assembly channel structure usually consists of three layers(Figure 5a).[87] It preparation requires complex semiconductor processing technology and 2D material transfer method (Figure 5b).[81] First, the bottom layer is transferred to the SiN_x surface, covering the entire microhole to ensure no leakage. The bottom layer is used to shield the roughness of the SiN_x substrate and serve as the bottom surface of the channel. Next, using electron beam lithography (EBL) and plasma etching, the center channel layer is processed on a silicon wafer to generate a set of parallel stripe arrays with a width of 130 nm. Subsequently, it is transferred to the bottom layer by wet transfer method. Then, using plasma etching and SiN_x microhole as a mask, the graphene suspended in the microhole is etched from the back to connect it up and down. Finally, graphene with a thickness exceeding 100 nm is chosen as the top layer of the channel and covers it.

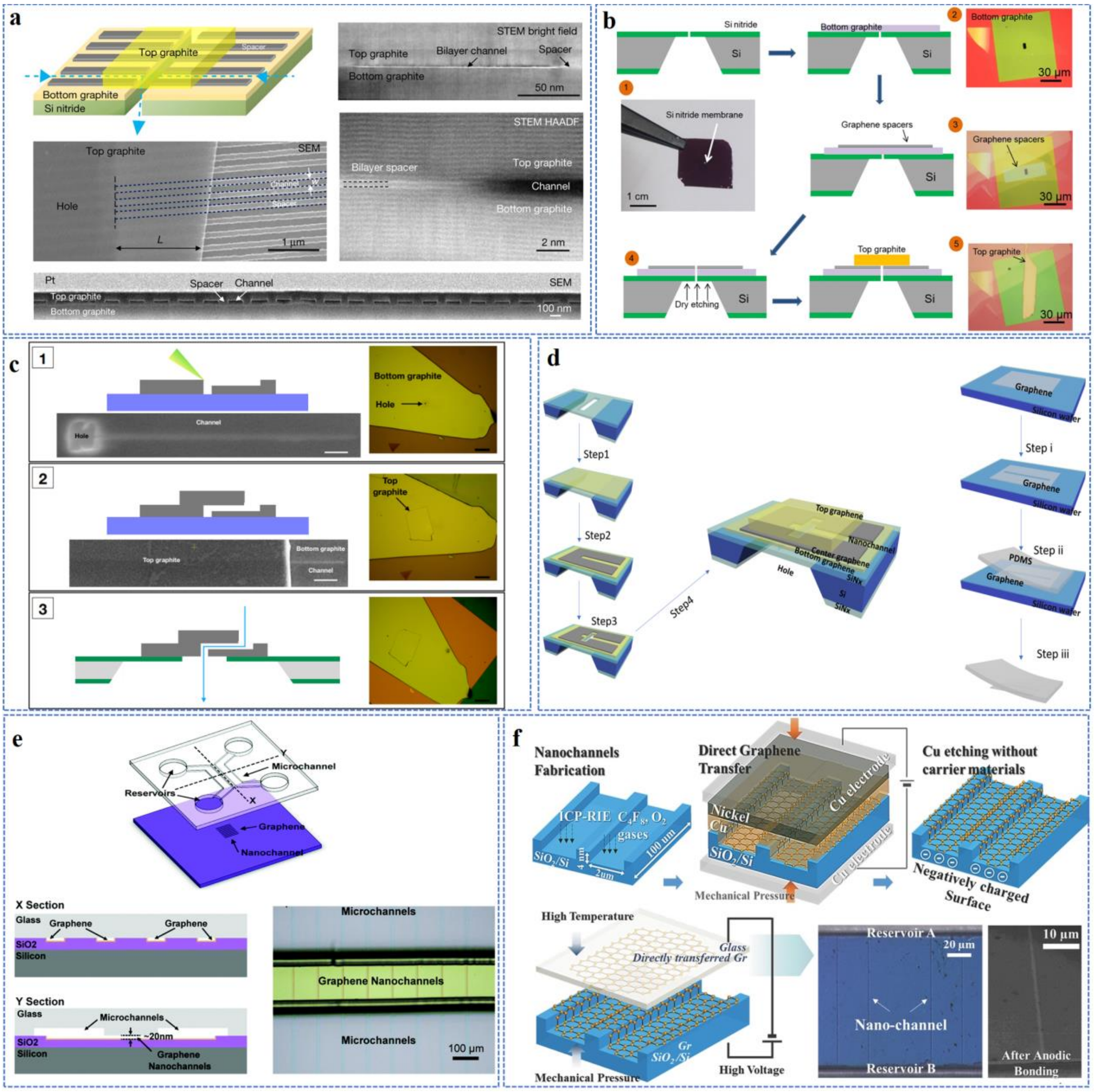

Figure 5. Structure and preparation of 2D material-based nanochannels. a) Structure and electron microscopy characterization of graphene nanochannels assembled in layers. Reproduced with permission from ref 81. Copyright 2016 Springer Nature. b) Assembly process of graphene material nanochannel. Reproduced with permission from ref 81. Copyright 2016 Springer Nature. c) The preparation process of the channel constructed by etching grooves

on the graphene surface. Reproduced with permission from ref 88. Copyright 2022 Springer Nature. d) Channel preparation process of femtosecond laser etching and water-assisted transfer. Reproduced with permission from ref 89. Copyright 2024 American Chemical Society. e) Graphene-covered silica channels. Reproduced with permission from ref 85. Copyright 2016 RSC Pub. f) Preparation of graphene-based nanochannels by direct transfer of monolayer graphene. Reproduced with permission from ref 86. Copyright 2017 John Wiley and Sons.

The preparation of channel seems simple, but it involves a series of extremely complicated operations. It is a challenge to ensure that the channel array with a width of only 130 nm and a height of one or more graphene layers is completely transferred, and to keep the surface clean throughout the whole process. Only a few laboratories have mastered the entire preparation process. Therefore, it is imperative to simplify this process. Bouquet et al. used electron beam-induced direct etching and reactive ion beam etching (RIE) to form channel grooves in the lower graphene, and then covered the upper graphene, thus simplifying the complicated interlayer transfer process (Figure 5c).[88] Liu et al. directly used a femtosecond laser to etch the graphene channel structure, and then used water-assisted graphene transfer to prepare a three-layer channel structure, without using complicated instruments and equipment, thus avoiding complicated transfer and repeated cleaning processes (Figure 5d).[89] However, this method is limited by the radius of the laser spot, and the width of the prepared channel is higher than 400 nm.

2.2.3 Fabrication of nanochannels with 2D material surfaces

The channel with a 2D material as the surface is typically fabricated on a SiO_2 sheet, where the grooves are processed using micro and nano-etching technology such as FIB and RIE. The key challenge was to transfer the 2D material into the grooves, attach it to the surface and keep it clean. Another is how to avoid the collapse of nanochannels resulting from electrostatic force. Xie et al. prepared silica nanochannels using lithography and controlled RIE (in CF_4). CVD graphene is transferred from copper foil to substrate by PMMA assisted wet transfer method (Figure 5e).[84, 85] After annealing in Ar/H_2, the substrate was subjected to an anodic bonding process (800 V, 450 °C) under vacuum (~10^{-4} Torr), with another glass substrate containing microchannels and reservoirs to form a stable channel structure. Han et al placed a nickel substrate on a copper foil/monolayer graphene, and then applied electrostatic force through the substrate under mechanical extrusion and thermal heating in a high vacuum environment (Figure 5f).[86] This nickel substrate will not ionize at high temperatures, and a uniform electric field will be generated on the surface of graphene/copper foil. This process creates a high negative charge on the SiO_2/Si surface and attracts the graphene/copper layer to the SiO_2/Si substrate. Then, 0.1 M ammonium persulfate (APS-100) was used to etch the copper foil on the surface of SiO_2. The graphene surface transferred by this method has a clean and smooth surface. This channel inside the transparent substrate allowing direct observation of fluid movement inside it, and facilitating integration with direct observation technologies such as fluorescence.

2.3 2D material-based laminar membranes

2.3.1 Advantages of 2D material-based laminar membranes

In some fields, such as ion/gas separation, osmotic power generation, etc., high water, ion or gas fluxes are required to meet the needs of practical applications. The nanopore or the channel mentioned above, it is limited by the size and volume, and the flux is limited. The laminar membrane is a good solution to the problem of low flux, which is a composite form of an infinite number of channels and pores. From the point of view of fluid transport, nanopores are the device where fluid passes through the edge of 2D material, while nanochannels are devices where fluid moving along the surfaces. Layered membranes are composed of stacked nanosheets, forming parallel sheet structure, with channels between adjacent nanosheets for fluid transmission in both out-of-plane and in-plane directions (Figure 6a).[18, 90] One direction involves transmission along the stacking direction, akin to transport within a 2D channel formed by layers of nanosheets. The other transport direction is perpendicular to the stacking direction, which occurs at the edge of the nanosheet. This means that the 2D material-based laminar membrane will integrate the transmission characteristics of pores and channels. The structural dimensions of the pores and channels correspond to the interlayer spacing and packing density, and the surface properties of the pores and channels correspond to the modification and doping of the membrane surface. The methods of adjusting the transport in the pores or channels can also be applied to the membrane. Layered membranes made of 2D material provide several advantages: 1) scalability, because the construction of these membranes is usually achieved by self-stacking of nanosheets, without being limited by area or thickness; 2) uniformity, that is, the dimensions of interlayer channels formed by stacked layers are relatively consistent, ensuring uniform transmission throughout the whole membrane; 3) adjustability, because the size and surface chemistry of interlayer channels can be customized, thus allowing flexible control over permeation channels.[90-92]

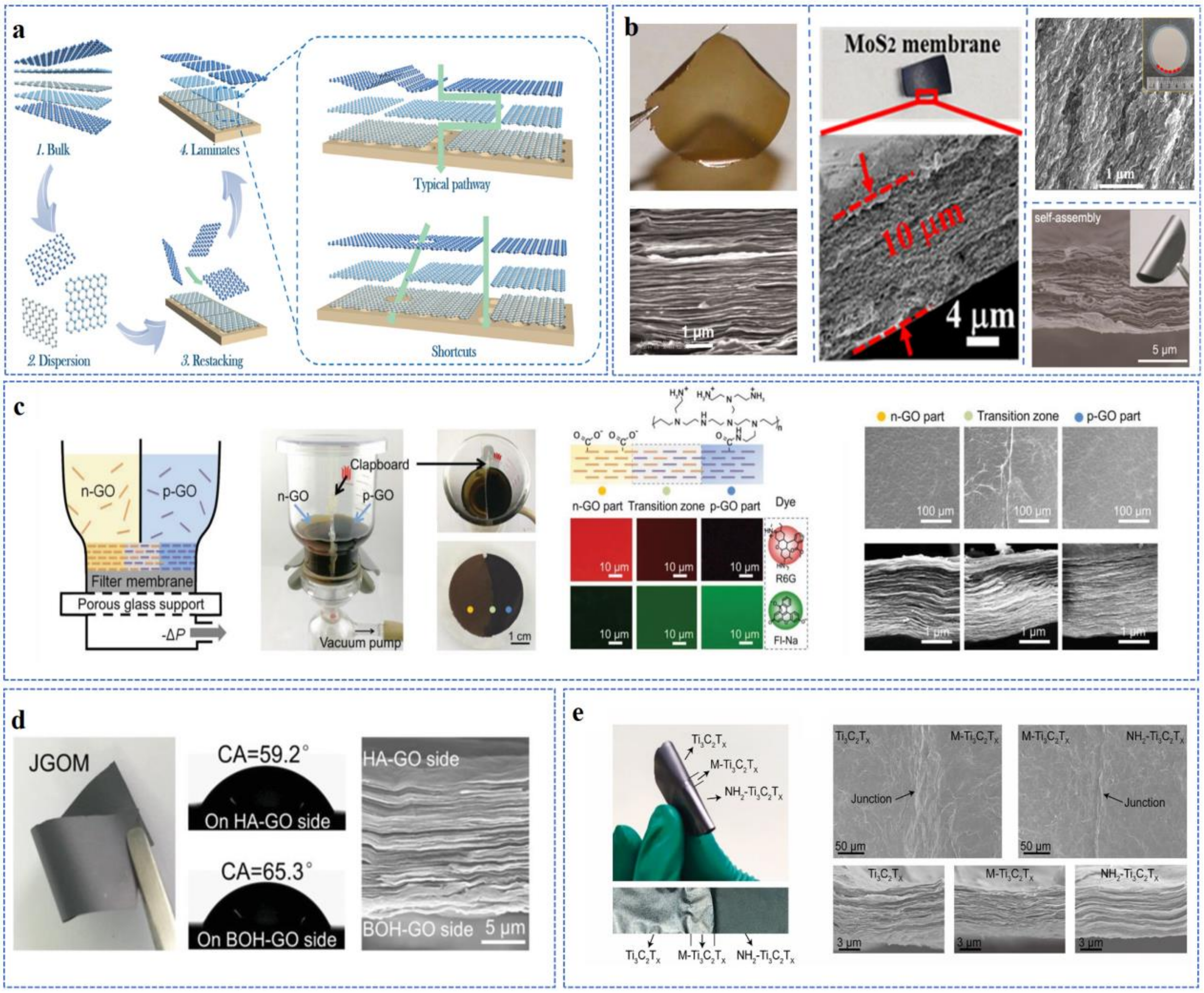

Figure 6. Structure and preparation of 2D material-based laminar membrane. a) The preparation process of 2D material-based laminar membrane. Reproduced with permission from ref 18. Copyright 2019 John Wiley and Sons. b) Laminar membrane assembled from a single 2D material (GO, MoS_2, h-BN, $Ti_3C_2T_x$). Reproduced with permission from ref 93. Copyright 2012 The American Association for the Advancement of Science. Reproduced with permission from ref 94. Copyright 2021 American Chemical Society. Reproduced with permission under a Creative Commons CC BY License from ref 95. Copyright 2023 RSC Pub.

Reproduced with permission from ref 96. Copyright 2018 Springer Nature. c) Transverse heterogeneous GOM. Reproduced with permission from ref 97. Copyright 2020 John Wiley and Sons. d) Longitudinal heterogeneous GOM. Reproduced with permission from ref 98, Copyright 2019 John Wiley and Sons. e) Transverse heterogeneous MXene laminar membrane. Reproduced with permission from ref 99. Copyright 2023 Elsevier.

2.3.2 Fabrication of single and heterogeneous 2D material-based laminar membranes

Common 2D materials such as graphene oxide (GO),[93, 98, 100, 101] h-BN,[95] TMDs,[94, 102, 103] and MXene[96, 104-106] can be utilized in the fabrication of 2D material-based laminar membrane (Figure 6b). The preparation process is generally consistent, being produced through vacuum filtration methods. Initially, the 2D material is dispersed from its bulk or powder phase into a suspension, followed by retacking of layers on a filter membrane using extraction filtration techniques.[18] Subsequently, the laminar membrane can be obtained by drying. In addition to using a single material, the membrane can also be designed as heterogeneous materials distributed horizontally or vertically. For example, in the preparation of GO membrane (GOM), the filter cartridge is separated from the middle, and in the pumping process, n-doped GO is added on one side and p-doped GO is added on the other side, thus forming a layered membrane with one side of n-type and the other side of p-type (Figure 6 c).[97] By controlling the order of filtration, after one layer is deposited, another layer is continuously deposited to form a longitudinally arranged heterogeneous membrane (Figure 6 d).[98] The surface-functionalized $Ti_3C_2T_x$ transverse heterogeneous laminar membrane was prepared by the same method (Figure 6e).[99] By controlling the surface structure and functionalization of 2D materials, heterogeneous laminar membrane are produced to expand the structural diversity and application range of laminar membrane.[98, 100, 107, 108]

2.3.3 Improve the stability of 2D material-based laminar membranes

The stability of a 2D material-based laminar membranes usually refers to the ability to maintain its structure and interlayer spacing. The stability difference between laminar membranes and channels is obvious, because the layer assembled channels are tightly bonded by van der Waals forces, while laminar membranes are deposited. There is a large space and weak van der Waals force between the layers, and the water molecules are easy to enter this space and separate the membrane. Therefore, it can not reach the structural robustness and durability of layer assembled channels. This instability hinders its application. GOM is easily dissolved, because there are a lot of oxidation groups in the inside and edges of GO sheets, such as hydroxyl and epoxy groups. The hydrogen bond between water and hydroxyl/epoxy groups can provide a strong hydration repulsion. In addition, the carboxyl groups are negatively charged in the hydration process, which can generate electrostatic repulsion between the GO sheets, thus leading to the expansion of the membrane spacing and the separation of the assembled GO sheets.

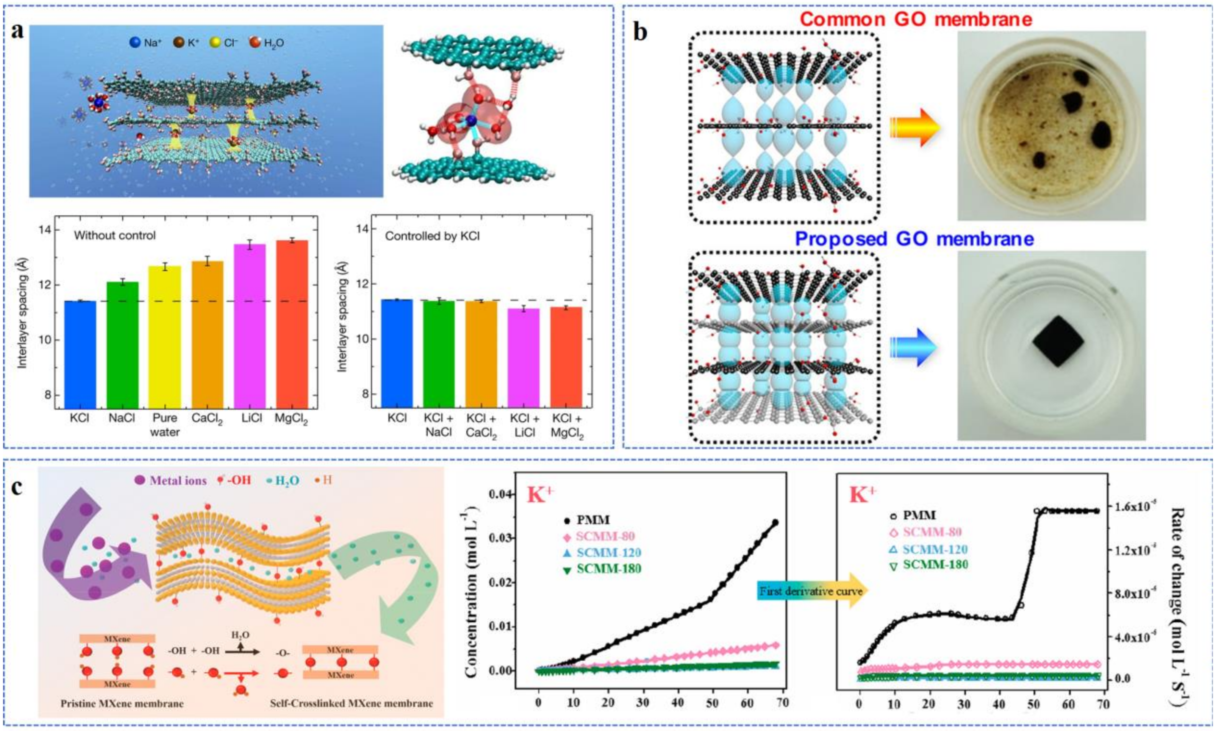

Figure 7. Improve the stability of 2D-based material laminar membrane. a) Metal ion intercalation fixed layer spacing. Reproduced with permission from ref 109. Copyright 2017 Springer Nature. b) Mixed reduced GO and π-π attraction prevents the membrane from dissolving. Reproduced with permission from ref 110. Copyright 2016 American Chemical Society. c) The self-crosslinking reaction of $Ti_3C_2T_x$ nanosheet improves the stability of the membrane. Reproduced with permission from ref 111. Copyright 2019 American Chemical Society.

The method to improve the stability of the membrane is to introduce an attractive force between the sheets to increase the connection strength. Chen et al. found that the GOM soaked in a cationic solution has the effect of fixing the layer spacing (Figure 7a).[109] The strong noncovalent hydration cation-π interaction between the GO sheet and the aromatic ring connects the adjacent layers, thus fixing the spacing between layers. Xi et al. reduced the repulsive effect of hydroxyl and epoxy band by doping partially reduced GO (Figure 7b).[110] The weakening of repulsion will lead to the strengthening of π - π attraction. The GOM prepared by this method has a controllable interlayer spacing, and shows excellent stability in water even in strong acid and alkali solutions. The membrane doped with 50% partially reduced GO can be soaked for one month. MXene membranes are similar to the GOM in that its lamellar surface contains rich groups. Lu et al. used dehydroxylation between $Ti_3C_2T_x$ nanosheets to generate a self-crosslinking process between nanosheets to form a Ti−O−Ti bond, requiring only a simple vacuum heat treatment (Figure 7c).[111] Once the Ti-O-Ti bond is formed, the swelling behavior of the MXene membrane will be restrained, because the interlayer spacing in the solution is relatively fixed. It showed good stability in the monovalent ion solution permeation experiment, and there was no obvious swelling in the experiment for more than 70 h.

The stabilization of 2D material-based laminar membrane has solved the problems of complex solution environment and working conditions in practical application and the economic problems of long-term work, which has taken an important step for its application in the fields of ion/gas separation, seawater desalination, blue energy and so on.

3.APPLICATIONS OF 2D MATERIAL-BASED NANOFLUIDIC DEVICES

3.1 Exploration of new physical mechanisms

3.1.1 Nonlinear ion transport in nanopores

The combination of nanofluids and 2D materials has produced new physical phenomena and transmission mechanisms. At the nanometer scale, traditional transport mechanisms are no longer applicable. Atomic thin nanopores provide a transmission path with diameters limited to the level of single molecule, allowing different molecules to be selected according to the pore size. In addition, the hydration and dehydration mechanisms of ions during the process of transport are also very interesting. Ions in solution do not exist in isolation. They attract polar water molecules, forming hydrated ions that move as a unit. The diameter of the hydrated ion reflects the spherical structure formed by the central ion and the surrounding water molecules.

But this binding is loose, strong force or space constraint can rearrange or displace the water molecules. 2D material nanofluidic devices provide the spatial constraints necessary to limit ionic hydration structures, making themselves an idea tool to study the ion hydration mechanism. Molecular dynamics (MD) simulations reveal that ionic currents and pore sizes in graphene exhibit non-linear behavior, characterized by a rapid decrease in ionic current as the pore size decreases.[112] This nonlinear behavior is attributed to the fact that water molecules need to be rearranged outside the atom-thick pores to keep the ions hydrated significantly. Barabash et al. simulated the complex interactions between ion hydration shell and hydration cloud and the edge atoms of the graphene nanopore was simulated (Figure 8a).[113] The ions must overcome the dehydration barrier caused by the redistribution of water molecules around them. Firstly, the existence of pores distorts the water layer near the membrane and water molecules exist in the pores. When hydrated ions enter the pore, the water layer attached to the pore of graphene overlaps with the spherical symmetric hydration shell of the ions, resulting in density remodeling, which makes the first hydration shell changes, and its symmetric distribution is concentrated on both sides of the pores. Sahu et al. found that when ions enter a graphene nanopore with a diameter similar to hydration radius, the water molecules can be rearranged outside the pore, and the ions need to lose about a quarter of the internal hydrated water molecules before entering the pore (Figure 8b). The energy penalty of K^+ is about 0.27 eV, while Cl^- is about 0.37 eV, which leads to nonlinear effects in the current.[112] The ionic flux can be described by the transition state theory and expressed in Arrhenius form:[77, 114]

$$J = A\exp\left(-\frac{E_b - E}{RT}\right) \tag{1}$$

where J is the ion flux, A is the pre-exponential factor, R is the universal gas constant, T is the temperature, and E_b is the energy barrier, E is the external force. Equation (1) indicates that the flux of ions through the pore is governed by the transport energy barrier. As ions passing through the sub-nanopore, an external driving force is required to remove their hydration shell upon entry and rehydrate them upon exit the pore. There is an exponential relationship between the transmission flux and external energy, resulting in nonlinear characteristics in the I-V curve. The formula also indicates an important source of ion selectivity in sub-nano pores, that is, different ions have different hydration layer structures. This difference in dehydration energy leads to difference in ion flux, enabling selectivity within the confined system.[74]

The impact of pore surface charge on ion transport in nano and sub-nano pores is significantly amplified. Xiong et al. conducted a whole-atom MD simulation to investigate ion translocation through negatively charged sub-nano graphene pores, revealing three distinct transport processes: (a) cation adsorption, (b) trapping - assisted cation translocation, and (c) selectivity - assisted anion translocation (Figure 8c).[115] The process involves the replacement of adsorbed K^+ by a K^+ translocating into the bottom chamber, leading to dissociation of the resident ion from the charged site and subsequent adsorption of the substituted ion at the same site, completing trapping-assisted K^+ translocation. The adsorption of K^+ at the negative site facilitates the passage of Cl^- through the nanopores. The charge on the pore surface can also lead to the nonlinearity of ion transmission. Feng et al. prepared nanopores with a thickness of 0.65 nm and a diameter of 0.6 nm on a single layer of MoS_2 by ECR, and evaluated the electrical characteristics of these nanopores (Figure 8d).[72] The *I-V* curve shows obvious nonlinear characteristics, and the electrical conductivity increases with the increase of voltage. Coulomb blockade explains the suppression of ion flow in sub-nano MoS_2 nanopores at low voltages, where the energy required to charge the system, combined with low capacitance and strong ionic interactions, resulting in a nonlinear *I-V* curve. The ion flow is observed only when the applied voltage exceeds a certain threshold.

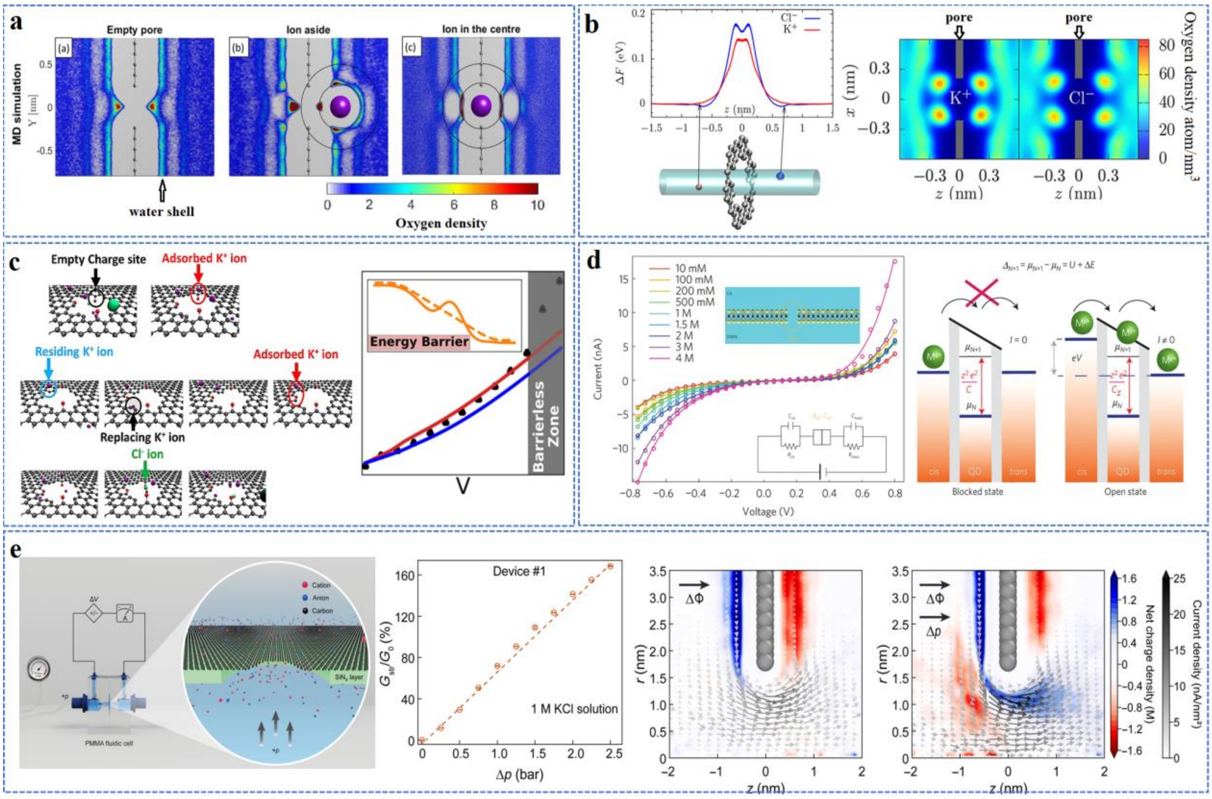

Figure 8. Nonlinearity of ion transport in nanopores. a) Dehydration simulation of ion transport in sub-nanopore. Left to right: changes of water shell distribution near graphene nanopore before and after ion entry. Reproduced with permission under a Creative Commons CC BY License from ref 113. Copyright 2021 Springer Nature. b) Transmission barrier (left) and oxygen atom distribution (right) of K^+ and Cl^- through graphene sub-nanopore. Reproduced with permission from ref 112. Copyright 2017 American Chemical Society. c) Ion trapping and thermionic emission across sub-nm pores. Reproduced with permission from ref 115. Copyright 2023 American Chemical Society. d) Nonlinear transport of ions in MoS_2 nanopores. Reproduced with permission from ref 40. Copyright 2016 Springer Nature. e) Nonlinear electrohydrodynamic ion transport in graphene nanopores. Left to right: schematic illustrating the pressure-integrated ion transport in graphene nanopores; ionic conductance increases as a function of applied pressure Δp; visualization of axisymmetric net charge distribution and current density vectors for $\Delta\phi = 3$ V with zero pressure bias, $\Delta\phi = 3$ V and $\Delta p = 200$ MPa. Reproduced with permission from ref 116. Copyright 2022 The American Association for the Advancement of Science.

Feng et al. measured ion conduction in graphene nanopores under pressure (Figure 8e). The streaming current $I_{str} = I - I_{\Delta p=0}$, conductance $G_{str} = I_{str}/\Delta\phi$. As show in Figure 8, $G_{str}/G_o \propto \Delta p$, where G_0 is the conductance without applied pressure Δp. So $I_{str} \propto \Delta\phi\Delta p$,which indicating a nonlinear electrohydrodynamic coupling in streaming current.[116] The ion flow generated by the pressure driving is symmetrical with the direction of the pressure gradient and controlled by the voltage. Through theoretical simulation show graphene capacitance accumulation result in a strong net ionic charge layer on the surface. When pressure is applied, ions on the surface are transported by a fluid driving force, resulting in nonlinear pressure-voltage coupling. This nonlinear coupling is also related to the slip on the surface of the graphene, which promotes the flow velocity of water on the surface of graphene and improves the pressure sensitivity of the graphene nanopores.

2D material-based nanopores provide a new platform for exploring the structural changes of ions and fluid transport from a microscopic point of view and exploring new physical mechanisms. A thorough understanding of the ion transport mechanism can provide guidance and a basis for designing, optimizing and controlling the permeability and selectivity of nanofluidic devices.

3.1.2 Transfer enhancement of graphene surface

In addition to the restriction at the entrance and exit, the interaction between the fluid and the surface also plays a key role in the fluid transport and structural characteristics in 2D material-based nanochannels.[117] Although 2D materials show high flatness, there are obvious differences between different types of materials. Graphene, as the flattest 2D material composed only of carbon atoms arranged in the same plane, has the smoothest surface.[118-120] h-BN also shows the lattice structure of layer assembly, but the composition of two kinds of atoms makes it surface fluctuation. The other 2D materials with non-coplanar atoms exhibit relatively more large surface roughness. Although this roughness may be neglected in the macroscopic systems, it can be significantly amplified at the nano or sub-nano scale, thus having an observable impact on fluid transport. The slip length is a linear extrapolation, which is the decreasing distance of velocity distribution in solid. Longer slip length means lower surface fluid resistance, which its correlation with low liquid-solid friction, as well as its influence on energy conversion efficiency.[121] To realize a large slip length in traditional solid materials is difficult. However, in carbon nanotubes and nanochannels, the slip length is exceptionally high, which is a feature not observed in other 2d materials.[119, 122, 123] This phenomenon is closely related to the smoothness of graphene surface. Tocci et al. used ab initio MD to model the connection between liquid water and friction in contact with graphene and h-BN (Figure 9a).[124] Although these two materials have a similar planar structure, the friction coefficient of water on the surface of h-BN is three times that of graphene. Due to the differences in atomic composition, electronic structures and energy fields, the maximum transport energy barrier of water transport on graphene surface is only 13 meV, while the maximum of h-BN is 21 meV. The height of the barrier determines the ease with which water moves on the surface. The higher the barrier, the greater the frictional resistance. In another work, they used the same method to prove that the speed of water sliding on graphene channel with different height (0.9 nm to 3.2 nm) is 5 times and 11 times higher than that of h-BN and MoS_2 (Figure 9b). [120] The energy landscape difference between 2D material surfaces provide the main static sources of water sliding difference. The transport energy barrier of water on graphene, h-BN and MoS_2 surfaces is about10 meV, 20 meV and 50 meV, respectively.

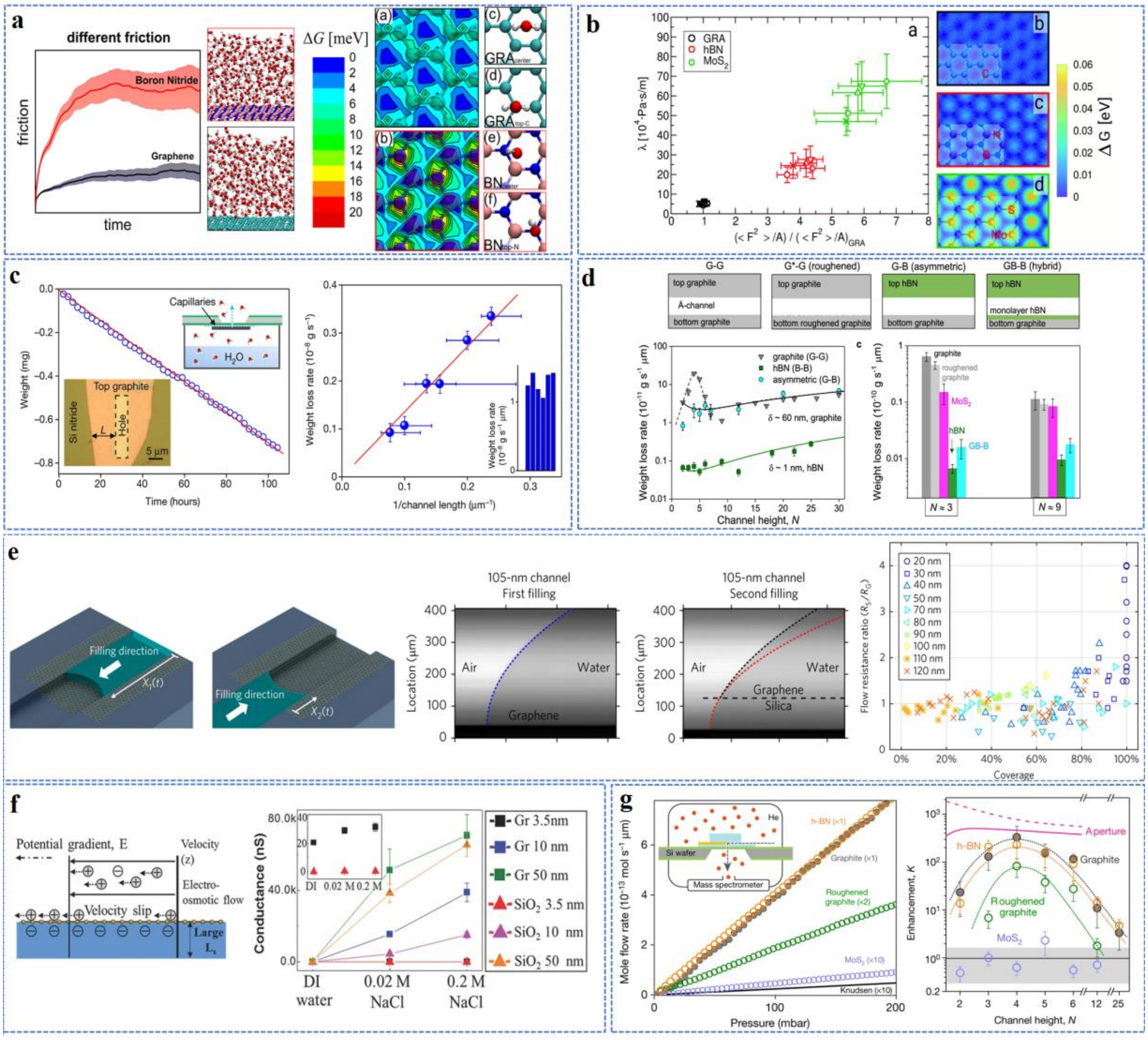

Figure 9. Transfer enhancement of graphene surface. a) Friction (left) and potential energy cloud distribution (right) of water on graphene and h-BN surfaces. Reproduced with permission from ref 124. Copyright 2014 American Chemical Society. b) Comparison of friction coefficients (left) and potential energy cloud (right) of graphene, h-BN and MoS_2 channels of different heights. Reproduced with permission under a Creative Commons CC BY License from ref 120. Copyright 2020 RSC Pub. c) Water permeation through graphene nanocapillaries. Reproduced with permission from ref 81, Copyright 2016 Springer Nature. d) Comparison of water permeation through graphene, etched graphene, h-BN and MoS_2. Reproduced with permission under a Creative Commons CC BY License from ref 125. Copyright 2021 Springer Nature. e) Fast water transport in graphene channels. Reproduced with permission from ref 84, Copyright 2018 Springer Nature. f) Ion enhanced transport on the surface of graphene. Reproduced with permission from ref 86. Copyright 2017 John Wiley and Sons. g) Ballistic

molecular transport through 2D channels. Reproduced with permission from ref 82, Copyright 2018 Springer Nature.

Geim et al. conducted an investigation on the transport of water molecules through graphene nanochannels, observing flow rates of up to 1 m s^{-1} for channels capable of accommodating only a few layers of water molecules (Figure 9c).[81] The authors attribute this observation to high capillary pressure (approximately 10^3 bar) and large slip lengths (60 nm) on the graphene surface, which are also associated with an increase in the structural order of nanoconfined water. Compared with graphene channel, the water transport speed and slip lengths of the h-BN or etched graphene channel with a certain roughness are lower (Figure 9d).[125] However, different from the theoretical simulation results, the water migration flux in h-BN channel is the lowest. Besides the difference of surface energy barrier, another source of water molecule friction is the electrostatic interaction of polar water molecules and OH^- adsorbed on the surface of h-BN, which inhibits the movement of the water molecules.[126] The interaction between OH^- and water also hinder the formation of long-range ordered water layers.

From the above analysis, it can be seen that covering other solid material channels with a graphene layer can reduce the surface roughness, lead to an increase in the surface slip length and enhance fluid transport. Xie et al. tested the slippage and transport resistance of water in a partially graphene-covered silica channel (Figure 9e).[84] It examined the relationship between the position and time of flowing into liquid surface from the graphene side and the silicon side was studied, and the mass flow resistance ratio was deduced. In the channel with water flow resistance ratio greater than 1, the higher the coverage rate of graphene, the lower the resistance of water transmission in the channel. The enhanced water transport due to longer slip length will also lead to enhanced ion transport in the channel, thereby improving the overall conductivity of ions in the channel. Han et al. detected a 115 times increase in ion conductivity within graphene-covered silica channels (3.5 nm).[86] Xie et al. observed a similar effect in their other work, in which the enhancement of electrical conductivity was limited because only one side of the channel was covered by graphene.[85] They believe that the conductance of graphene channel is enhanced because the sliding of the graphene surface enhances the electroosmosis flow of ions. The solution in the channel flows directionally under the action of electric field, ionic friction and viscous force, and the sliding of the graphene surface enhances the speed of this directional flow, which makes the mobility of ions partially increase on the original basis, thus generating greater conductivity.

Surface roughness plays significant role in gas transport within the nanoconfined space. When gas molecules move in a space smaller than their mean free path, the gas flow is governed by Knudsen theory, where surface-molecule collision has higher probability than molecule-molecule collision. This surface-molecule interaction leads to diffusion scattering, hindering the transport of molecules. Keerthi et al. reported that gas molecules have specular reflections in sub-nano channels with atomic-level surface flatness, resulting in gas ballistic transport and frictionless flow, thereby increasing transport speed (Figure 9g).[82] In MoS_2 channels, the height of atomic fluctuation is comparable to the size of a He atom and its de Broglie wavelength, resulting in a substantial diffuse scattering and gas transport behavior consistent with Knudsen theory. Conversely, h-BN and graphene channels, with their superior flatness, exhibit specular surface reflection, and greatly enhancing the gas transport. In the channel with 4 layers of graphene height, gas transport enhancement reaches to 300, highlighting the significant contribution of flat surface in optimizing gas permeability.

Generally speaking, the enhanced transfer of fluid on the surface of graphene reduces the transport resistance caused by the friction between the fluid and the solid surface. This is beneficial to improving the efficiency of energy conversion. In the pressure-driven channels, the energy conversion efficiency can be improved by more than one order of magnitude on the graphene surface.[127] This is expected to open up new opportunities for applications such as rapid desalination, as well as energy harvesting in nanofluid confinement.

3.1.3 Conformational changes of fluids in confined spaces

The limitation of nano-scale also amplifies the Coulomb potential and Leonard-Jones potential, which can extend throughout the whole channel, thus affecting the structure and distribution of molecules, and ultimately affecting the structure and transport of fluid.[128] Aluru et al. performed a multiscale study of water within graphene channels using a variety of models (Figure 10a).[129] The molecular accumulation of water near the interface is different from that in bulk solution. The interface region is bound by the Leonard-Jones potential and presents a layered arrangement. Compared with the radial distribution function of the center of mass, the radial distribution of the contact layer is more polarization, and it obviously showed a higher degree of order in a liquid. The water dipole is preferentially parallel to the hydrophobic surface, and the contribution of hydrogen bonding is also suppressed.[130] The layered arrangement of water molecules on the surface of the channel, shows a lower dielectric constant than that of bulk phase water. In the nanochannel with h-BN as the wall, when the height of the channel is less than 2 nm, the dielectric constant of the internal water is only 2.1 (Figure 10b).[131] When the channel height increases to 100 nm, the dielectric constant of the water in electrolyte returns to the bulk value of 80 (pure water, pH = 7).

Multibody Coulomb interactions between ions become more complex under strong space constraints, such as the Coulomb blocking effect mentioned above. Nanochannels confine the solution to narrow spaces (0.7-1.4 nm), where ions can form tight Bjerrum pairs under such strong spatial constraints (Onsager's Wien effect).[132] These Bjerrum pairs, consisting of a cation and an anion, are uncharged, but can be separated by an electric field, contributing to the conduction, thus producing a nonlinear *I-V* response. Bocquet et al. extended this concept with fractional Wien effect.[133] The authors constructs a gated charge, the number of charge is not an integer, but a fraction. It can bind an integer number of ions, but the binding of one ion is relatively weak. Under an external electric field, this weakly bound ion may dissociate from the gated charge, resulting in a non-zero conductance. Additionally, the authors proposed a theory to explain the strong nonlinear effects of ion transport at sub-nanometer scale (Figure 10c).[134] MD simulations reveal another mechanism. Under an electric field in the nanochannel, Bjerrum pairs do not dissociate but instead form a wormlike structure - Bjerrum polyelectrolytes. As the field strength increases, these structures break down slowly, leading to slow dynamics and long memory times. This phenomenon retains structural information of Bjerrum polyelectrolytes, like leaving behind some kind of memory that can be used to build basic neurons.

New physical mechanisms for nanofluidic devices based on 2D materials are still emerging, benefiting from their ground-breaking scale limitations and rich surface properties. 2D material-based nanofluidic devices provide a broad platform to explore the unknown mechanism in the field of nano, and the exploration of mechanism will promote the progress of its technology in the field of condensed matter physics, fluid mechanics, bionic fluid devices and biosensing.

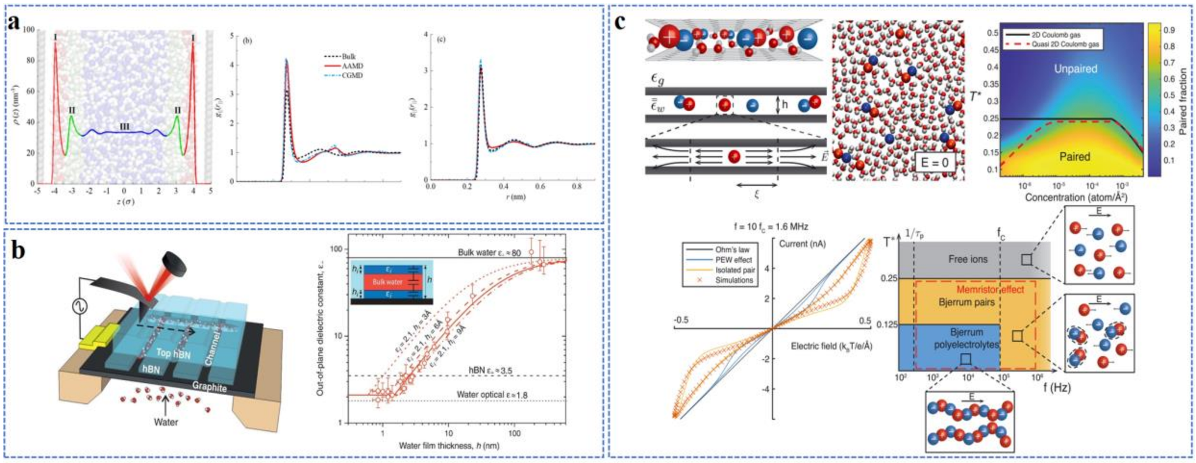

Figure 10. Conformational change of fluid in confined space. a) Conformational change of water in a graphene channel. Reproduced with permission from ref 129. Copyright 2018 The American Physical Society. Left: the radial density distribution of water molecules in graphene nanochannels. Right: the radial distribution of molecular centroid in contact layer (the left corresponds to I; the right corresponds to II). b) Dielectric constant of water under strong confinement. Reproduced with permission from ref 131, Copyright 2018 The American Association for the Advancement of Science. c) Nonlinear effects of ion transport under strong constraints and memristor effects with time-dependent mechanisms. Reproduced with permission from ref 134, Copyright 2021 The American Association for the Advancement of Science.

3.2 Detection of single biological molecule

3.2.1 Principles of nanofluidic devices for analyte detection

By applying the Coulter counter principle to nanopore or nanochannel sensors, analyte detection and characterization can be realized at the single molecular level.[20, 135-137] When a voltage is applied across a pore or channel, ions flow through it, resulting in a steady-state ion current (Figure 11). When the analyte passes through, the ionic current is disturbed due to the hindrance of its structure or the charge it carries. The structural information of the analyte can be analyzed by capturing these subtle changes. It provides a low-cost, label-free, high-throughput single-molecule bio sensing technology. The latest DNA sequencing technology, known as the third generation, uses nanopores to identify the base information on DNA and obtain sequence. At present, the most advanced nanopore DNA sequencing technology is based on biological nanopore, which involves the cultivation of natural proteins with pore structures, such as α-hemolysin, virus pore, mycobacterial pore protein and so on.[19] Solid state nanopores or channels offer a more stable option with adjustable physical and chemical properties that are more adaptable to multiple environments (temperature, pH, salinity), and they have higher controllability of pore size and shape. It can also be combined with advanced semiconductor technology, which contributes to the miniaturization of devices and the integration of testing and analysis equipment.

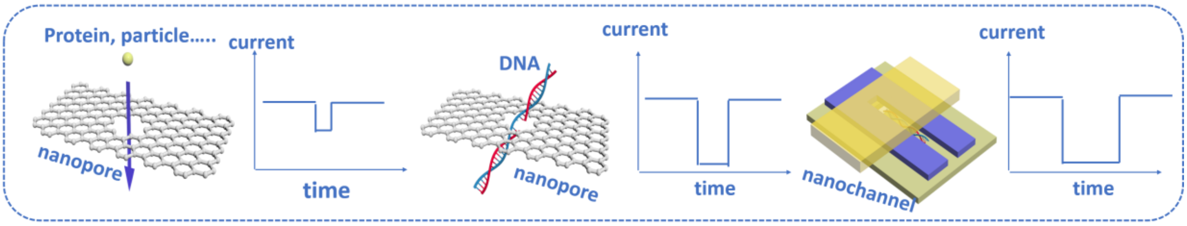

Figure 11. Schematic of 2D material-based nanofluidic devices for label-free single-molecule sensing.

3.2.2 DNA detection using 2D material nanopores

The monolayer of 2D material is the thinnest material, and its thickness is equivalent to the spacing between nucleotides, so it provides high spatial resolution, making it an ideal candidate material for DNA sequencing.[19] Dekker et al. observed a variety of DNA folding states in nanopores with a diameter of about 20 nm on single-layer graphene, which proved the feasibility of realizing and utilizing single molecule DNA translocation in ultra-thin nanopores (Figure 12a).[39] Liu et al. proposed a method for preparing nanopores based on MoS_2 for detecting DNA translocations through pores (Figure 12b). The observed signal amplitude during DNA translocation was found to be 5 times higher than that obtained with SiN_x nanopores, while maintaining a signal-to-noise ratio exceeding 10 fold.[35] Although MoS_2 is thicker than graphene, it doesn't need special surface treatment to reduce the strong interactions between DNA and surface.[138] The inherent electrical conductivity of the 2D material enables the DNA molecule to not only trigger a signal through ionic currents as it passes through the nanopore, but also cause a lateral current perturbation applied to the 2D material.[44, 69, 139-141]

This necessitates the fabrication of electrodes on the 2D material and application of a current. Graf and Heerema et al., respectively, made MoS_2 and graphene nanoribbons integrated with nanopores and connected them to electrodes (Figure 12c). DNA can be detected by the signals related to the ion current flowing through the nanopore and a transverse current flowing through the nanoribbon.[69, 140] The integration of complementary information from signals and dimensions will significantly improve the accuracy of nanopore identification.

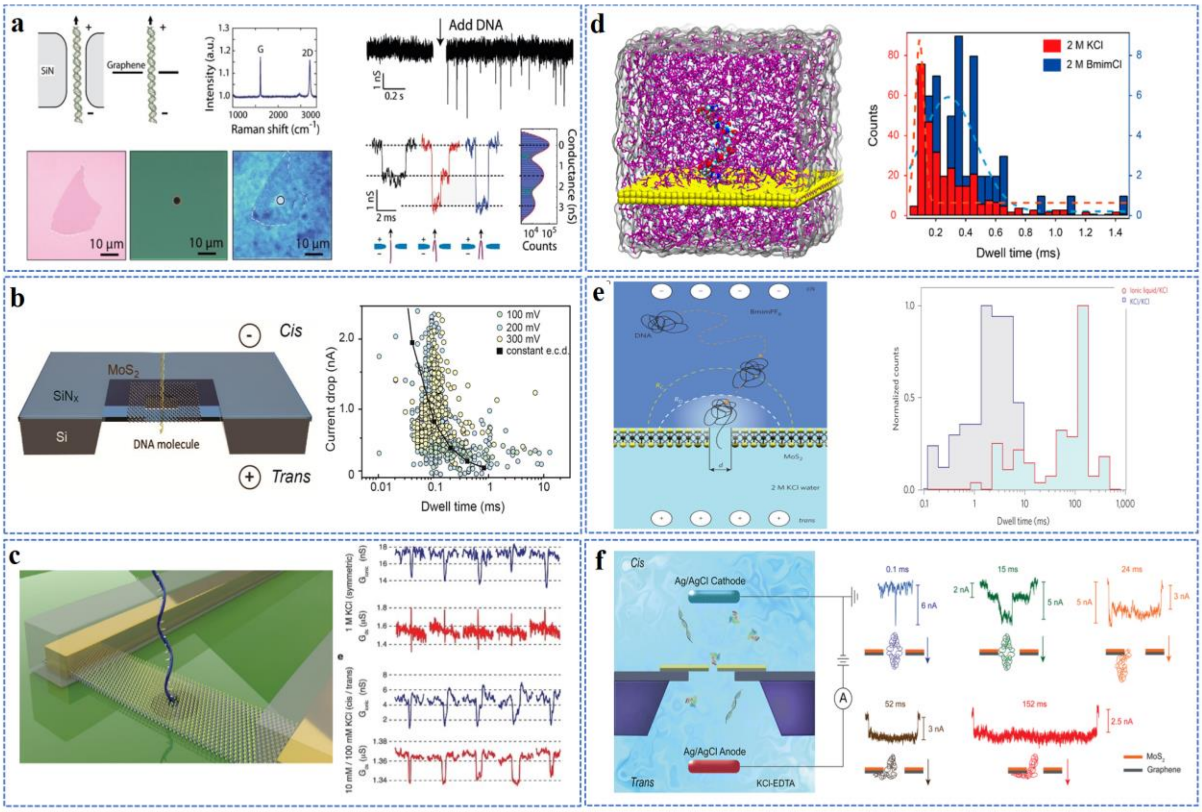

Figure 12. The 2D material-based nanopore detects DNA and slows its transmission. a) DNA translocation through graphene nanopores. Reproduced with permission from ref 39, Copyright 2010 American Chemical Society. b) DNA translocation through MoS_2 nanopores. Reproduced with permission from ref 35, Copyright 2014 American Chemical Society. c) Transverse detection of DNA using a MoS_2 nanopore. Reproduced with permission from ref 140. Copyright 2019 American Chemical Society. d) Ionic liquid decelerates single-stranded DNA transport through MoS_2 nanopores. Reproduced with permission from ref 142, Copyright 2022 American Chemical Society. e) Viscosity gradient slows down DNA translocation in MoS_2 nanopores. Reproduced with permission from ref 143, Copyright 2015 Springer Nature. f) The graphene-MoS_2 heterostructure nanopore is used to slow down the transport of biomolecules. Reproduced

with permission from ref 46, Copyright 2022 RSC Pub.

3.2.3 Slowing DNA transport through nanopores

Although 2D material-based nanopores have great potential in DNA sequencing, their development has been hindered by some challenges. A key obstacle is the rapid transport of DNA, which impairs the time resolution for identifying single bases. Voltage manipulation emerges as a pivotal approach for regulating the transmission rate of DNA, with higher voltage resulting in accelerated DNA translocation driven by electric field. However, it is also need to consider the influence of voltage adjustment on the stability, signal-to-noise ratio and noise control of membrane structures. Researchers shift their focus towards structural control and ion solution selection. Zhou et al. conducted simulations and experiments which confirmed that the strong interaction between $Bmim^+$ and ssDNA creates significant drag force and forms π-π stacks with bases in BmimCl solution, ultimately slowing down the electrophoretic movement of ssDNA in MoS_2 nanopores (Figure 12d).[142] Feng et al. observed the slow transport of DNA by adding 2 M potassium chloride (KCl) solution to one side of the MoS_2 nanopore and $BmimPF_6$ to the other (Figure 12e).[143] The transfer time extended from several ms to more than 100 ms. This method produces the best single nucleotide translocation speed for DNA sequencing, while keeping the signal-to-noise ratio above 10. Due to the limitation of graphene on the movement of biomolecules and the relatively weak limitation of MoS_2, Liu et al. devoted themselves to controlling the transport speed of DNA and proteins by using graphene-MoS_2 heterojunction (Figure 12f).[46] The strong π-π interaction between graphene and DNA slows down the transport of DNA, while the positively charged Mo atoms are more likely to attract negatively charged DNA into the pores.[42] The results showed that it can inhibit the transfer speed of bovine serum albumin, but it had no obvious effect on DNA. There is still room for improvement in this method, and a good delay effect may be obtained by trying a combination of various 2D materials.

3.2.4 Detection of DNA conformations in 2D material-based nanochannels

2D material-based nanochannel is also used for DNA detection. Unlike nanopores, these channels are limited by their length being significantly longer than bases, so they can not recognize a single base. However, they are capable of discerning the curled and folded state of

DNA. The restriction and stretching of DNA within these channels is also the focus of attention.[7, 144-146] Unlike traditional channels, which are limited by processing technology and struggle to achieve dimensions on the scale of the DNA hydration radius (less than 10 nm), graphene channels provide a smooth surface, facilitating the smooth transfer of DNA. This makes graphene nanochannels an ideal solution to overcome these limitations. Graphene nanochannel is a perfect solution to this problem. Yang et al. fabricated graphene nanochannels measuring 6.5 nm in height, 400 nm in length, and 110 nm in width (Figure 13a).[147] In the ionic current, two different events can be observed: a prolonged current interruption indicating DNA translocation, and a brief peak indicating DNA entry and exit. The DNA translocation events manifest three discernible stages in their current blocking trajectory: loading, translation, and exit. Liu et al. prepared graphene nanochannels with extremely high cleanliness, enabling smooth transmission of DNA in channels with a very high length-to-height ratio (4.3 nm high, 10 μm long), and found a certain linear relationship between the length of DNA and its transmission time, demonstrating the ability of the channel to recognize different lengths of DNA (Figure 13b).[89] Scale effects in confined space can also stretch DNA and make it linear. If the DNA is stretched into the channel first, so that the bases are fully exposed, and then it is transferred into the pore, it is expected to solve another big problem of solid nanopore detection, that is, the situation that DNA is curled and folded in the bulk solution, and it is difficult to identify single base. In addition, the friction and adhesion of the channel surface to DNA will also slow down the transmission speed of DNA, and this delaying effect will be enhanced by the design of the channel direction. The combination of channels and pores may also significantly reduce the speed of DNA passing through pores. Although the channel can not directly achieve the function of gene detection, it is expected to play a role in the front-end processing of sequencing.

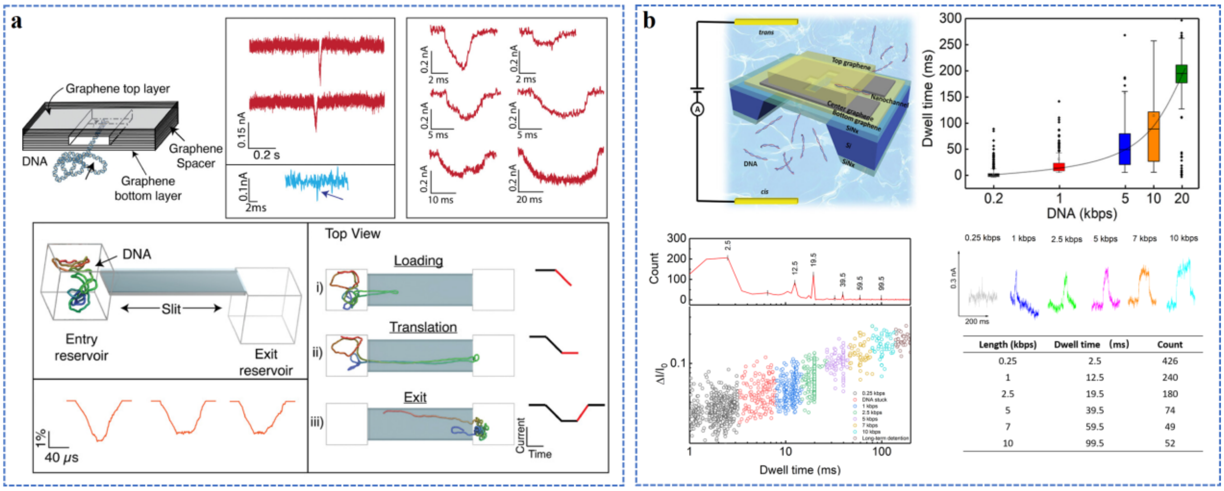

Figure 13. Detection of DNA transmission by 2D material-based nanochannels. a) Translocation of DNA through graphene ultrathin nanochannels. Reproduced with permission from ref 147, Copyright 2021 John Wiley and Sons. b) Graphene nanochannels recognize DNA of different lengths. Reproduced with permission from ref 89, Copyright 2024 American Chemical Society.

3.2.5 Identification of proteins using 2D material-based nanopores

The atomic-level thickness of the 2D material-based nanopore provide a high resolution for the identification of proteins. Compared to DNA, proteins are affected by their viscosity and charge distribution, and their adsorption on the surface of graphene is stronger. Shan et al. observed the ferritin translocation event only after modifying the graphene nanopore with phospholipid-PEG (DPPE-PEG750) amphiphilic reagent, and the signal of bovine serum protein was not captured (Figure 14a).[148] The hydrophobicity of graphene is also an important factor to prevent proteins from entering the nanopores. Gaurav et al. improved the preparation process to prepare clean, defect-free, and hydrophilic graphene nanopore chips.[149] Electron beam-induced drilling and shrinkage techniques were used to prepare nanopores of different scales. The nanopore successfully detected Fc-specific rabbit anti-goat IgG, Fc fragment of goat IgG and the specific binding of both. The adsorption between biomolecules on the surface of MoS_2 is relatively weak, and the prepared nanopores can capture protein signals relatively easily. Gu et al. successfully captured the transmission signal of bovine serum protein using MoS_2 nanopores (Figure 14b).[150] Compared with SiN_x nanopores, although they show higher pulse amplitude, their noise is much higher and their stability needs to be further improved. The identification of protein sequences is also of great significance for understanding the structure and function of proteins.[151] The subtle differences between natural amino acids challenges the spatial resolution in nanopore sequencing. Wang et al. successfully utilized sub-nano MoS_2 nanopores to achieve direct identification of individual amino acids with a resolution of less than 1 Dalton (Figure 14c).[45] They can distinguish the differences of chemical group in a single amino acids (including amino acid isomers), and have proved to successfully identify 16 of 20 natural amino acids.

DNA and protein sequencing using 2D material-based nanopores or channels has a broad application prospect, and may become the most cost-effective, rapid, convenient and effective genome sequencing technology available to human beings in the future. This progress is expected to catalyze the substantive progress in biological and medical research. However, there are still many challenges in this field, including equipment life, recognition accuracy, integration with electronic equipment, signal recognition and analysis using artificial intelligence technology and simplification of sample pretreatment procedures. In addition, compared with the widely used biological channels, the problem of noise suppression of 2D material-based nanofluidic devices is as difficult as reducing the transmission speed. The mechanical vibration, membrane capacitance, wettability and defects of 2D materials will all interfere with the identification effect.[71, 152, 153] The source of some of the noise is still unclear. To solve these problems, it is necessary to further explore the source mechanism of noise and optimize the device structure. So far, it has not been possible to read long sequences of DNA bases in solid-state nanopores or channels. It still needs the close cooperation and progress of many disciplines to achieve the goal of gene monitoring and protein sequencing by using 2D material-based nanofluidic devices, and there is still a long way to go.

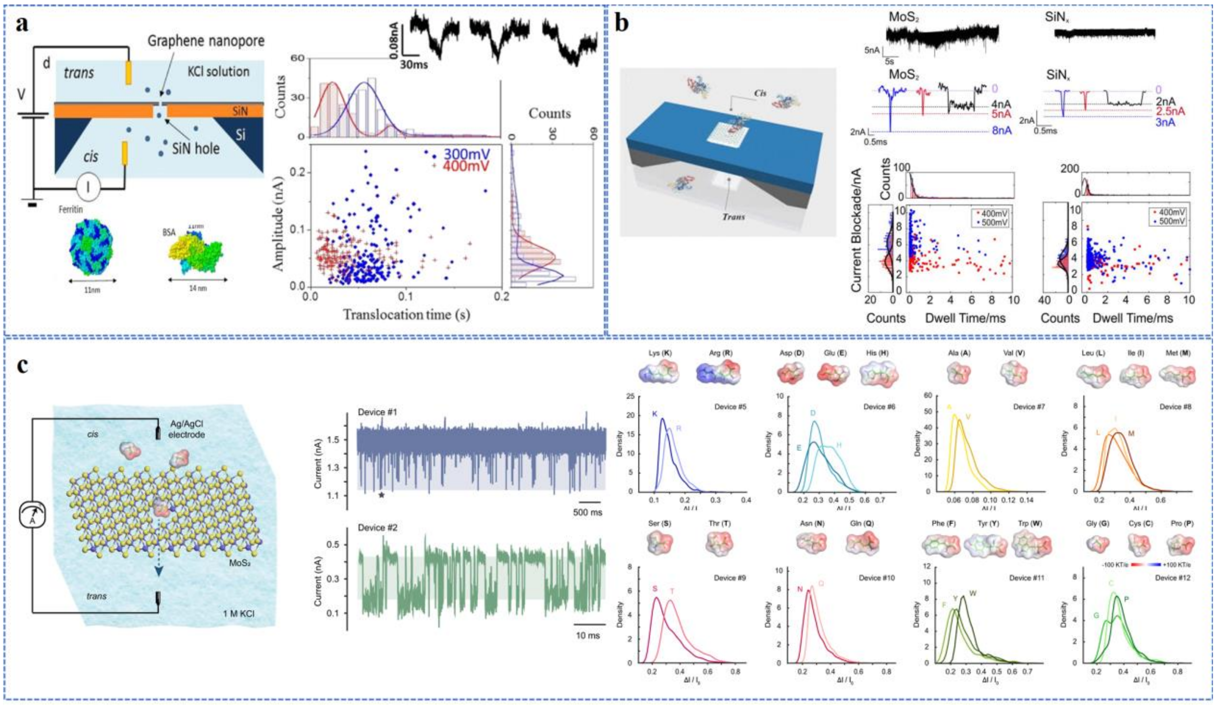

Figure 14. 2D material-based nanopore identification of proteins. a) Modified graphene nanopores capture single proteins. Reproduced with permission from ref 148, Copyright 2013 IOP Publishing. b) Capture of bovine serum protein by MoS_2 nanopores. Reproduced with permission from ref 150, Copyright 2019, AIP Publishing. c) MoS_2 nanopore identifies single amino acids with sub-1 Dalton resolution. Reproduced with permission under a Creative Commons CC BY License from ref 45, Copyright 2021 Springer Nature.

3.3 2D material-based iontronics and bionic devices

3.3.1 Research value of iontronics devices

Integrated circuits are the key to promoting the development of science and technology today, especially the development of artificial intelligence technology, which depends on advanced chips. Traditional integrated circuits are composed of diodes, transistors and other electronic components, and the signal carrier is electrons. Ions are also conductive substances, which have a wide variety, different structures, volumes, charge, positive and negative charges, ion mobility, etc., and can carry more information than electrons theoretically. Nanofluid devices are carriers of ions, which can also respond to a variety of stimuli such as applied electric field, pH, temperature, light, thereby regulating the transport of internal ions, and realizing the biology-like function of sensing external stimuli. Because of their superior photothermal and photoelectrical properties, 2D materials have more advantages than other traditional materials in the field of iontronics and bionic devices. The transmission of information between the various life activities of the human body depends on the transmission of ions. For biocompatibility, the development of iontronics devices is of great significance. The combination of brain and computer, the hottest topic in medical and engineering research today, can realize the seamless connection of ionic electrical signals by using ionic electrical devices, without converting ionic signals to electronic signals, which is beneficial to the integrity of information reception and response speed.

3.3.2 2D material-based nanofluidic devices as logic devices

It is the theoretical basis of constructing ionic-electric devices to realize ion directional transport or flow control through spatial electric field and structure control. Yao et al. prepared single graphene nanopores supported by polyethylene terephthalate (PET) membranes with the help of rapid heavy ion irradiation and asymmetric etching techniques (Figure 15a).[154] The surface of the prepared graphene nanopores is positively charged and has good anion selectivity. By using hydrochloric acid to change the surface charge state of the PET cone-shaped nanopores from negative to positive, the rectification ratio is as high as 190. Chen et al. prepared a GO based heterogeneous membrane. By using the formation of charge heterojunction caused by pH or ultraviolet irradiation changes, pH-light double-responsivity and ion rectification functions are integrated into 2D nanofluid systems (Figure 15b).[108] The rectification ratio reaches 56 at pH = 3 and 140 under ultraviolet light. The construction of nanofluidic devices with asymmetric structures is an important way to realize fluid diodes. Dong et al. cut the $Ti_3C_2T_x$ membrane ladder into a triangle to achieve a rectification ratio of 22.38, and successfully applied it to the logic circuit to achieve the logical operation of "AND" and "OR" (Figure 15c).[105]

The photoelectric response of 2D materials can be used to prepare photonic nanofluidic devices, such as photonic ion switches, photonic ion diodes, photonic ion transistors and so on. Guo et al. proposed that the local potential reduction of GOM by light irradiation follows a carrier diffusion mechanism (Figure 15d).[101] When light is struck off-center, it can create a voltage difference on the surface of graphene to drive the transport of ionic. Under asymmetric illumination, the voltage in the same direction can be balanced by using the photo-induced voltage difference, thus blocking the transmembrane ion current and forming a closed state. Its switching ratio is close to 10^3 - 10^4. By controlling light and alternating electric fields, using asymmetric light illumination, blocking the ion current at the desired voltage polarity, forming an efficient ion diode with a rectification ratio of up to ~10^4. The local low voltage in the illuminated area can be viewed as a light-induced gate voltage to control the horizontal ion conductance, forming an ion transistor. The source-drain current increases with the increase of light intensity, showing p-type gating behavior. In addition to GO, 2D materials with strong photoelectrical response, such as TMDs, MXene are also used to prepare similar devices.[94, 103, 106, 155] Compared with graphene-based materials, the size of the ionic photocurrent of these materials can be increased by tens of times, its photo-responsiveness can be improved by 2 - 3.5 times.

In addition to using light to control ion transport to prepare iontronics devices, gate voltage regulation is a more direct way, and it is more suitable for miniaturization and integration. However, gate voltage regulation requires higher device preparation, because it needs to work in an ionic solution, so it needs to be packaged to isolate the regulating electrode from the solution to prevent electrical crosstalk. Zhang et al. used redox graphene to fabricate an atomic-scale (interlayer spacing H ≈ 4.5 Å, length L ≈ 6 μm and width W ≈ 20 μm) ion transistor (Figure 15e). Since the channel height is smaller than the hydration diameter of metal ions, ions cannot enter the channel and the channel is in the "OFF" state. When a gate voltage is applied to the channel surface, the hydration shell can be twisted or partially stripped to overcome the energy barrier for ions to enter, allowing ions to insert into the channel as capacitive charges. When the inserted ions accumulate in the channel, the seepage threshold is exceeded, and the permeated ion transport is initialized, indicating the "ON" state of ion permeation.

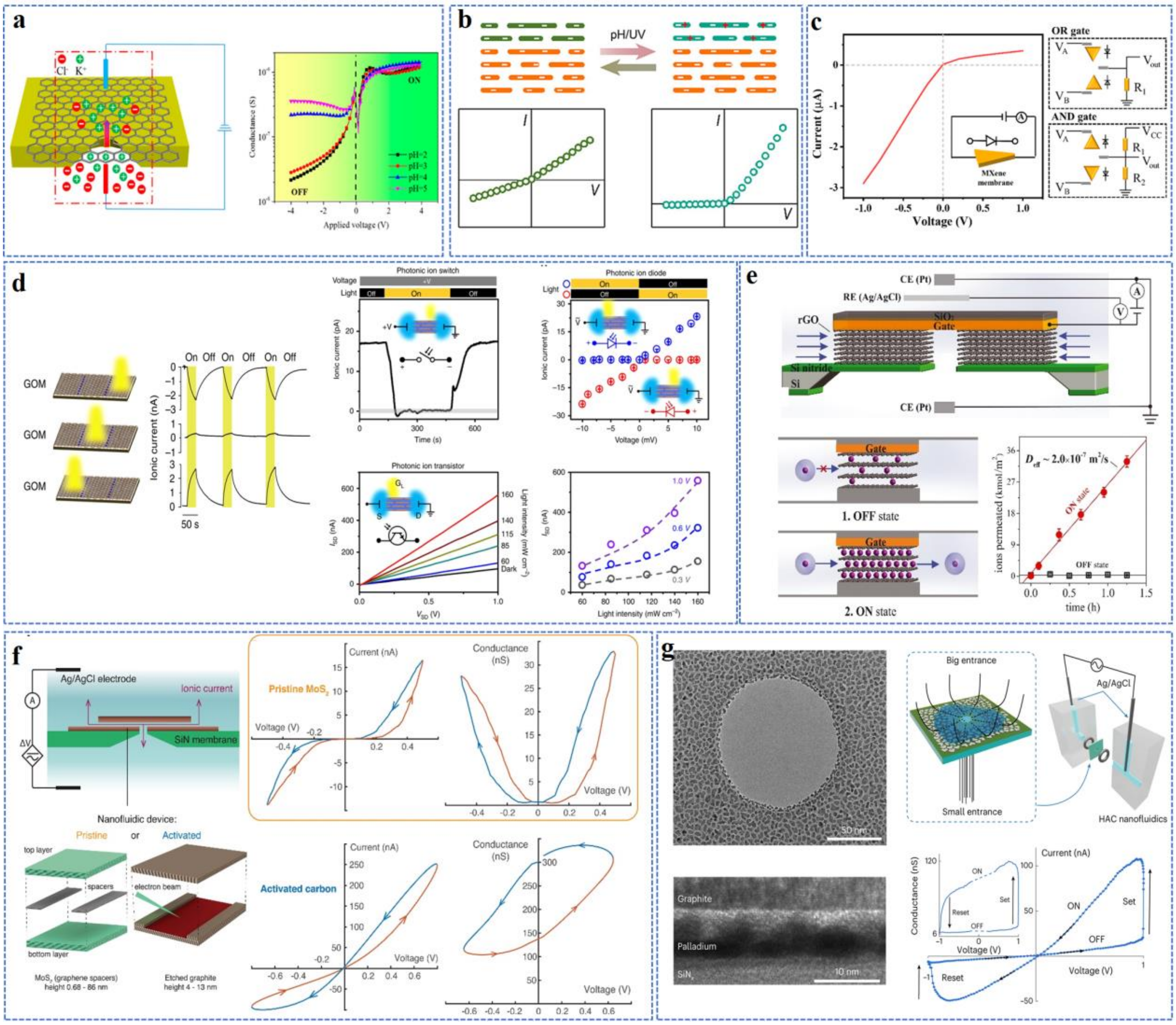

Figure 15. a) Large rectification effect of single graphene nanopore supported by PET membrane. Reproduced with permission from ref 154, Copyright 2017 American Chemical Society. b) Dual-riven binary heterogeneous nanofluidic ionic diodes. Reproduced with permission from ref 108, Copyright 2022 American Chemical Society. c) Geometric tailoring of macroscale $Ti_3C_2T_x$ membrane for logic gate circuits. Reproduced with permission from ref 105, Copyright 2021 American Chemical Society. d) Photo-induced ion transport through GOMs and photonic nanofluidic devices. Reproduced with permission under a Creative Commons CC BY License from ref 101. Copyright 2019 Springer Nature. e) Atomic-scale ion GOM transistor with ultrahigh diffusivity. Reproduced with permission from ref 156, Copyright 2021 The American Association for the Advancement of Science. f) MoS_2 and activated graphene nanochannel to achieve two kinds of memristor effect. Reproduced with permission from ref 157, Copyright 2023 The American Association for the Advancement of Science. g)

Nanofluidic logic with mechano–ionic memristive switches.

3.3.3 2D material-based nanofluidic devices as memristors

The nerve conduction in living beings operates through changes in membrane permeability, which lead to a reversal of membrane potential and ion flow upon external stimuli, resulting in action potential.[159] 2D material-based nanofluidic devices can also be used to generate similar ion pulse currents and realize the function of neurons. Robin et al. theoretically predicted the Hodgkin-Huxley model in nanochannels of 2D materials, and then they implemented two types of memristors in MoS_2 and activated graphene channels, bipolar memristors with self-crossing *I-V* curves and unipolar memristors with self-crossing conductivity evolution (*G-V*) curves (Figure 15f).[134, 157] The nonlinear effect of the unipolar memristor can be explained by the formation of a polyelectrolyte by the tightly combined Bjerrum pair, which hinders the conduction of ions and can be destroyed by a strong enough electric field. The nonlinearity of bipolar devices depends on the polarity of the applied voltage, so their memory is derived from the asymmetric structure of the device. When cations flow from the side with low resistance to entry, because it is easier to enter than to leave, ions accumulate in the channel, resulting in an increase in conductivity. If the voltage is reversed, cations will flow out from the side with higher resistance, the channel will be exhausted, and the conductivity will decrease. For these two types of memristors, the memory time scale can reach from a few minutes to a few hours. Long-term memory comes from ion pairing or ion adsorption on the surface of the channel. The authors use this channel to realize a basic form of Hebbian learning, simulating the activation and connection of neurons. Emmerich et al. designed a nanofluidic device for circuit-level memory processing (Figure 15g).[158, 160] Graphene covered the heterogeneous palladium layer deposited on a SiN_x layer. Ions and water molecules flow around the palladium island in nano-scale channels formed by the graphene and substrates. Their large inlet asymmetry and quantity limitation lead to the switching behavior related to the formation of reversible liquid bubbles. When the counter ions enter the channel through the crystal edge, the ions accumulate, and when they enter through the microhole, the ion accumulation is exhausted. At 1M KCl solution, they operate in the range of 30-300 mHz with conductance ratios between 9 and 60. Using these mechanical-ionic memory switches can be used to assemble logic circuits consisting of two interactive devices and an ohm resistor.

The appearance of nanoscale or even sub-nanoscale artificial nanofluidic devices based on 2D materials has greatly promoted the development of nanofluidic iontronics. The ultimate goal of nanofluidic iontronics is to construct an integrated ion sensing system, which can carry out seamless signal transduction between external stimulation, conduction, treatment and biological systems. 2D materials have shown great advantages in many aspects, and it is believed that iontronics devices based on 2D materials will appear in brain like computing architectures in the future.

3.4 Ion selectivity

3.4.1 Principle of ion selectivity

An important method to achieve ion separation is the membrane filtration, which realizes by adsorption or charge, size limitation. Ion separation means that the target ion has a very high transmittance, while shielding other non-target ions requires a very high selective transmittance. Ion selectivity application can be subdivided into three categories. One is the selective of water molecules and ions. The main purpose is seawater desalination. The second, the selectivity between ions of different types and valence states is of great value in the reuse of ion recovery plasma. The third is the separation of anion and cation, which is related to energy collection and conversion efficiency.[161] The precise and ultra-fast ion selection technology is the best choice to extract fresh water and minerals from seawater.

The size of 2D material-based nanofluidic devices, whether nanopores, nanochannels or membranes, can be limited to the sub-nano scale, which is equivalent to the size of hydrated ion. Size design allows ion screening at different spatial scales (Figure 16, left). The transport space is much smaller than the size of the hydrated ions, which allows only water molecules to pass through, and as the space increases, some hydrated ions must overcome the barrier of dehydration to pass through, which we have discussed above.

At the same time, the charge properties of 2D materials can realize the selectivity of valence state, anion and cation (Figure 16, right). The charge carried on 2D materials, defects or charged groups adsorbed by impurities, generates electric field on the surface of pores or channels, known as electric double layer (EDL). Within the EDL, the electric potential decreases with distance from the surface, eventually reaching electric neutrality at the boundary of the diffusion layer. The EDL thickness is usually expressed as Debye length (λ_D):[3, 162]

$$\lambda_D = \frac{1}{\sqrt{8\pi l_B C}} \tag{2}$$

Here, Bjerrum length (l_B) is given as

$$l_B = \frac{z^2 e^2}{4\pi\varepsilon_r\varepsilon_0 k_B T} \tag{3}$$

and C is concentration of the salt in the reservoirs, ε_r is the relative permittivity of the medium, ε_0 is the permittivity of free space, k_B is the Boltzmann constant, z is the cation and anion valances, e is the elementary charge, T is the temperature. Thus, the thickness of EDL is related to the ion concentration. According to Gauss theorem, the electric field strength is related to the surface charge density, with the higher the charge density, the stronger the internal electric field. When EDL thickness matches the restricted size of the channel, ion movement is governed by the electric field within the EDL, resulting in charge selectivity - attracting opposite charged particles and repelling ions with same charge.

The ratio of ion mobility represents the ion selectivity of the fluid device, which can be calculated by the conductivity and osmotic potential as follows:[3, 162]

$$\sigma = F(z^+\mu^+C^+ + z^-\mu^-C^-) \tag{4}$$

$$\frac{\mu^+}{\mu^-} = -\frac{z^+}{z^-}\frac{\ln\left(\frac{C_H}{C_L}\right) - \frac{z^+FE_{osm}}{RT}}{\ln\left(\frac{C_H}{C_L}\right) - \frac{z^-FE_{osm}}{RT}} \tag{5}$$

where, σ is ionic conductivity of the nanofluidic devices, μ is the electrophoretic mobility, F is Faraday's constant, E_{osm} is the osmotic potential, C^+ and C^- are the concentrations of anion and cation, respectively, C_H and C_L are the concentration of salt on the high and low concentration sides, z^+ and z^- are the cation and anion valances, R is the universal gas constant. To obtain the ion selectivity, it is necessary to measure the ion conductivity in the nanofluidic device, and the osmotic potential caused by the asymmetric diffusion of anions, which is caused by the device's surface charge under a certain concentration gradient. These values enable the calculation of ion mobility, and eventually the evaluation of the ion selectivity according to Eq. (4-5).

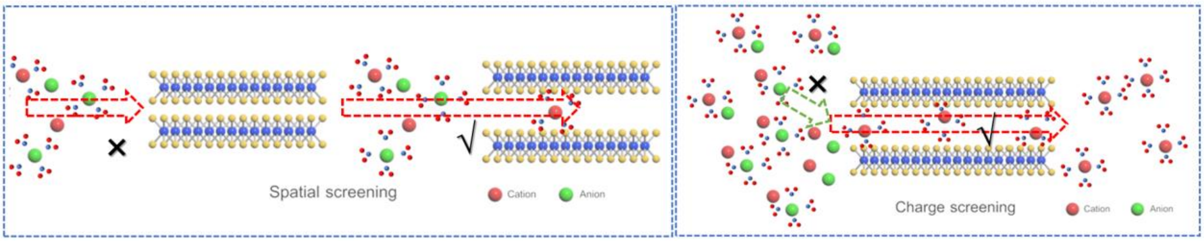

Figure 16. Schematic of 2D material-based nanofluidic devices for ion selectivity.

3.4.2 Spatial selectivity and charge selectivity of 2D material-based nanofluidic devices

2D materials will be charged in the solution environment, which is related to the pH and concentration of the solution, as well as the doping and defects on the surface. Therefore, in most cases, space selectivity and charge selectivity may work at the same time, depending on which factor accounts for the high proportion. Mechanically stripped, defect-free graphene and h-BN only allow proton transport.[25] Sumedh et al. used the oxygen plasma etching to create pore defects on graphene, and at low defect densities, the graphene membrane exhibited a near 100% salt rejection rate and rapid water transport.[61] Using the different dehydration effects of ions in different valence states passing through the nanopore can achieve the function of ion selectivity.[74, 77] For graphene nanopore with a radius of 0.2 nm, theoretical simulations show that the selection ratio of K^+ to Cl^- is about 2.5, which is due to the smaller dehydration barrier of K^+ than Cl^-.[112] With the pores size increase, the difference of potential barrier between the two ions decreases, and the selectivity decreases. Fu et al. used the direct Au ion bombardment technique to prepare sub-nanopores with an average diameter of 0.8 ± 0.16 nm in a single layer of graphene, enabling cation screening based on ion dehydration difference (Figure 17a). For example, Na^+ has only one water shell with a hydration radius of 3.06 Å, while Ca^{2+} has two water shells with a hydration radius of 4.34 Å.[163, 164] When passing through the graphene nanopore with a diameter of 0.85 nm, Na^+ needs to remove 2 water molecules, while Ca^{2+} needs to remove 6, so the transmission barrier of Ca^{2+} is higher than Na^+. The energy barrier for cation translocation through the nanopore follows the order $K^+ < Na^+ < Li^+ < Ca^{2+} < Mg^{2+}$, which attributed to ion size and hydration strength.[74] In contrast to controlling pores and using ion dehydration to achieve selectivity, the selectivity of Na^+/Cl^- in monolayer graphene nanopore with a diameter of 20 nm can still exceed 100, and the conductivity of univalent cations can reach 5 times that of bivalent cations (Figure 17b).[29] The high surface charge density of the graphene pore surface is the fundamental source for achieving high ion selectivity. Therefore, preparation of highly selective nanopores does not need to rely on strict size limitations.

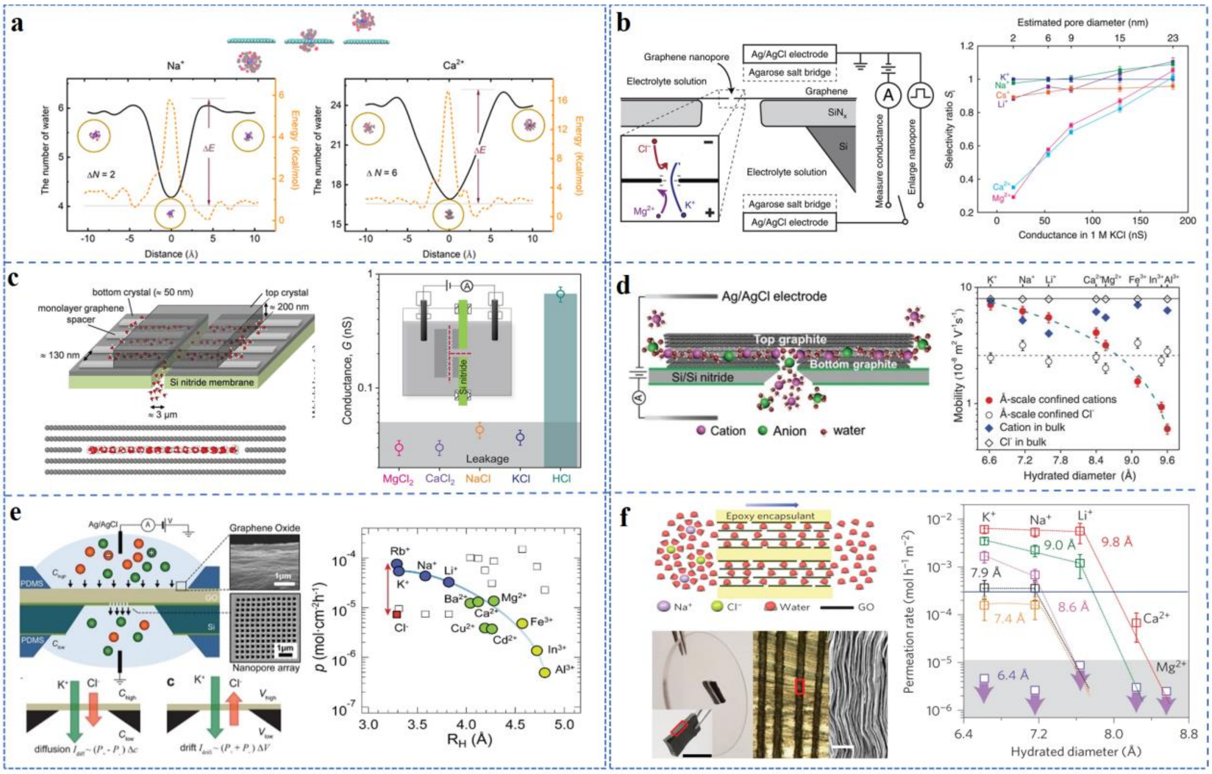

Figure 17. Spatial and charge selectivity of 2D material-based nanofluidic devices. a) Graphene sub-nanopores enable the selectivity of different cations. Reproduced with permission from ref 74, Copyright 2020 American Chemical Society. b) The surface charge improves the selectivity of graphene nanopores. Reproduced with permission under a Creative Commons CC BY License from ref 29, Copyright 2016 Springer Nature. c) Complete steric exclusion of ions and proton transport through confined monolayer water. Reproduced with permission from ref 83, Copyright 2019 The American Association for the Advancement of Science. d) Size effect in ion transport through Å-scale slits. Reproduced with permission from ref 165, Copyright 2017 The American Association for the Advancement of Science. e) Scalable graphene-based membranes for ionic sieving with ultrahigh charge selectivity. Reproduced with permission from ref 166, Copyright 2017 American Chemical Society. f) Controlled layer spacing enables tunable screening of ions by GOM. Reproduced with permission from ref 167, Copyright 2017 Springer Nature.

The selectivity of ions of different scales can also be realized by controlling the channel height of 2D material nanochannels.[117, 165, 168] The nanochannel at the height of a single layer of graphene (0.34 nm) allows only protons to pass through (Figure 17c).[83] The ionic mobility through a monolayer MoS_2 channel (height = 0.67 nm) decreases with the increase of the hydrated ion scale (Figure 17d).[165] Ions with a hydration diameter larger than the slit size can still penetrate it, which is consistent with the mechanism of ion dehydration in the sub-nanopore. Compared with nanopores, although the long transmission path can realize high filtration, it also limits the transmission flux. Laminar membranes have great advantages in ion selectivity. Its multi-layer space and multi-dimensional transmission path mean that it has a high transmission flux, and controllable interlayer spacing can realize the selection of ions of different sizes. And the surface is easy to functionalize, which makes it easy to achieve high density surface charge modification. Hong et al. achieved extremely high charge selectivity in GOM, up to 96%, which is a combination of spatial selective and charge selective (Figure 17e).[166] Taking into account the volume expansion of laminar membrane in solution, which affects the height between layers, Abraham et al. controlled the layer spacing of GOM through physical constraints, also achieving accurate and adjustable ion selectivity (Figure 17f).[167] The interlayer spacing ranges from 9.8 to 6.4 Å, which is smaller than the diameter of the hydrated ion. With the decrease of layer spacing, the permeability efficiency of ions and the diameter of ions that can pass through are reduced, but the water flux remains high. The surface of MXene is rich in negatively charged surface functional groups, and it is also used to selectively separate different ions. Wang et al. reported a non-expansive MXene membrane.[169] The strong interaction between the oxygen functional groups on the surface of Al^{3+} and MXene prevents expansion. These membranes exhibit good non-swelling stability in aqueous solution for 400 h and have a fast water flux (~1.1 - 8.5 $l\ m^{-2}\ h^{-1}$) with a high rejection rate of KCl (~ 89.5 - 99.6 %).

3.4.3 Improving ion selectivity through modifications and external fields

The transport space and surface charge are the two main factors affecting the selectivity of 2D material-based nanofluidic devices. In addition to the example of compressed GOM space discussed above, it is not easy to achieve continuous changes in space on nanofluidic devices. To improve selectivity, it is best to find a breakthrough in the surface charge. There are some methods to control the surface charge. One is to add groups (such as -OH, -COOH) to the surface by modification. These groups are adsorbed on the surface and carry a lot of negative charges. Modification methods include plasma cleaning, chemical solution immersion, etc., and sample reconstruction is not needed. High density sub-nano pores can be produced on graphene membranes by plasma etching process. Due to the synergistic effect of nanopore size and surface charge, this process can not only select cations with different hydration radii, but also distinguish cations and anions with high selectivity. Nanoporous graphene membranes generated by oxygen plasma show a high Na^+/Cl^- selectivity ratio of more than 8, while graphene membranes generated by hydrogen plasma have almost no Na^+/Cl^- selectivity (Figure 18a).[66] The oxygen plasma introduces a large amount of negative charge on the graphene surface and in the pores. Guo et al. achieved functionalization of graphene nanopore through etching combined with in situ covalent modification to coordinate pore size and chemical properties (Figure 18b).[78] The modified graphene nanopore has asymmetric ion transport behavior and highly efficient monovalent metal ion selectivity performance (K^+/Li^+ selectivity ~ 48.6). It also allows preferential transport of cations, and the resulting membrane has a K^+/Cl^- selectivity of 76 and H^+/Cl^- selectivity of 59.3. The synergistic effect of steric hindrance and electrostatic interaction gives Cl^- or Li^+ a higher energy barrier across the nanopore, resulting in super-selective H^+ or K^+ transport.

Another way is to adjust the charge distribution on the surface of 2D materials by external field. 2D materials have abundant photoelectric properties. Electric field, light field and the movement of electrons will all change the charge density distribution of 2D materials. In some experimental reports of light field controlling ion diffusion in 2D material-based nanofluidic devices, we find that the ion diffusion potential is enhanced after light incidence.[34, 68] The enhancement of diffusion potential reflects that the light field increases the surface charge density of 2D material and improves their ion selectivity. However, most of light incidence experiments focus on its application in the field of blue energy and ion photoelectric devices, and few experiments have studied its value in ion selectivity. The significance of improving ion selectivity by controlling surface charge density by light field needs to be explored.

In addition to size and charge control, ambient temperature and structure also affect ion selectivity. 2D materials has a strong photothermal effect, which will bring about an increase in temperature under light, also lead to an increase in ionic mobility. Xia et al. demonstrated the feasibility of photothermal enhanced ion selective in MXene membrane (Figure 18c).[170] Using the photothermal effect of MXene membrane, the permeability of Na^+ increased by 429 % to 62.6 mol m^{-2} h^{-1}. The transport of heavy metal ions is inhibited because heavy metal ions are strongly repelled by the increase in the number of permeated Na^+ under Angstrom confinement. Using a conical structure with a voltage-dependent ion enrichment/depletion effect, Xue et al. prepared heterogeneous graphene-based PET membranes to achieve voltage-controlled ion selectivity (Figure 18d).[171] The ion selectivity between K^+, Na^+, Li^+, Ca^{2+}, and Mg^{2+} can be adjusted simply by adjusting the applied voltage. At negative voltage, most bivalent cations are blocked from passing through. The ion enrichment/depletion of asymmetric structures are essentially due to the screening of surface charges.

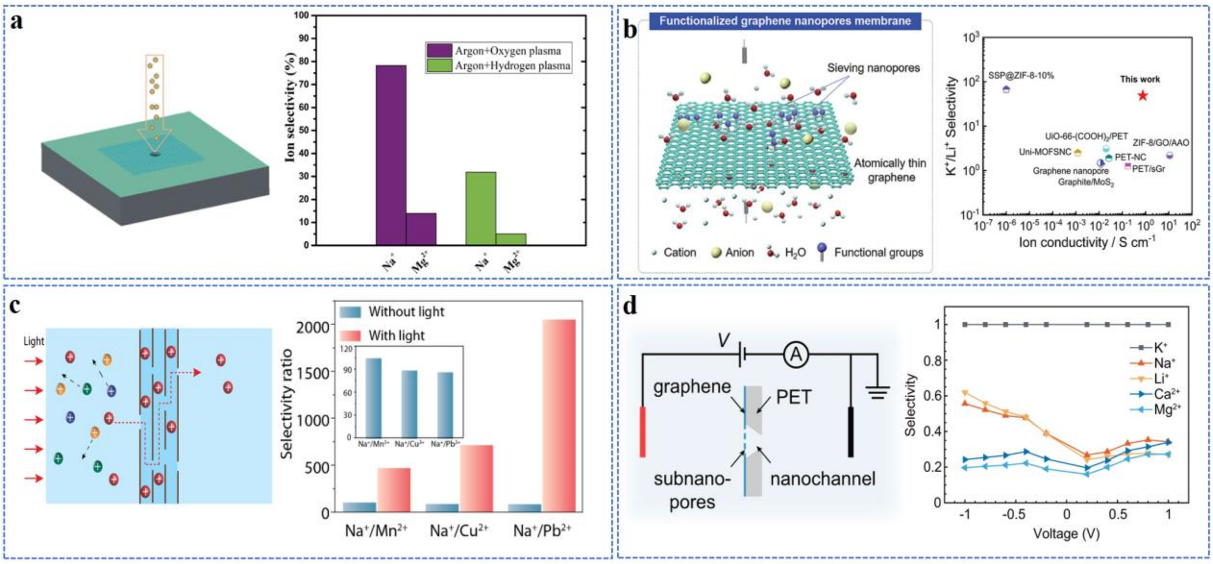

Figure 18. Modification and external field improve ion selectivity. a) OIE improves the selectivity of graphene nanopore. Reproduced with permission from ref 66, Copyright 2020 American Chemical Society. b) Modified functional groups improve the selectivity of graphene nanopores. Reproduced with permission from ref 78, Copyright 2024 John Wiley and Sons. c) Photothermal effect improves ion selectivity of MXene membrane. Reproduced with permission from ref 170, Copyright 2023 American Chemical Society. d) Multifunctional graphene heterogeneous nanochannel with voltage-tunable ion selectivity. Reproduced with permission under a Creative Commons CC BY License from ref 171, Copyright 2022 Springer

Nature.

2D material-based laminar membranes show the potential to replace commercial polymer membranes in traditional water purification and desalination applications, but it still needs to solve severe challenges. The research on the failure mechanism of membrane structure, improvement of its stability and durability, the adsorption and blockage of pollutants in complex water environment remains insufficient, along with the cost control and large-scale preparation, restricting its further development. In the future, only by breaking through the structural limitations of laboratory miniaturization can we truly replace traditional membranes and give full play to their advantages in industrial applications.

3.5 Osmotic energy generation

3.5.1 Principle of osmotic energy generation

Nowadays, replacing fossil energy with clean energy and reduce the emission of greenhouse gases and other pollutants such as carbon dioxide have become the common pursuit of all countries. Clean energy sources, such as light, wind and tidal energy, have been used to realize the effective conversion of electric energy. The ocean is a huge treasure house of energy. The clean energy obtained from the ocean is called "blue energy". Seawater contains a high concentration of salt and can be used to generate energy. Infiltration energy is considered as a sustainable and environment-friendly "blue" energy source, which comes from the salt gradient between fresh water and salt solutions. Pressure-retarded osmosis (PRO) and reverse electrodialysis (RED) are two very promising methods for harnessing osmotic energy. [172-174] In PRO, a salt-resistant porous semi-permeable membrane is placed between two solutions with a concentration gradient, which leads to the volume expansion of high-concentration solution caused by water permeating the membrane and the pressure accumulation, and part of the pressure is released by the outlet flow of the turbine power generation. The RED method makes the ion selective membrane placed between the high concentration solution and the low concentration solution. At osmotic pressure, due to the selectivity of the membrane, the ion diffusion rate of specific charges is very high, resulting in directional charge movement, thus producing osmotic current and voltage (Figure 19). Compared with the two methods, the RED method has attracted much attention because it can directly convert osmotic pressure energy into electric energy. Traditional ion exchange membranes are faced with the challenges of high membrane resistance, high cost and low output power density. The high cost lies not only in the cost of preparing the membrane, but also in the cost of water pretreatment. If the surface of the membrane is easy to accumulate pollutants and block, then the water needs to be purified in advance, and the energy consumed by purification may be higher than that brought by self-power.

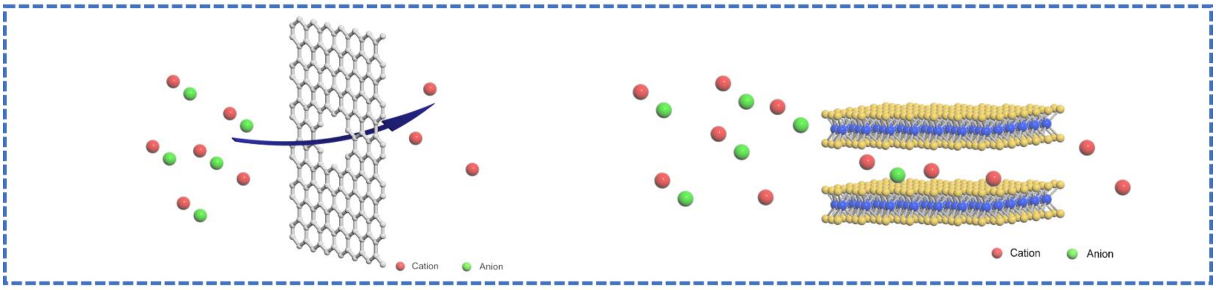

Figure 19. Schematic of 2D material-based nanofluidic devices for osmotic energy.

The osmotic voltage (V_{OS}), can be described as:[3, 175]

$$V_{OS} = (t_+ - t_-)\frac{RT}{F}\ln\left[\frac{\gamma_H C_H}{\gamma_L C_L}\right] \tag{6}$$

Here, t_+ and t_- are the transference number for cations and anions, which is defined as the fraction of the current carried either by the cation (t_+) or the anion (t_-) to the total ionic current. γ_H and γ_L correspond to the activity coefficient of ions. As can be seen from the formula, there are two key factors that affect the osmotic voltage. One is the selective permeability of anion and cation of the osmotic membrane, which is determined by the internal charge quantity and pore size of the membrane material. The second, the difference in solution concentration on both sides of the membrane is determined by the working environment. Therefore, in order to obtain higher power density, it is necessary to improve the membrane's selectivity for anions and cations.

We have reviewed the excellent performance of 2D material-based nanofluidic devices in the field of ion selectivity, which also means that they have certain advantages in the field of osmotic power generation, especially in the aspect of high energy density and external field adjustment to improve power generation efficiency.

3.5.2 High energy density in energy generation using 2D material-based nanofluidic devices

Feng et al. used MoS_2 nanopores with a single atomic layer thickness as permeable membranes (Figure 20a). There are osmotic currents and voltages in the *I-V* curve at 10^3 times the concentration gradient. It needs to be excluded because of the additional redox effect of the test electrode on the current. The greater the concentration gradient, the higher the osmotic current and voltage it produces, which means it has a higher power generation capacity. The pore size also affects the efficiency of power generation. Smaller pore sizes have higher anion and cation selectivity, which means higher osmotic voltage, but the osmotic current is suppressed because of the flux limitation. The larger pore sizes have weaker ion selectivity, but there is a higher osmotic current. Therefore, in order to achieve the best power generation, it is necessary to find a suitable size to balance the osmotic current and voltage. At a diameter of 10 nm, the power density is expected to reach 10^6 W m^{-2}.[41] The electricity power generated by the nanopore can be used to power MoS_2 transistors. h-BN nanopores have ultra-thin atomic thickness and high surface charge density, and because of their chemical stability, they can maintain good ion selectivity in high acid environment. At the ion gradient of 10^3, Chen et al. achieved a pure permeation-driven proton gradient power of 3 nW (Figure 20b).[30] The robustness of the h-BN membrane at extreme pH conditions allows the generation of ion gradient power from acid-base neutralization. With 1 M HCl / KOH, the power generated can be increased to the 4.5 nW level. Surface functionalization is an important way to improve the surface charge density, which can effectively improve the selective permeability of anions and cations. Wang et al. pre-anchored the nanopore through positively charged octa-ammonium-polyhedral-oligomeric-silsesquioxane (POSS) and electrostatic interaction with negatively charged 4-carboxybenzenediazonium tetrafluoroborate (4-CBD), attracting 4-CBD reactants and limiting modifications near the pore (Figure 20c).[176] This directional modification can break the shrinkage of random reaction sites, the refinement of effective functional groups and the inevitable defects in the traditional modification process, thus improving the modification efficiency. Compared with other graphene-based nano-porous graphene membranes, the oriented modified graphene membranes prepared by this method have excellent power density, can reach of 81.6 W m^{-2} with an energy conversion efficiency of 35.4% under a 100-fold salinity gradient. Bocquet et al. developed the fabrication of "activated" 2D carbon nanochannels (Figure 20d).[88] By SEM etching in water and oxygen environment, the channel surface is rich in negative electric groups, and high ion transport flux is generated due to its low friction. The power density of its single-pore channels can reach 100 kW m^{-2}, which is several orders of magnitude higher than that of h-BN nanotubes and other single-channel fluid devices, and comparable to atomically thin MoS_2 nanopores.

Although experiments have verified that nanopores or channels can generate extremely high-power density, the power generated by a single sample can only reach the nW level, which is not enough to drive a single electronic device, because of the low ion flux caused by its small aperture. The ion flux of 2D material membrane is higher, which means it can generate higher power generation. Ji et al. used the surface modification of GO nanosheets, to achieve surface charge adjusted from negative (−123 mC m^{-2}) to positive (+147 mC m^{-2}), resulting in a strong cation or anion-selective (Figure 20e).[100] The complementary dual-channel ion diffusion is achieved by combining two charge properties of the membrane. Driven by osmotic pressure, anion and cation produce two opposite transmission forces due to the selectivity of the membrane. This produces an effective charge separation process, leading to superimposed electrochemical potential differences and ion fluxes. At a concentration gradient of 50 times, the device has an output voltage of up to 160 mV and an output power of up to 0.77 W m^{-2}. The series of multiple membrane groups can reach an output voltage of more than 2 V, which can drive the normal operation of calculators, timers, clocks and light-emitting diodes.

Single-layer COFs with ordered pore arrangement can achieve extremely low membrane resistivity and high ionic conductivity. Yang et al. used a single-layer zinc tetraphenyl porphyrin-based COF (MTPP-COF) to achieve a power output of 135.8 Wm^{-2} under a 50-fold NaCl concentration gradient, and produced more than 200 Wm^{-2} in simulated seawater and river water gradient.[53] Even centimeter-sized samples can reach 14.6 Wm^{-2} and show good operational stability under continuous flow conditions.

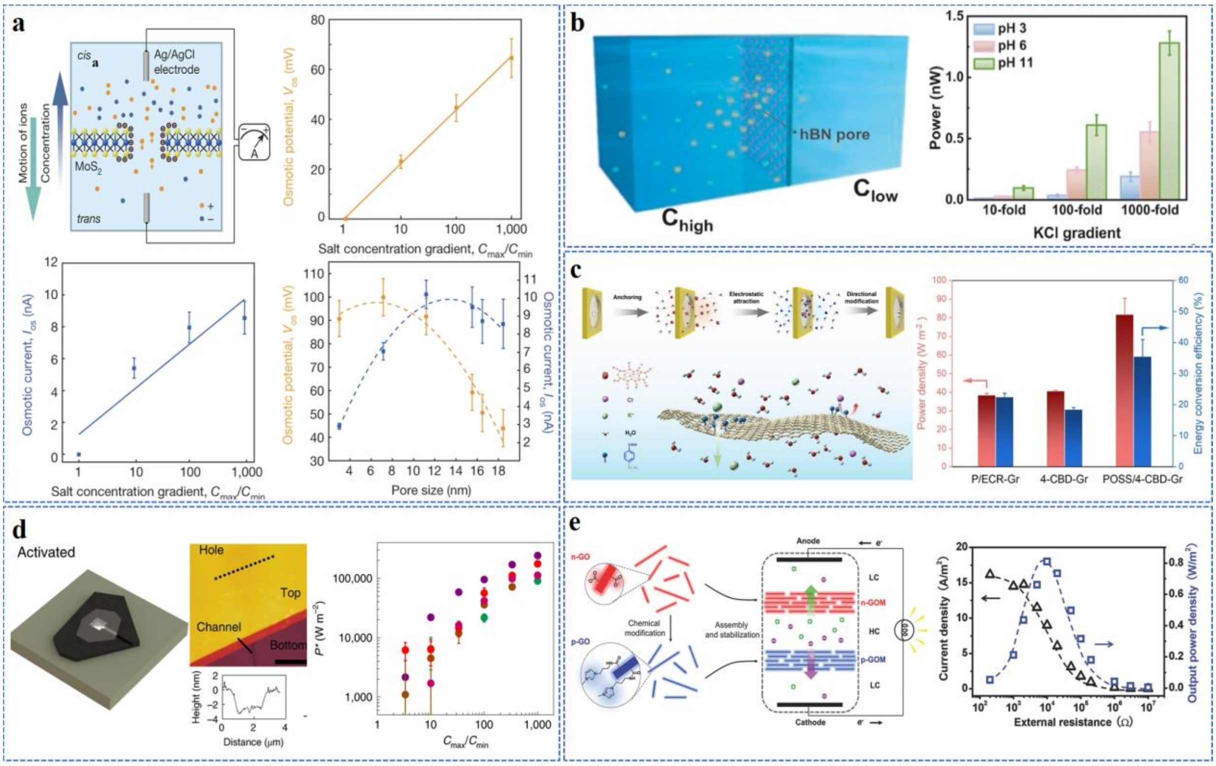

Figure 20. a) Single layer MoS_2 nanopores as nano-power generators. Reproduced with permission from ref 41, Copyright 2016 Springer Nature. b) Single layer h-BN nanopores as high-performance ionic gradient power generators. Reproduced with permission from ref 30, Copyright 2023 John Wiley and Sons. c) Pre-anchoring for high-performance osmotic energy generation on graphene nanopore. Reproduced with permission from ref 176, Copyright 2023 American Chemical Society. d) Enhanced osmotic energy generation in activated carbon nanochannel. Reproduced with permission from ref 88, Copyright 2022 Springer Nature. e) Osmotic power generation with positively and negatively charged GOM pairs. Reproduced with permission from ref 100, Copyright 2016 John Wiley and Sons.

3.5.3 Photo—thermo-electric effects for generating electricity and improving efficiency

In addition to surface modifications to improve charge density, the rich photoelectric properties of 2D materials mean that their surface charge density can be regulated optically to achieve higher power density. MoS_2 is a good photoelectric material. The surface charge of MoS_2 can be increased by laser irradiation to adjust the ion selectivity of MoS_2 nanopores through photoelectric effect (Figure 21a).[68] And, the increase of the surface charge of the membrane enhances the surface conductance, resulting in a larger osmotic current. The combination of the two increases the osmotic power generated. At neutral pH, the method can double the osmotic power generated by a single nanopore. In addition to photoelectric properties, photothermal properties can also be used to achieve the conversion of osmotic energy. Luo et al. placed a thin membrane of MXene on an ionic solution and exposed part of the membrane to light (Figure 21b).[177] MXene unique photothermal properties convert asymmetric light irradiation into a water evaporation gradient that moves water through nanofluid channels in the membrane, thereby transferring cations and generating ionic currents. At similar optical power densities, nanofluid photocurrents are an order of magnitude higher than those of other 2D materials. Based on their photoelectric response, van der Waals heterojunctions can be used to construct various functional optoelectronic devices, such as solar cells, photodetectors, etc. Feng et al reported photoinduced ion pumping based on graphene-MoS_2 nanopores (Figure 21c).[34] The device uses the photogenerated voltage of the p-n junction to drive the active transport of ions through the 2D van der Waals heterojunction nanopore. When illuminated by a light source with a wavelength of 365 nm, the heterojunction region of the nanopore wall generates a photovoltage of about 80 mV, driving ions through the pore. The induced current through a single nanopore reaches tens of pA. Under no light condition, the open circuit voltage and short circuit current of the ion circuit is 0. Under 365 nm wavelength illumination, the short circuit current is about -8 pA and the open circuit voltage is about 70 μV, which proves the ability of light-energy conversion.

Although 2D material-based nanofluidic devices have shown excellent performance and great potential in the field of blue energy, their application prospects are still controversial, facing the same problems as ion-selective membranes, especially the benefit between power generation efficiency and energy consumption of water pretreatment. The large area preparation and good stability of 2D crystal materials such as COFs help bridge the gap between laboratory-scale demonstrations and industrial-scale devices, which is difficult to achieve in other 2D fluid devices at this stage. We believe that this research field will be further developed in improving power density and solving pretreatment problems, and the ultimate goal is to establish a truly efficient new technology to obtain blue energy.

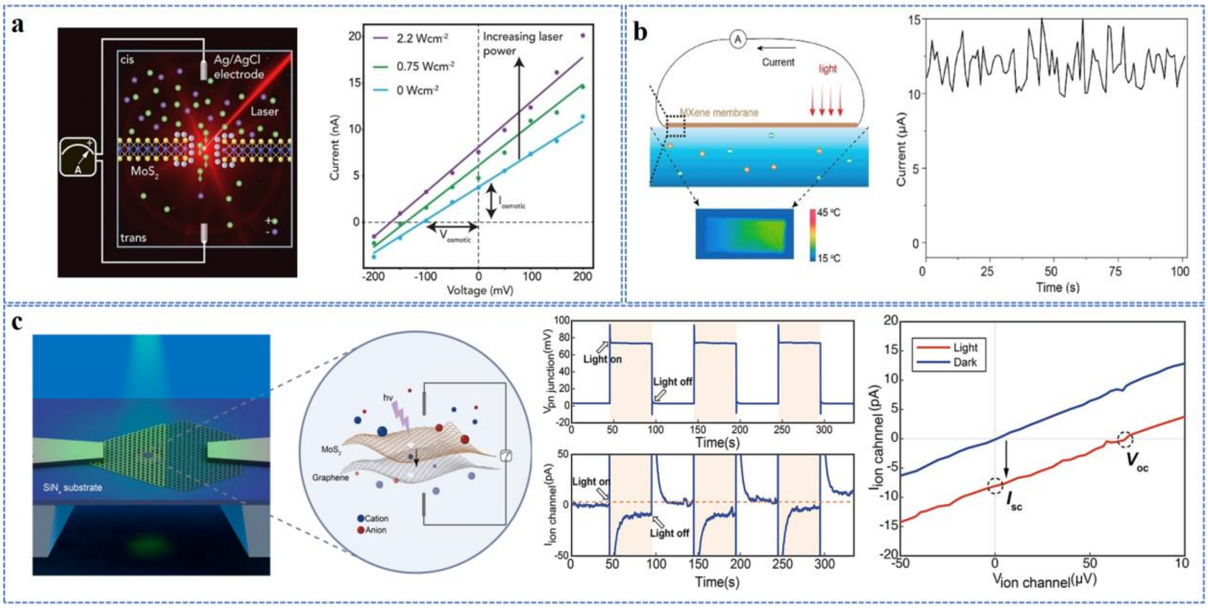

Figure 21. a) Photoelectric response improves the power generation of MoS_2 nanopore. Reproduced with permission from ref 68, Copyright 2013 Elsevier. b) The photothermal response achieve self-electricity of the MXene membrane. Reproduced with permission from ref 177, Copyright 2020 Elsevier. c) Photoinduced ion pumping by graphene-MoS_2 heterojunction nanopores. Reproduced with permission from ref 34, Copyright 2023 American Chemical Society.

3.6 Gas separation and carbon capture

Gas separation and purification are crucial industrial processes that also plays a key role in environmental protection and the development of renewable energy sources, such as carbon capture and hydrogen purification. Traditional gas separation processes, such as low temperature distillation, chemisorption, etc., are energy-cost. In contrast, membrane filtration for gas separation only requires pressure control or spontaneous gas diffusion, with small energy consumption. 2D materials-based nanofluidic devices also offer an energy effective approach for gas permeation, separation and carbon capture. The atomic thickness of the 2D material means higher permeability compared to conventional three-dimensional membranes. At the same time, the angstrom scale of 2D material preparation poses a transport barrier for molecules with a certain kinetic diameter, which will lead to huge selectivity.

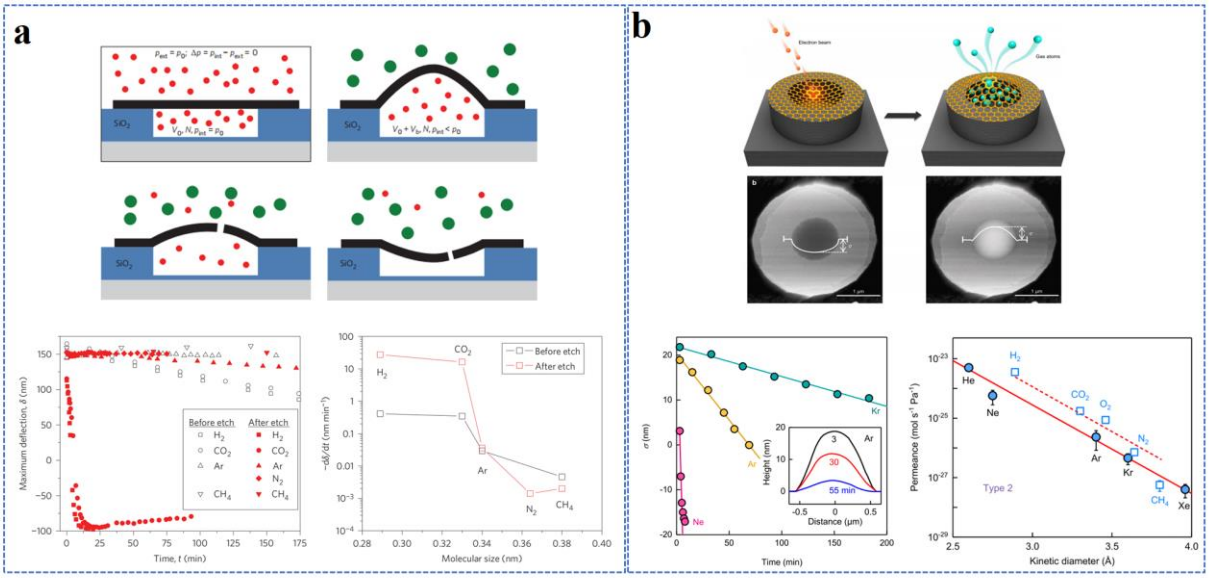

Figure 22. a) Selective molecular sieving through porous graphene. Reproduced with permission from ref 178, Copyright 2012 Springer Nature. b) Exponentially selective molecular sieving through angstrom pores. Reproduced with permission under a Creative Commons CC BY License from ref 179, Copyright 2021 Springer Nature.

Steven et al. were the first to demonstrate the selective penetration of gases by graphene nanopores (Figure 22a).[178] They devised an ingenious experiment in which the graphene membrane expands and deforms by controlling the internal and external pressure by encapsulating the gas in a non-porous graphene microchamber. Subsequently, ultraviolet induced oxidation etching is used to create pores in the graphene membrane, and micro-indoor gas permeates to the outside world. On the deformation of the graphene membrane, the permeability rate of the gas can be reflected by the morphology of the graphene membrane tested by AFM. The results show that there is an obvious positive correlation between gas permeation rate and molecular dynamics size, and molecules larger than pore diameter cannot permeate. Sun et al. further used this method to study the gas transport of a single graphene pore with an effective diameter estimated to be around ~ 2 Å (Figure 22b).[179] He and H_2 easily permeate through these pores, while larger gases such as Xe and CH_4 are blocked. The gas permeation rate is exponentially related to the kinetic diameter of the gas molecules. Therefore, strong permeability selectivity to gas molecules of different scales can be achieved. It is suggested that this exponential correlation may come from the adsorption and diffusion of gas molecules in the pore.

For 2D material pores with larger pore sizes, although they do not reach the pore size limit of gas molecular scale, they can also realize the high selectivity. Kemal et al. created nanopore arrays on a bilayer graphene with pore sizes ranging from 7.6 nm to micrometers, and explained the gas penetration and separation through the collision of gas molecules within the nanopores.[180] The flux of N_2 depends on the nanopore diameter (Figure 23a, left). For diameter between 7.6 to 50 nm, the mean free path of the N_2 molecules is longer than the pore diameter. The minimal collisions near the pore leads to a free-flow state, which maintain the gas diffusion at a minimum. As the pore size increases, more molecules interact near the pore, and the collisions between them lead to collective molecular flow. The authors reported that the gas permeability is inversely proportional to the molecular weight squared (MW^{-2}). This means that nanopores can separate gases based on their molecular weights. For gases mixture, intermolecular collisions during transport through the pore can transfer momentum from the lighter to the heavier molecules, leading to a collective flow, thereby reducing separation. Smaller nanopore apertures reduce the probability of collisions, which enhance the separation of different gas molecules. A pore diameter of 7.6 nm performs the best separation that is close to the theoretical maximum value of 4.69 predicted by H_2/CO_2 separation theory (Figure 23a, right). As the diameter increases, the separation efficiency decreases sharply until it is close to no separation.

Based on these principles and findings, researchers focus on porous membranes with a smaller aperture range to achieve higher gas permeability and separation efficiency. Although sub-nanoscale pores, comparable in size togas molecules, can generate permeability difference similar to the ion transport, their scale limitation also causes a gas permeability limitation.[179, 181] Separating gas solely by pore size control requires balancing between permeability and selectivity to optimize separation effect. Karl et al. expanded the nanopore from sub-nano to 5 nm by introducing atomic defects and selectively etching graphene edge atoms.[182] The resulting membranes exhibited unprecedented hydrogen permeability of up to 10^7 gas permeation units, which is three orders of magnitude higher than the state-of-the-art membranes and is comparable to H_2/CH_4 selectivity. Liu et al. used a decoupling strategy of defect expansion by helium ion irradiation and hydrogen plasma treatment to precisely generate nanopore with the desired diameter and density in bilayer graphene membranes (Figure 23b).[182] He ion irradiation can effectively generates carbon vacancies under controlled conditions, which are then enlarged through plasma treatment. The resulting membrane selectivity of H_2/N_2 and H_2/CH_4 can reach 495 and 877.

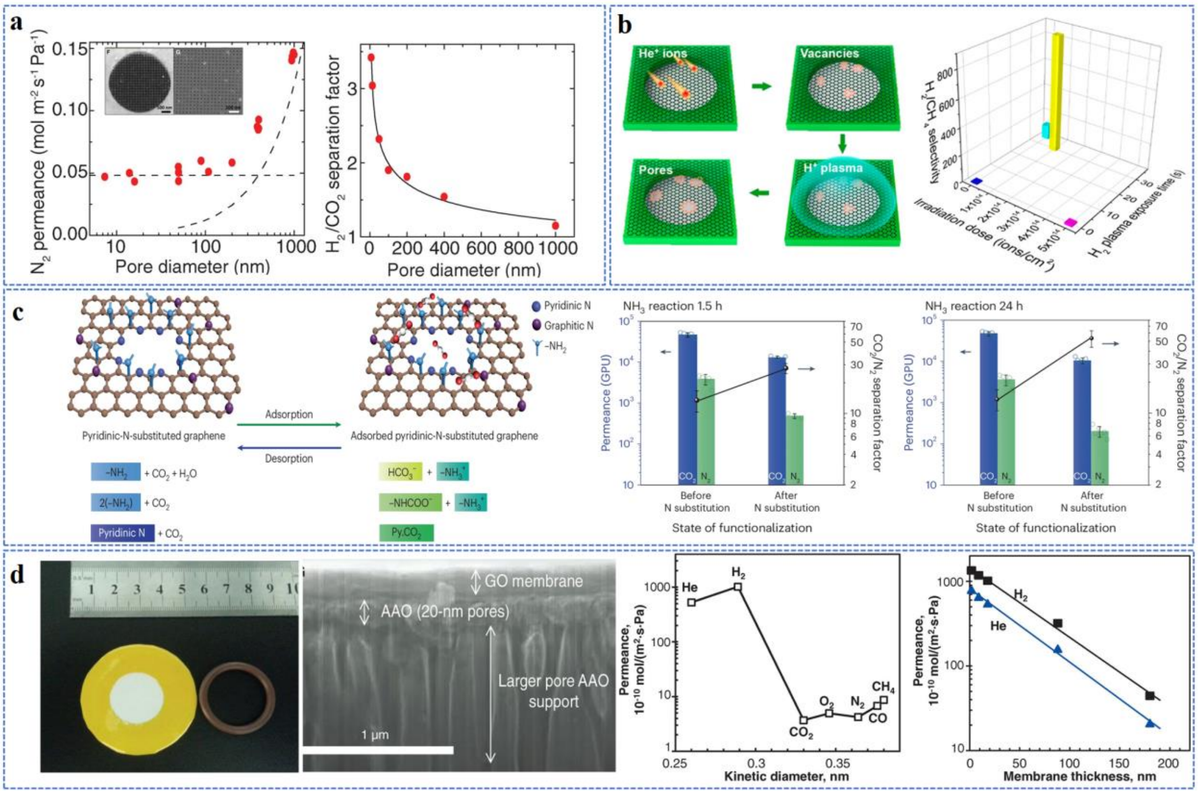

Figure 23. a) Ultimate permeation across atomically thin porous graphene. Reproduced with permission from ref 180, Copyright 2014 The American Association for the Advancement of Science. b) Selective gas permeation in defect-engineered bilayer graphene. Reproduced with permission from ref 183, Copyright 2021 American Chemical Society. c) Graphene membranes with pyridinic nitrogen at pore edges for high-performance CO_2 capture. Reproduced with permission from ref 184, Copyright 2024 Springer Nature. d) Molecular-sieving GOM for selective hydrogen separation. Reproduced with permission from ref 185, Copyright 2023 The American Association for the Advancement of Science.

Modification and doping of pore surface are other important approaches to improve gas permeability and selectivity. Introducing groups with strong adsorption for the target gas molecules can significantly improve the performance. Hsu et al. introduced pyridinic-N into the edge of graphene pores using O_3 oxidation and NH_3 treatment. [184] Pyridinic-N groups selectively and strongly bind CO_2 from gas mixtures (Figure 23c), increasing the residence time of CO_2 at the pore. The CO_2/N_2 separation factor of untreated graphene membrane was 13.7. This value increased to 30 and 53.3, after NH_3 exposure for 1.5 h and 24 h, respectively.

While nanochannels provide comparable scale, their long transport path limits the permeation flux, therefore cannot reach to the efficiency comparable to porous membranes. Laminar membranes, offering the spatial constrains, high channel density and large membrane area, show excellent characteristics in gas penetration. Li et al. prepared GOM on AAO films with thickness ranging from 1.8 to 180 nm, whose centimeter scale ensures a large gas flux (Figure 23d).[185] An 18-nm membrane achieved H_2 permeability 300 times higher than that of CO_2, indicating an average pore size of 0.289~0.33 nm in the membrane, allowing passing H_2 (0.298 nm) while shielding CO_2 (0.33 nm). Permeability of H_2 and He decreased exponentially with the thickness of the membrane, suggesting that structural defects rather than the interlayer spacing are the main transport pathway of molecules. For GOM, MXene membrane or Graphene/h-BN composite membrane, the nanosheet spacing of 0.35-0.4 nm enables H_2 transport while restricting larger gas molecules, demonstrating their high application value in H_2 separation.[186-188]

4. CHALLENGES AND PROSPECTS

In this paper, we review the structure, preparation and application of 2D material-based nanofluidic devices, which show high research and application value. Although 2D material-based nanofluidic devices have made great progress, their opportunities and challenges coexist.

i) The scalability of preparation. The large-scale preparation of 2D material-based nanofluidic devices is crucial for their commercialization. The main challenge lies in the large area or mass production, which requires improving production efficiency and reducing costs. Mechanical exfoliation is unsuitable for large-scale preparation 2D materials due to its low efficiency and the time-consuming, labor-intensive sample screening process. While CVD creates larger sample size, its scalability is limited by the complicated transfer process. Thakur et al. demonstrated the CVD growth of a continuous MoS_2 membrane on a 7.62 cm sapphire substrate, followed by PDMS transfer at the wafer scale. [189] This technique allows simultaneously preparation of 128 devices that can cover a through-microhole with non-leakage rate above 70%, demonstrating the potential for batch preparation and commercialization. Although CVD-grow samples enable large-scale transfer, their applications are limited due to the higher defect density, lower lattice quality and stability compare to mechanically exfoliated. Nanochannel preparation requires specialized equipment, experience, and complex transfer processes, leading to a low success rate and limiting large-scale preparation. In contrast, laminar membrane preparation is relatively simple and requires no complex equipment, making it feasible for large-area preparation. Spray and spin coating methods are suitable for large area preparation, but they might lack of uniformity. Tape casting method offers both uniformity and large-area membranes, making it high commercial value for membrane separation field.

Another challenge for scalability is standardization. Processing nanopores or channels with specific structures demands strict control of conditions such as temperature, humidity, power, ion beam focusing degree and vacuum levels during the drilling processing. These factors affect aperture size, porous densities and the resulting application performance. Even in professional laboratories, it remains very difficult to maintain consistent processing quality.

ii) In-depth exploration of mechanisms. 2D material-based nanofluidic devices compress space to the limit scale, breaking the research scope of classical physics. In some cases, the fluid is no longer regarded as a continuous existence, but as discrete molecular individuals. The influence of the individual's nature on the whole can not be neglected. The use of nanofluidic devices, such as nanopores, can be used as observation devices for ions and molecules. For example, the changes of ion hydration structure can be reflected in the nonlinearity of the ion current signal. It can also be used to deeply explore the structural changes in confined space and the difference between spatial distribution and physical appearance. The influence of the surface of 2D materials on fluid still attracting a lot of attention, and new 2D materials are constantly emerging. The 2D materials with flatness or anisotropic periodic surface structure are used to construct nanofluidic devices. New structures, such as angular graphene grids with Moiré periodic potential fields, their lattice structure and electron distribution, which will influence fluid transport, are still being explored in depth. Some new transport mechanisms or spatial conformations described in this paper may be just the tip of the iceberg. New device structures and new material combinations may bring about new transmission phenomena that are difficult to understand with traditional and existing mechanisms. Only by relying on profound theoretical foundation can we develop a new theoretical model to guide the progress of practice. They are complementary. Nowadays, more and more scholars are beginning to pay attention to the physical mechanisms of 2D material-based nanofluidic devices. We believe that in the future, new physical phenomena and mechanisms will emerge continuously, whether from experimental or simulation research, providing guidance for its application prospects.

iii) The prospects and difficulties of sequencing. DNA sequencing using 2D material-based nanopores or channels is considered to be the most promising method to replace biological pores. Its advantage lies in the stability of the environment and the integration of the equipment, and can realize the complementary detection of ion current and transverse current. But the transmission speed of DNA is fast, which reduces the time resolution of nanopores. Using ionic liquid or heterojunction to slow down the transmission speed of DNA has certain effect, but it still has not achieved the ideal recognition effect. We believe that in addition to the above schemes, the transfer speed can be slowed down by modifying the surface of the channel and adding chemical groups with certain adsorption or viscosity to the substrate. Front-end treatment may be feasible by using the friction effects before entering the channel. In addition, the noise level must be suppressed. The electromagnetic noise in the external environment can be shielded by a faraday cage, but the capacitive noise of the device, the vibration of the membrane and even the blocking of DNA during transmission will interfere with the acquisition of effective signals. Therefore, it is necessary to strengthen the stability of the structure and choose insulating materials with low dielectric constant to package the device. Single molecule detection technology combined with artificial intelligence algorithms can analyze the collected signal, which has certain advantages in improving the accuracy of signal recognition and eliminating noise interference. In addition to electrical sensing methods, 2D material-based nanopore and channel technology is expected to be combined with advanced optical single molecule detection technologies, such as interference scattering microscope (iSCAT), optical nano tweezers, etc., which can directly observe the molecular structure and motion state from more dimensions without labeling, and can realize synchronous feedback of electro-optic signals.

In the future, the detection process of single molecules or DNA must be the integration of analyte purification, detection, signal processing and analysis, in order to truly realize the function of the lab on a chip. Nanofluidic devices made of 2D materials will play an irreplaceable role.

iv) Application and development of ionic electronic devices. 2D material-based iontronics devices have better characteristics than the traditional material devices, showing broad application prospect. But generally speaking, ion electrical equipment is still in the primary stage of development. One is the application scope is limited. Compared with electronic devices, which have been inseparable from people's lives, iontronics devices have only attracted the attention of a few researchers, and the emphasis is different. On the other hand, because the transmission speed of ions is slower than that of electrons, the response time of ion transistors is undoubtedly longer than that of electron transistors, which is unfavorable for the control of electrical appliances. From its own performance, 2D material-based nanofluidic devices still need to explore new mechanisms and structures, such as heterostructures, asymmetric devices, asymmetric transmission interfaces, etc. To improve the performance of ion electrical devices, so as to promote faster practical application.

v) Industrial application limitation. Although the 2D material-based nanofluidic devices have achieved high ion/gas separation and power generation efficiency in laboratory demonstration, several challenges remain to be addressed before their industrial application. One key issue is the flux. The efficiency of a single pore does not reflect the overall device performance. To replace traditional membrane materials with 2D materials and unlock their commercial value, large-scale production and improved permeation flux are required beyond laboratory-scale setups. Additionally, the blockage and pollution of impurity are other challenges. While the ultra-small size of nanofluidic devices help avoid pollutants in the laboratory environment, pollution is inevitable in real-word applications. Potential solutions include front-end treatment to removes pollutants through layer-by-layer filtration, and surface coating to reduce the adsorption of pollutants on the pores. These approaches, however, inevitably affect the original surface properties of 2D materials. Future research will focus on mitigating clogging and pollutant adsorption in 2D material-based nanofluidic devices.

AUTHOR INFORMATION

Corresponding Authors

Zhibo Liu - *The Key Laboratory of Weak Light Nonlinear Photonics, Ministry of Education, School of Physics and Teda Applied Physics Institute, Renewable Energy Conversion and Storage Center, State Key Laboratory of Photovoltaic Materials and Cells, Nankai University, Tianjin 300071, China. The collaborative Innovation Center of Extreme Optics, Shanxi University, Taiyuan, Shanxi 030006, China.*

E-mail: liuzb@nankai.edu.cn

Jianguo Tian - *The Key Laboratory of Weak Light Nonlinear Photonics, Ministry of Education, School of Physics and Teda Applied Physics Institute, Renewable Energy Conversion and Storage Center, State Key Laboratory of Photovoltaic Materials and Cells, Nankai University, Tianjin 300071, China.*

E-mail: jjtian@nankai.edu.cn

Cuifeng Ying - *Advanced Optics & Photonics Laboratory, Department of Engineering, School of Science & Technology, Nottingham Trent University, Nottingham NG11 8NS, UK.*

E-mail: cuifeng.ying@ntu.ac.uk

Authors

Yangjun Cui - *The Key Laboratory of Weak Light Nonlinear Photonics, Ministry of Education, School of Physics and Teda Applied Physics Institute, Renewable Energy Conversion and Storage Center, Nankai University, Tianjin 300071, China.*

Long Gao - *The Key Laboratory of Weak Light Nonlinear Photonics, Ministry of Education, School of Physics and Teda Applied Physics Institute, Renewable Energy Conversion and Storage Center, Nankai University, Tianjin 300071, China.*

NOTES

The authors declare no competing financial interest.

ACKNOWLEDGMENTS

This work was supported by the National Natural Science Foundation of China (Grant 12174207). C.Y. acknowledges the funding by UK-India Education and Research Initiative (UKIERI).

VOCABULARY

Nanofluidics: Nanofluidics is the study of the behavior, manipulation, and control of fluids that are confined to structures of nanometer (typically 1-100 nm) characteristic dimensions.

2D material-based nanofluidic devices: Fluid devices constructed on the basis of two-dimensional materials are transmitted at the spatial scale of nanometer or sub-nanometer.

Iontronics devices: Electrical devices that rely on ions as carriers to transmit signals.

Heterojunction: The interface region formed by the contact of two different semiconductors.

Ion/gas selectivity: Differences in the permeability of fluid devices to different ions and gas.

REFERENCES

(1) Xu, Y., Nanofluidics: A New Arena for Materials Science. *Adv. Mater.* **2018,** *30* (3), e1702419.

(2) Aluru, N. R.; Aydin, F.; Bazant, M. Z.; Blankschtein, D.; Brozena, A. H.; de Souza, J. P.; Elimelech, M.; Faucher, S.; Fourkas, J. T.; Koman, V. B.; Kuehne, M.; Kulik, H. J.; Li, H. K.; Li, Y.; Li, Z.; Majumdar, A.; Martis, J.; Misra, R. P.; Noy, A.; Pham, T. A.; Qu, H.; Rayabharam, A.; Reed, M. A.; Ritt, C. L.; Schwegler, E.; Siwy, Z.; Strano, M. S.; Wang, Y.; Yao, Y. C.; Zhan, C.; Zhang, Z., Fluids and Electrolytes under Confinement in Single-Digit Nanopores. *Chem. Rev.* **2023,** *123* (6), 2737-2831.

(3) You, Y.; Ismail, A.; Nam, G.-H.; Goutham, S.; Keerthi, A.; Radha, B., Angstrofluidics: Walking to the Limit. *Annu. Rev. Mater. Res.* **2022,** *52* (1), 189-218.

(4) Stephenson, A.; Nivala, J., Barcoding biomarkers with nanopore sequencing. *Nat. Nanotechnol.* **2023,** *18* (12), 1385–1386.

(5) Ying, Y.-L.; Hu, Z.-L.; Zhang, S.; Qing, Y.; Fragasso, A.; Maglia, G.; Meller, A.; Bayley, H.; Dekker, C.; Long, Y.-T., Nanopore-based technologies beyond DNA sequencing. *Nat. Nanotechnol.* **2022,** *17* (11), 1136-1146.

(6) Bocquet, L., Nanofluidics coming of age. *Nat. Mater.* **2020,** *19* (3), 254-256.

(7) Reccius, C. H.; Stavis, S. M.; Mannion, J. T.; Walker, L. P.; Craighead, H. G., Conformation, length, and speed measurements of electrodynamically stretched DNA in nanochannels. *Biophys J.* **2008,** *95* (1), 273-286.

(8) Castillo-Fernandez, O.; Salieb-Beugelaar, G. B.; van Nieuwkasteele, J. W.; Bomer, J. G.; Arundell, M.; Samitier, J.; van den Berg, A.; Eijkel, J. C., Electrokinetic DNA transport in 20

nm-high nanoslits: evidence for movement through a wall-adsorbed. *Electrophoresis* **2011,** *32* (18), 2402-2409.
(9) Kovarik, M. L.; Jacobson, S. C., Attoliter-scale dispensing in nanofluidic channels. *Anal. Chem.* **2007,** *79* (4), 1655-1660.
(10) Awasthi, S.; Ying, C.; Li, J.; Mayer, M., Simultaneous Determination of the Size and Shape of Single alpha-Synuclein Oligomers in Solution. *ACS Nano* **2023,** *17* (13), 12325-12335.
(11) Song, Y.; Zhou, T.; Liu, Q.; Liu, Z.; Li, D., Nanoparticle and microorganism detection with a side-micron-orifice-based resistive pulse sensor. *Analyst* **2020,** *145* (16), 5466-5474.
(12) van Kan, J. A.; Zhang, C.; Perumal Malar, P.; van der Maarel, J. R. C., High throughput fabrication of disposable nanofluidic lab-on-chip devices for single molecule studies. *Biomicrofluidics* **2012,** *6* (3), 036502.
(13) Sen, Y. H.; Jain, T.; Aguilar, C. A.; Karnik, R., Enhanced discrimination of DNA molecules in nanofluidic channels through multiple measurements. *Lab. Chip.* **2012,** *12* (6), 1094-1101.
(14) Liu, Y.; Yobas, L., Slowing DNA Translocation in a Nanofluidic Field-Effect Transistor. *ACS Nano* **2016,** *10* (4), 3985-3994.
(15) Leitao, S. M.; Navikas, V.; Miljkovic, H.; Drake, B.; Marion, S.; Blanchet, G. P.; Chen, K.; Mayer, S. F.; Keyser, U. F.; Kuhn, A.; Fantner, G. E.; Radenovic, A., Spatially multiplexed single-molecule translocations through a nanopore at controlled speeds. *Nat. Nanotechnol.* **2023,** *18* (9), 1078-1084.
(16) Bošković, F.; Keyser, U. F., Nanopore microscope identifies RNA isoforms with structural colours. *Nat. Chem.* **2022,** *14* (11), 1258-1264.
(17) Macha, M.; Marion, S.; Nandigana, V. V. R.; Radenovic, A., 2D materials as an emerging platform for nanopore-based power generation. *Nat. Rev. Mater.* **2019,** *4* (9), 588-605.
(18) Kang, Y.; Xia, Y.; Wang, H.; Zhang, X., 2D Laminar Membranes for Selective Water and Ion Transport. *Adv. Funct. Mater.* **2019,** *29* (29), 1902014.
(19) Xu, J.; Jiang, X.; Yang, N., Carbon nanopores for DNA sequencing: a review on nanopore materials. *Chem. Commun.* **2023,** *59* (33), 4838-4851.
(20) Arjmandi-Tash, H.; Belyaeva, L. A.; Schneider, G. F., Single molecule detection with graphene and other two-dimensional materials: nanopores and beyond. *Chem. Soc. Rev.* **2016,**

45 (3), 476-493.
(21) Lu, J.; Jiang, Y.; Yu, P.; Jiang, W.; Mao, L., Light-Controlled Ionic/Molecular Transport through Solid-State Nanopores and Nanochannels. *Chem. – Asian J.* **2022,** *17* (10), e202200158
(22) Xiao, K.; Schmidt, O. G., Light-Driven Ion Transport in Nanofluidic Devices: Photochemical, Photoelectric, and Photothermal Effects. *CCS Chem.* **2022,** *4* (1), 54-65.
(23) Pakulski, D.; Czepa, W.; Buffa, S. D.; Ciesielski, A.; Samorì, P., Atom-Thick Membranes for Water Purification and Blue Energy Harvesting. *Adv. Funct. Mater.* **2019,** *30* (2), 1902394.
(24) Yu, X.; Ren, W., Ion and Water Transport in 2D Nanofluidic Channels. *Adv. Funct. Mater.* **2024**, *34* (30), 2313968.
(25) Mogg, L.; Zhang, S.; Hao, G. P.; Gopinadhan, K.; Barry, D.; Liu, B. L.; Cheng, H. M.; Geim, A. K.; Lozada-Hidalgo, M., Perfect proton selectivity in ion transport through two-dimensional crystals. *Nat. Commun.* **2019,** *10* (1), 4243.
(26) Wang, S.; Li, H.; Sawada, H.; Allen, C. S.; Kirkland, A. I.; Grossman, J. C.; Warner, J. H., Atomic structure and formation mechanism of sub-nanometer pores in 2D monolayer MoS_2. *Nanoscale* **2017,** *9* (19), 6417-6426.
(27) Govind Rajan, A.; Silmore, K. S.; Swett, J.; Robertson, A. W.; Warner, J. H.; Blankschtein, D.; Strano, M. S., Addressing the isomer cataloguing problem for nanopores in two-dimensional materials. *Nat. Mater.* **2019,** *18* (2), 129-135.
(28) Thakur, M.; Cai, N.; Zhang, M.; Teng, Y.; Chernev, A.; Tripathi, M.; Zhao, Y.; Macha, M.; Elharouni, F.; Lihter, M.; Wen, L.; Kis, A.; Radenovic, A., High durability and stability of 2D nanofluidic devices for long-term single-molecule sensing. *npj 2D Mater. Appl.* **2023,** *7* (1), 11.
(29) Rollings, R. C.; Kuan, A. T.; Golovchenko, J. A., Ion selectivity of graphene nanopores. *Nat. Commun.* **2016,** *7*, 11408.
(30) Liu, T. R.; Fung, M. Y. T.; Yeh, L. H.; Chiang, C. H.; Yang, J. S.; Kuo, P. C.; Shiue, J.; Chen, C. C.; Chen, C. W., Single-Layer Hexagonal Boron Nitride Nanopores as High-Performance Ionic Gradient Power Generators. *Small* **2023,** *20* (16), 2306018.
(31) Liu, K.; Lihter, M.; Sarathy, A.; Caneva, S.; Qiu, H.; Deiana, D.; Tileli, V.; Alexander, D. T. L.; Hofmann, S.; Dumcenco, D.; Kis, A.; Leburton, J.-P.; Radenovic, A., Geometrical

Effect in 2D Nanopores. *Nano Lett.* **2017,** *17* (7), 4223-4230.
(32) Mojtabavi, M.; VahidMohammadi, A.; Liang, W.; Beidaghi, M.; Wanunu, M., Single-Molecule Sensing Using Nanopores in Two-Dimensional Transition Metal Carbide (MXene) Membranes. *ACS Nano* **2019,** *13* (3), 3042-3053.
(33) Mojtabavi, M.; Tsai, W. Y.; VahidMohammadi, A.; Zhang, T.; Gogotsi, Y.; Balke, N.; Wanunu, M., Ionically Active MXene Nanopore Actuators. *Small* **2022,** *18* (11), e2105857.
(34) Niu, M.; Chen, Y.; Chen, F.; Zhao, C.; Yang, Y.; Xu, Y.; Feng, J., Light-Driven Ion Transport through Single-Heterojunction Nanopores. *Nano Lett.* **2023,** *23* (3), 1010-1016.
(35) Liu, K.; Feng, J.; Kis, A.; Radenovic, A., Atomically thin molybdenum disulfide nanopores with high sensitivity for DNA translocation. *ACS Nano* **2014,** *8* (3), 2504-2511.
(36) Danda, G.; Masih Das, P.; Chou, Y.-C.; Mlack, J. T.; Parkin, W. M.; Naylor, C. H.; Fujisawa, K.; Zhang, T.; Fulton, L. B.; Terrones, M.; Johnson, A. T. C.; Drndić, M., Monolayer WS_2 Nanopores for DNA Translocation with Light-Adjustable Sizes. *ACS Nano* **2017,** *11* (2), 1937-1945.
(37) Schneider, G. F.; Xu, Q.; Hage, S.; Luik, S.; Spoor, J. N.; Malladi, S.; Zandbergen, H.; Dekker, C., Tailoring the hydrophobicity of graphene for its use as nanopores for DNA translocation. *Nat. Commun.* **2013,** *4*, 2619.
(38) Deng, Y.; Huang, Q.; Zhao, Y.; Zhou, D.; Ying, C.; Wang, D., Precise fabrication of a 5 nm graphene nanopore with a helium ion microscope for biomolecule detection. *Nanotechnology* **2017,** *28* (4), 045302.
(39) Schneider, G. F.; Kowalczyk, S. W.; Calado, V. E.; Pandraud, G.; Zandbergen, H. W.; Vandersypen, L. M.; Dekker, C., DNA translocation through graphene nanopores. *Nano Lett.* **2010,** *10* (8), 3163-3167.
(40) Feng, J. D.; Liu, K.; Graf, M.; Dumcenco, D.; Kis, A.; Di Ventra, M.; Radenovic, A., Observation of ionic Coulomb blockade in nanopores. *Nat. Mater.* **2016,** *15* (8), 850-855.
(41) Feng, J.; Graf, M.; Liu, K.; Ovchinnikov, D.; Dumcenco, D.; Heiranian, M.; Nandigana, V.; Aluru, N. R.; Kis, A.; Radenovic, A., Single-layer MoS_2 nanopores as nanopower generators. *Nature* **2016,** *536* (7615), 197-200.
(42) Luan, B.; Zhou, R., Spontaneous Transport of Single-Stranded DNA through Graphene-

MoS_2 Heterostructure Nanopores. *ACS Nano* **2018,** *12* (4), 3886-3891.

(43) Sen, P.; Gupta, M., Single nucleotide detection using bilayer MoS_2 nanopores with high efficiency. *RSC Adv.* **2021,** *11* (11), 6114-6123.

(44) Traversi, F.; Raillon, C.; Benameur, S. M.; Liu, K.; Khlybov, S.; Tosun, M.; Krasnozhon, D.; Kis, A.; Radenovic, A., Detecting the translocation of DNA through a nanopore using graphene nanoribbons. *Nat. Nanotechnol.* **2013,** *8* (12), 939-945.

(45) Wang, F.; Zhao, C.; Zhao, P.; Chen, F.; Qiao, D.; Feng, J., MoS_2 nanopore identifies single amino acids with sub-1 Dalton resolution. *Nat. Commun.* **2023,** *14* (1), 2895.

(46) Gu, C.; Yu, Z.; Li, X.; Zhu, X.; Jin, C.; Cao, Z.; Dong, S.; Luo, J.; Ye, Z.; Liu, Y., Experimental study on single biomolecule sensing using MoS_2-graphene heterostructure nanopores. *Nanoscale* **2022,** *15* (1), 266-274.

(47) Yuan, Z. S.; Liang, Z. H.; Yang, L. S.; Zhou, D. M.; He, Z. H.; Yang, J. Y.; Wang, C. Y.; Jiang, L.; Guo, W., Light-Driven Ionic and Molecular Transport through Atomically Thin Single Nanopores in MoS_2/WS_2 Heterobilayers. *ACS Nano* **2024,** *18* (35), 24581-24590.

(48) Zhang, Q.; Cao, P. S.; Cheng, Y.; Yang, S. S.; Yin, Y. D.; Lv, T. Y.; Gu, Z. Y., Nonlinear Ion Transport through Ultrathin Metal–Organic Framework Nanosheet. *Adv. Funct. Mater.* **2020,** *30* (42), 2004854.

(49) Wang, X.; Chi, C.; Zhang, K.; Qian, Y.; Gupta, K. M.; Kang, Z.; Jiang, J.; Zhao, D., Reversed thermo-switchable molecular sieving membranes composed of two-dimensional metal-organic nanosheets for gas separation. *Nat. Commun.* **2017,** *8*, 14460.

(50) Zhou, Y.; Wu, Y.; Wu, H.; Xue, J.; Ding, L.; Wang, R.; Wang, H., Fast hydrogen purification through graphitic carbon nitride nanosheet membranes. *Nat. Commun.* **2022,** *13,* 5852.

(51) Dakhchoune, M.; Villalobos, L. F.; Semino, R.; Liu, L.; Rezaei, M.; Schouwink, P.; Avalos, C. E.; Baade, P.; Wood, V.; Han, Y.; Ceriotti, M.; Agrawal, K. V., Gas-sieving zeolitic membranes fabricated by condensation of precursor nanosheets. *Nat. Mater.* **2020,** *20* (3), 362-369.

(52) Liu, Q.; Miao, Y.; Villalobos, L. F.; Li, S.; Chi, H.-Y.; Chen, C.; Vahdat, M. T.; Song, S.; Babu, D. J.; Hao, J.; Han, Y.; Tsapatsis, M.; Agrawal, K. V., Unit-cell-thick zeolitic

imidazolate framework films for membrane application. *Nat. Mater.* **2023,** *22* (11), 1387-1393.
(53) Yang, J.; Tu, B.; Zhang, G.; Liu, P.; Hu, K.; Wang, J.; Yan, Z.; Huang, Z.; Fang, M.; Hou, J.; Fang, Q.; Qiu, X.; Li, L.; Tang, Z., Advancing osmotic power generation by covalent organic framework monolayer. *Nat. Nanotechnol.* **2022,** *17* (6), 622-628.
(54) Graf, M.; Lihter, M.; Thakur, M.; Georgiou, V.; Topolancik, J.; Ilic, B. R.; Liu, K.; Feng, J.; Astier, Y.; Radenovic, A., Fabrication and practical applications of molybdenum disulfide nanopores. *Nat. Protoc.* **2019,** *14* (4), 1130-1168.
(55) Su, S.; Wang, X.; Xue, J., Nanopores in two-dimensional materials: accurate fabrication. *Mater, Horiz,* **2021,** *8* (5), 1390-1408.
(56) Guo, H. W.; Hu, Z.; Liu, Z. B.; Tian, J. G., Stacking of 2D Materials. *Adv. Funct. Mater.* **2020,** *31* (4), 2007810.
(57) Macha, M.; Marion, S.; Tripathi, M.; Thakur, M.; Lihter, M.; Kis, A.; Smolyanitsky, A.; Radenovic, A., High-Throughput Nanopore Fabrication and Classification Using Xe-Ion Irradiation and Automated Pore-Edge Analysis. *ACS Nano* **2022,** *16* (10), 16249-16259.
(58) Kuan, A. T.; Lu, B.; Xie, P.; Szalay, T.; Golovchenko, J. A., Electrical pulse fabrication of graphene nanopores in electrolyte solution. *Appl. Phys. Lett.* **2015,** *106* (20), 203109.
(59) Fried, J. P.; Swett, J. L.; Nadappuram, B. P.; Mol, J. A.; Edel, J. B.; Ivanov, A. P.; Yates, J. R., In situ solid-state nanopore fabrication. *Chem. Soc. Rev.* **2021,** *50* (8), 4974-4992.
(60) Feng, J.; Liu, K.; Graf, M.; Lihter, M.; Bulushev, R. D.; Dumcenco, D.; Alexander, D. T. L.; Krasnozhon, D.; Vuletic, T.; Kis, A.; Radenovic, A., Electrochemical Reaction in Single Layer MoS_2: Nanopores Opened Atom by Atom. *Nano Lett.* **2015,** *15* (5), 3431-3438.
(61) Surwade, S. P.; Smirnov, S. N.; Vlassiouk, I. V.; Unocic, R. R.; Veith, G. M.; Dai, S.; Mahurin, S. M., Water desalination using nanoporous single-layer graphene. *Nat. Nanotechnol.* **2015,** *10* (5), 459-64.
(62) Kadoguchi, N.; Uesugi, Y.; Nagasako, M.; Kobayashi, T.; Kozawa, Y.; Sato, S., Nanoprocessing of Self-Suspended Monolayer Graphene and Defect Formation by Femtosecond-Laser Irradiation. *Nano Lett.* **2023,** *23* (11), 4893-4900.
(63) Wei, G.; Quan, X.; Chen, S.; Yu, H., Superpermeable Atomic-Thin Graphene Membranes with High Selectivity. *ACS Nano* **2017,** *11* (2), 1920-1926.

(64) Wang, W. L.; Santos, E. J. G.; Jiang, B.; Cubuk, E. D.; Ophus, C.; Centeno, A.; Pesquera, A.; Zurutuza, A.; Ciston, J.; Westervelt, R.; Kaxiras, E., Direct Observation of a Long-Lived Single-Atom Catalyst Chiseling Atomic Structures in Graphene. *Nano Lett.* **2014,** *14* (2), 450-455.

(65) Qi, H.; Li, Z.; Tao, Y.; Zhao, W.; Lin, K.; Ni, Z.; Jin, C.; Zhang, Y.; Bi, K.; Chen, Y., Fabrication of sub-nanometer pores on graphene membrane for ion selective transport. *Nanoscale* **2018,** *10* (11), 5350-5357.

(66) Qi, H.; Zhang, Z.; Li, Z.; Nan, H.; Bi, K.; Chen, Y., Synergic Effects of the Nanopore Size and Surface Charge on the Ion Selectivity of Graphene Membranes. *J. Phys. Chem. C* **2020,** *125* (1), 507-514.

(67) Huang, S.; Villalobos, L. F.; Li, S.; Vahdat, M. T.; Chi, H. Y.; Hsu, K. J.; Bondaz, L.; Boureau, V.; Marzari, N.; Agrawal, K. V., In Situ Nucleation-Decoupled and Site-Specific Incorporation of Å-Scale Pores in Graphene Via Epoxidation. *Adv. Mater.* **2022,** *34* (51), 2206627..

(68) Graf, M.; Lihter, M.; Unuchek, D.; Sarathy, A.; Leburton, J. P.; Kis, A.; Radenovic, A., Light-Enhanced Blue Energy Generation Using MoS_2 Nanopores. *Joule* **2019,** *3* (6), 1549-1564.

(69) Heerema, S. J.; Vicarelli, L.; Pud, S.; Schouten, R. N.; Zandbergen, H. W.; Dekker, C., Probing DNA Translocations with Inplane Current Signals in a Graphene Nanoribbon with a Nanopore. *ACS Nano* **2018,** *12* (3), 2623-2633.

(70) Keneipp, R. N.; Gusdorff, J. A.; Bhatia, P.; Shin, T. T.; Bassett, L. C.; Drndić, M., Nanoscale Sculpting of Hexagonal Boron Nitride with an Electron Beam. *J. Phys. Chem. C* **2024,** *128* (21), 8741-8749.

(71) Park, K.-B.; Kim, H.-J.; Kim, H.-M.; Han, S. A.; Lee, K. H.; Kim, S.-W.; Kim, K.-B., Noise and sensitivity characteristics of solid-state nanopores with a boron nitride 2-D membrane on a pyrex substrate. *Nanoscale* **2016,** *8* (10), 5755-5763.

(72) Feng, J.; Liu, K.; Graf, M.; Dumcenco, D.; Kis, A.; Di Ventra, M.; Radenovic, A., Observation of ionic Coulomb blockade in nanopores. *Nat. Mater.* **2016,** *15* (8), 850-855.

(73) Alibakhshi, M. A.; Kang, X.; Clymer, D.; Zhang, Z.; Vargas, A.; Meunier, V.; Wanunu, M., Scaled-Up Synthesis of Freestanding Molybdenum Disulfide Membranes for Nanopore

Sensing. *Adv. Mater.* **2023,** *35* (12), 2207089.
(74) Fu, Y.; Su, S.; Zhang, N.; Wang, Y.; Guo, X.; Xue, J., Dehydration-Determined Ion Selectivity of Graphene Subnanopores. *ACS Appl. Mater. Interfaces* **2020,** *12* (21), 24281-24288.
(75) Thiruraman, J. P.; Fujisawa, K.; Danda, G.; Das, P. M.; Zhang, T.; Bolotsky, A.; Perea-Lopez, N.; Nicolai, A.; Senet, P.; Terrones, M.; Drndic, M., Angstrom-Size Defect Creation and Ionic Transport through Pores in Single-Layer MoS_2. *Nano Lett.* **2018,** *18* (3), 1651-1659.
(76) Lee, W.-C.; Ronghe, A.; Villalobos, L. F.; Huang, S.; Dakhchoune, M.; Mensi, M.; Hsu, K.-J.; Ayappa, K. G.; Agrawal, K. V., Enhanced Water Evaporation from Å-Scale Graphene Nanopores. *ACS Nano* **2022,** *16* (9), 15382-15396.
(77) Zhao, K.; Lee, W.-C.; Rezaei, M.; Chi, H.-Y.; Li, S.; Villalobos, L. F.; Hsu, K.-J.; Zhang, Y.; Wang, F.-C.; Agrawal, K. V., Tuning Pore Size in Graphene in the Angstrom Regime for Highly Selective Ion–Ion Separation. *ACS Nano* **2024,** *18* (7), 5571-5580.
(78) Guo, L.; Liu, Y.; Zeng, H.; Zhang, S.; Song, R.; Yang, J.; Han, X.; Wang, Y.; Wang, L., Covalently Functionalized Nanopores for Highly Selective Separation of Monovalent Ions. *Adv. Mater.* **2024,** *36* (1), 2307242.
(79) Mashiyama, D.; Tobe, T.; Ogino, T., Nanopatterning of Suspended Graphene Films by Local Catalytic Etching Using Atomic Force Microscopy Equipped with an Ag-Coated Probe. *J. Phys. Chem. C* **2015,** *119* (21), 11914-11921.
(80) Yazda, K.; Bleau, K.; Zhang, Y.; Capaldi, X.; St-Denis, T.; Grutter, P.; Reisner, W. W., High Osmotic Power Generation via Nanopore Arrays in Hybrid Hexagonal Boron Nitride/Silicon Nitride Membranes. *Nano Lett.* **2021,** *21* (10), 4152-4159.
(81) Radha, B.; Esfandiar, A.; Wang, F. C.; Rooney, A. P.; Gopinadhan, K.; Keerthi, A.; Mishchenko, A.; Janardanan, A.; Blake, P.; Fumagalli, L.; Lozada-Hidalgo, M.; Garaj, S.; Haigh, S. J.; Grigorieva, I. V.; Wu, H. A.; Geim, A. K., Molecular transport through capillaries made with atomic-scale precision. *Nature* **2016,** *538* (7624), 222-225.
(82) Keerthi, A.; Geim, A. K.; Janardanan, A.; Rooney, A. P.; Esfandiar, A.; Hu, S.; Dar, S. A.; Grigorieva, I. V.; Haigh, S. J.; Wang, F. C.; Radha, B., Ballistic molecular transport through two-dimensional channels. *Nature* **2018,** *558* (7710), 420-424.

(83) Gopinadhan, K.; Hu, S.; Esfandiar, A.; Lozada-Hidalgo, M.; Wang, F. C.; Yang, Q.; Tyurnina, A. V.; Keerthi, A.; Radha, B.; Geim, A. K., Complete steric exclusion of ions and proton transport through confined monolayer water. *Science* **2019,** *363* (6423), 145-147.

(84) Xie, Q.; Alibakhshi, M. A.; Jiao, S.; Xu, Z.; Hempel, M.; Kong, J.; Park, H. G.; Duan, C., Fast water transport in graphene nanofluidic channels. *Nat. Nanotechnol.* **2018,** *13* (3), 238-245.

(85) Xie, Q.; Xin, F.; Park, H. G.; Duan, C., Ion transport in graphene nanofluidic channels. *Nanoscale* **2016,** *8* (47), 19527-19535.

(86) Jung, W.; Kim, J.; Kim, S.; Park, H. G.; Jung, Y.; Han, C. S., A Novel Fabrication of 3.6 nm High Graphene Nanochannels for Ultrafast Ion Transport. *Adv. Mater.* **2017,** *29* (17), e1605854.

(87) Bhardwaj, A.; Surmani Martins, M. V.; You, Y.; Sajja, R.; Rimmer, M.; Goutham, S.; Qi, R.; Abbas Dar, S.; Radha, B.; Keerthi, A., Fabrication of angstrom-scale two-dimensional channels for mass transport. *Nat. Protoc.* **2023,** *19* (1), 240-280.

(88) Emmerich, T.; Vasu, K. S.; Nigues, A.; Keerthi, A.; Radha, B.; Siria, A.; Bocquet, L., Enhanced nanofluidic transport in activated carbon nanoconduits. *Nat. Mater.* **2022,** *21* (6), 696-702.

(89) Cui, Y.; Ying, C.; Huang, X.-Y.; Ye, Q.; Tian, J.; Liu, Z., Electrical Transport and Dynamics of Confined DNA through Highly Conductive 2D Graphene Nanochannels. *Nano Lett.* **2024,** *24* (15), 4485-4492.

(90) Guan, K.; Wang, S.; Ji, Y.; Jia, Y.; Zhang, L.; Ushio, K.; Lin, Y.; Jin, W.; Matsuyama, H., Nanochannel-confined charge repulsion of ions in a reduced graphene oxide membrane. *J. Mater. Chem. A* **2020,** *8* (48), 25880-25889.

(91) Guan, K.; Jia, Y.; Lin, Y.; Wang, S.; Matsuyama, H., Chemically Converted Graphene Nanosheets for the Construction of Ion-Exclusion Nanochannel Membranes. *Nano Lett.* **2021,** *21* (8), 3495-3502.

(92) Guan, K.; Guo, Y.; Li, Z.; Jia, Y.; Shen, Q.; Nakagawa, K.; Yoshioka, T.; Liu, G.; Jin, W.; Matsuyama, H., Deformation constraints of graphene oxide nanochannels under reverse osmosis. *Nat. Commun.* **2023,** *14* (1), 1016.

(93) Nair, R. R.; Wu, H. A.; Jayaram, P. N.; Grigorieva, I. V.; Geim, A. K., Unimpeded Permeation of Water Through Helium-Leak–Tight Graphene-Based Membranes. *Science* **2012,** *335* (6067), 442-444.

(94) Su, Y.; Liu, D.; Yang, G.; Wang, L.; Razal, J. M.; Lei, W., Light-Controlled Ionic Transport through Molybdenum Disulfide Membranes. *ACS Appl. Mater. Interfaces* **2021,** *13* (29), 34679-34685.

(95) Das, A.; Yadav, V.; Krishnamurthy, C. V.; Jaiswal, M., Percolative proton transport in hexagonal boron nitride membranes with edge-functionalization. *Nanoscale Adv.* **2023,** *5* (18), 4901-4910.

(96) Lao, J.; Lv, R.; Gao, J.; Wang, A.; Wu, J.; Luo, J., Aqueous Stable Ti_3C_2 MXene Membrane with Fast and Photoswitchable Nanofluidic Transport. *ACS Nano* **2018,** *12* (12), 12464-12471.

(97) Wen, Q.; Jia, P.; Cao, L.; Li, J.; Quan, D.; Wang, L.; Zhang, Y.; Lu, D.; Jiang, L.; Guo, W., Electric-Field-Induced Ionic Sieving at Planar Graphene Oxide Heterojunctions for Miniaturized Water Desalination. *Adv. Mater.* **2020,** *32* (16), 1903954.

(98) Wang, L.; Wen, Q.; Jia, P.; Jia, M.; Lu, D.; Sun, X.; Jiang, L.; Guo, W., Light-Driven Active Proton Transport through Photoacid- and Photobase-Doped Janus Graphene Oxide Membranes. *Adv. Mater.* **2019,** *31* (36), e1903029.

(99) Wang, J.; Liu, S.; Zheng, S.; Li, S.; Wang, D.; He, M.; Wang, L.; Wang, X., Ion transport behavior in a vertically-oriented asymmetric $Ti_3C_2T_x$ nanochannel membrane. *J. Membr. Sci.* **2023,** *668*, 121232.

(100) Ji, J.; Kang, Q.; Zhou, Y.; Feng, Y.; Chen, X.; Yuan, J.; Guo, W.; Wei, Y.; Jiang, L., Osmotic Power Generation with Positively and Negatively Charged 2D Nanofluidic Membrane Pairs. *Adv. Funct. Mater.* **2016,** *27* (2), 1603623.

(101) Yang, J.; Hu, X.; Kong, X.; Jia, P.; Ji, D.; Quan, D.; Wang, L.; Wen, Q.; Lu, D.; Wu, J.; Jiang, L.; Guo, W., Photo-induced ultrafast active ion transport through graphene oxide membranes. *Nat. Commun.* **2019,** *10* (1), 1171.

(102) Tong, X.; Liu, S.; Zhao, Y.; Chen, Y.; Crittenden, J., Influence of the Exclusion-Enrichment Effect on Ion Transport in Two-Dimensional Molybdenum Disulfide Membranes.

ACS Appl. Mater. Interfaces **2021,** *13* (23), 26904-26914.

(103) Jia, P.; Wen, Q.; Liu, D.; Zhou, M.; Jin, X.; Ding, L.; Dong, H.; Lu, D.; Jiang, L.; Guo, W., Highly Efficient Ionic Photocurrent Generation through WS_2-Based 2D Nanofluidic Channels. *Small* **2019,** *15* (50), 1905355.

(104) Hong, S.; Al Marzooqi, F.; El-Demellawi, J. K.; Al Marzooqi, N.; Arafat, H. A.; Alshareef, H. N., Ion-Selective Separation Using MXene-Based Membranes: A Review. *ACS Macro Lett.* **2023,** *5*, 341-356.

(105) Dong, Q.; Jiang, J.; Wang, Y.; Zhai, J., Geometric Tailoring of Macroscale $Ti_3C_2T_x$ MXene Lamellar Membrane for Logic Gate Circuits. *ACS Nano* **2021,** *15* (12), 19266-19274.

(106) Hong, S.; Zou, G.; Kim, H.; Huang, D.; Wang, P.; Alshareef, H. N., Photothermoelectric Response of $Ti_3C_2T_x$ MXene Confined Ion Channels. *ACS Nano* **2020,** *14* (7), 9042-9049.

(107) Feng, Y.; Ding, L.; Ji, D.; Wang, L.; Guo, W., Highly rectified ion transport through 2D WSe_2/MoS_2 bi-layered membranes. *Chin. Chem. Lett.* **2018,** *29* (6), 892-894.

(108) Wang, L.; Chen, Y., Bioinspired Dual-Driven Binary Heterogeneous Nanofluidic Ionic Diodes. *Langmuir* **2022,** *38* (41), 12450-12456.

(109) Chen, L.; Shi, G.; Shen, J.; Peng, B.; Zhang, B.; Wang, Y.; Bian, F.; Wang, J.; Li, D.; Qian, Z.; Xu, G.; Liu, G.; Zeng, J.; Zhang, L.; Yang, Y.; Zhou, G.; Wu, M.; Jin, W.; Li, J.; Fang, H., Ion sieving in graphene oxide membranes via cationic control of interlayer spacing. *Nature* **2017,** *550* (7676), 380-383.

(110) Xi, Y.-H.; Hu, J.-Q.; Liu, Z.; Xie, R.; Ju, X.-J.; Wang, W.; Chu, L.-Y., Graphene Oxide Membranes with Strong Stability in Aqueous Solutions and Controllable Lamellar Spacing. *ACS Appl. Mater. Interfaces* **2016,** *8* (24), 15557-15566.

(111) Lu, Z.; Wei, Y.; Deng, J.; Ding, L.; Li, Z.-K.; Wang, H., Self-Crosslinked MXene ($Ti_3C_2T_x$) Membranes with Good Antiswelling Property for Monovalent Metal Ion Exclusion. *ACS Nano* **2019,** *13* (9), 10535-10544.

(112) Sahu, S.; Di Ventra, M.; Zwolak, M., Dehydration as a Universal Mechanism for Ion Selectivity in Graphene and Other Atomically Thin Pores. *Nano Lett.* **2017,** *17* (8), 4719-4724.

(113) Barabash, M. L.; Gibby, W. A. T.; Guardiani, C.; Smolyanitsky, A.; Luchinsky, D.

G.; McClintock, P. V. E., Origin and control of ionic hydration patterns in nanopores. *Commun. Mater.* **2021,** *2* (1), 65.

(114) Epsztein, R.; DuChanois, R. M.; Ritt, C. L.; Noy, A.; Elimelech, M., Towards single-species selectivity of membranes with subnanometre pores. *Nat. Nanotechnol.* **2020,** *15* (6), 426-436.

(115) Xiong, M.; Athreya, N.; Chakraborty, R.; Leburton, J.-P., Ion Trapping and Thermionic Emission across Sub-nm Pores. *Nano Lett.* **2023,** *23* (24), 11719-11726.

(116) Jiang, X. W.; Zhao, C. X.; Noh, Y. C.; Xu, Y.; Chen, Y. A.; Chen, F. F.; Ma, L. P.; Ren, W. C.; Aluru, N. R.; Feng, J. D., Nonlinear electrohydrodynamic ion transport in graphene nanopores. *Sci. Adv.* **2022,** *8* (2), eabj2510.

(117) Yu, Y.; Fan, J.; Xia, J.; Zhu, Y.; Wu, H.; Wang, F., Dehydration impeding ionic conductance through two-dimensional angstrom-scale slits. *Nanoscale* **2019,** *11* (17), 8449-8457.

(118) Tocci, G.; Joly, L.; Michaelides, A., Friction of water on graphene and hexagonal boron nitride from ab initio methods: very different slippage despite very similar interface structures. *Nano Lett.* **2014,** *14* (12), 6872-6877.

(119) Falk, K.; Sedlmeier, F.; Joly, L.; Netz, R. R.; Bocquet, L., Molecular origin of fast water transport in carbon nanotube membranes: superlubricity versus curvature dependent friction. *Nano Lett.* **2010,** *10* (10), 4067-4073.

(120) Tocci, G.; Bilichenko, M.; Joly, L.; Iannuzzi, M., Ab initio nanofluidics: disentangling the role of the energy landscape and of density correlations on liquid/solid friction. *Nanoscale* **2020,** *12* (20), 10994-11000.

(121) Bocquet, L.; Charlaix, E., Nanofluidics, from bulk to interfaces. *Chem. Soc. Rev.* **2010,** *39* (3), 1073-1095.

(122) Mouterde, T.; Bocquet, L., Interfacial transport with mobile surface charges and consequences for ionic transport in carbon nanotubes. *Eur. Phys. J. E Soft Matter.* **2018,** *41* (12), 148.

(123) Cui, G.; Xu, Z.; Li, H.; Zhang, S.; Xu, L.; Siria, A.; Ma, M., Enhanced osmotic transport in individual double-walled carbon nanotube. *Nat. Commun.* **2023,** *14* (1), 2295.

(124) Tocci, G.; Joly, L.; Michaelides, A., Friction of Water on Graphene and Hexagonal Boron Nitride from Methods: Very Different Slippage Despite Very Similar Interface Structures. *Nano Lett.* **2014,** *14* (12), 6872-6877.

(125) Keerthi, A.; Goutham, S.; You, Y.; Iamprasertkun, P.; Dryfe, R. A. W.; Geim, A. K.; Radha, B., Water friction in nanofluidic channels made from two-dimensional crystals. *Nat. Commun.* **2021,** *12* (1), 3092.

(126) Joly, L.; Tocci, G.; Merabia, S.; Michaelides, A., Strong Coupling between Nanofluidic Transport and Interfacial Chemistry: How Defect Reactivity Controls Liquid-Solid Friction through Hydrogen Bonding. *J. Phys. Chem. Lett.* **2016,** *7* (7), 1381-1386.

(127) Ren, Y. Q.; Stein, D., Slip-enhanced electrokinetic energy conversion in nanofluidic channels. *Nanotechnology* **2008,** *19* (19), 195707.

(128) Celebi, A. T.; Beskok, A., Molecular and Continuum Transport Perspectives on Electroosmotic Slip Flows. *J. Phy. Chem. C* **2018,** *122* (17), 9699-9709.

(129) Motevaselian, M. H.; Mashayak, S. Y.; Aluru, N. R., Extended coarse-grained dipole model for polar liquids: Application to bulk and confined water. *Phys. Rev. E* **2018,** *98* (5), 052135.

(130) Zhang, C.; Gygi, F.; Galli, G., Strongly Anisotropic Dielectric Relaxation of Water at the Nanoscale. *J. Phys. Chem. Lett.* **2013,** *4* (15), 2477-2481.

(131) Fumagalli, L.; Esfandiar, A.; Fabregas, R.; Hu, S.; Ares, P.; Janardanan, A.; Yang, Q.; Radha, B.; Taniguchi, T.; Watanabe, K.; Gomila, G.; Novoselov, K. S.; Geim, A. K., Anomalously low dielectric constant of confined water. *Science* **2018,** *360* (6395), 1339-1342.

(132) Kaiser, V.; Bramwell, S. T.; Holdsworth, P. C. W.; Moessner, R., Onsager's Wien effect on a lattice. *Nat. Mater.* **2013,** *12* (11), 1033-1037.

(133) Kavokine, N.; Marbach, S.; Siria, A.; Bocquet, L., Ionic Coulomb blockade as a fractional Wien effect. *Nat. Nanotechnol.* **2019,** *14* (6), 573-578.

(134) Robin, P.; Kavokine, N.; Bocquet, L., Modeling of emergent memory and voltage spiking in ionic transport through angstrom-scale slits. *Science* **2021,** *373* (6555), 687-691.

(135) Gilboa, T.; Meller, A., Optical sensing and analyte manipulation in solid-state nanopores. *Analyst* **2015,** *140* (14), 4733-4747.

(136) Harms, Z. D.; Haywood, D. G.; Kneller, A. R.; Jacobson, S. C., Conductivity-based detection techniques in nanofluidic devices. *Analyst* **2015,** *140* (14), 4779-4791.

(137) Ahmed, S. A.; Liu, Y.; Xiong, T.; Zhao, Y.; Xie, B.; Pan, C.; Ma, W.; Yu, P., Iontronic Sensing Based on Confined Ion Transport. *Anal. Chem.* **2024,** *96* (20), 8056-8077.

(138) Cao, Z.; Yadav, P.; Barati Farimani, A., Which 2D Material is Better for DNA Detection: Graphene, MoS_2, or MXene? *Nano Lett.* **2022,** *22* (19), 7874-7881.

(139) Farimani, A. B.; Min, K.; Aluru, N. R., DNA Base Detection Using a Single-Layer MoS_2. *ACS Nano* **2014,** *8* (8), 7914-7922.

(140) Graf, M.; Lihter, M.; Altus, D.; Marion, S.; Radenovic, A., Transverse Detection of DNA Using a MoS_2 Nanopore. *Nano Lett.* **2019,** *19* (12), 9075-9083.

(141) de Souza, F. A. L.; Sivaraman, G.; Fyta, M.; Scheicher, R. H.; Scopel, W. L.; Amorim, R. G., Electrically sensing Hachimoji DNA nucleotides through a hybrid graphene/h-BN nanopore. *Nanoscale* **2020,** *12* (35), 18289-18295.

(142) Gu, Z.; He, Z.; Chen, F.; Meng, L.; Feng, J.; Zhou, R., Ionic Liquid Decelerates Single-Stranded DNA Transport through Molybdenum Disulfide Nanopores. *ACS Appl. Mater. Interfaces* **2022,** *14* (28), 32618-32624.

(143) Feng, J.; Liu, K.; Bulushev, R. D.; Khlybov, S.; Dumcenco, D.; Kis, A.; Radenovic, A., Identification of single nucleotides in MoS_2 nanopores. *Nat. Nanotechnol.* **2015,** *10* (12), 1070-1076.

(144) Morrin, G. T.; Kienle, D. F.; Schwartz, D. K., Diffusion of Short Semiflexible DNA Polymer Chains in Strong and Moderate Confinement. *ACS Macro Lett.* **2021,** *10* (10), 1191-1195.

(145) Kim, Y.; Kim, K. S.; Kounovsky, K. L.; Chang, R.; Jung, G. Y.; dePablo, J. J.; Jo, K.; Schwartz, D. C., Nanochannel confinement: DNA stretch approaching full contour length. *Lab. Chip* **2011,** *11* (10), 1721-1729.

(146) Strychalski, E. A.; Levy, S. L.; Craighead, H. G., Diffusion of DNA in Nanoslits. *Macromolecules* **2008,** *41* (20), 7716-7721.

(147) Yang, W.; Radha, B.; Choudhary, A.; You, Y.; Mettela, G.; Geim, A. K.; Aksimentiev, A.; Keerthi, A.; Dekker, C., Translocation of DNA through Ultrathin Nanoslits. *Adv. Mater.*

2021, *33* (11), e2007682.

(148) Shan, Y. P.; Tiwari, P. B.; Krishnakumar, P.; Vlassiouk, I.; Li, W. Z.; Wang, X. W.; Darici, Y.; Lindsay, S. M.; Wang, H. D.; Smirnov, S.; He, J., Surface modification of graphene nanopores for protein translocation. *Nanotechnology* **2013,** *24* (49), 495102.

(149) Goyal, G.; Lee, Y. B.; Darvish, A.; Ahn, C. W.; Kim, M. J., Hydrophilic and size-controlled graphene nanopores for protein detection. *Nanotechnology* **2016,** *27* (49) , 495301.

(150) Gu, C.; Yu, Z.; Li, X.; Zhu, X.; Cao, Z.; Ye, Z.; Jin, C.; Liu, Y., Experimental study of protein translocation through MoS_2 nanopores. *Appl. Phys. Lett.* **2019,** *115* (22), 223702.

(151) Hu, Z. L.; Huo, M. Z.; Ying, Y. L.; Long, Y. T., Biological Nanopore Approach for Single-Molecule Protein Sequencing. *Angew. Chem. Int. Ed.* **2021,** *60* (27), 14738-14749.

(152) Fragasso, A.; Schmid, S.; Dekker, C., Comparing Current Noise in Biological and Solid-State Nanopores. *ACS Nano* **2020,** *14* (2), 1338-1349.

(153) Robin, P.; Lizee, M.; Yang, Q.; Emmerich, T.; Siria, A.; Bocquet, L., Disentangling 1/f noise from confined ion dynamics. *Faraday Discuss.* **2023,** *246* (0), 556-575.

(154) Yao, H.; Zeng, J.; Zhai, P.; Li, Z.; Cheng, Y.; Liu, J.; Mo, D.; Duan, J.; Wang, L.; Sun, Y.; Liu, J., Large Rectification Effect of Single Graphene Nanopore Supported by PET Membrane. *ACS Appl. Mater. Interfaces* **2017,** *9* (12), 11000-11008.

(155) Liu, P.; Zhou, T.; Teng, Y.; Fu, L.; Hu, Y.; Lin, X.; Kong, X.-Y.; Jiang, L.; Wen, L., Light-Induced Heat Driving Active Ion Transport Based on 2D MXene Nanofluids for Enhancing Osmotic Energy Conversion. *CCS Chem.* **2021,** *3* (4), 1325-1335.

(156) Xue, Y. H.; Xia, Y.; Yang, S.; Alsaid, Y.; Fong, K. Y.; Wang, Y.; Zhang, X., Atomic-scale ion transistor with ultrahigh diffusivity. *Science* **2021,** *372* (6541), 501-503.

(157) Robin, P.; Emmerich, T.; Ismail, A.; Niguès, A.; You, Y.; Nam, G. H.; Keerthi, A.; Siria, A.; Geim, A. K.; Radha, B.; Bocquet, L., Long-term memory and synapse-like dynamics in two-dimensional nanofluidic channels. *Science* **2023,** *379* (6628), 161-167.

(158) Emmerich, T.; Teng, Y.; Ronceray, N.; Lopriore, E.; Chiesa, R.; Chernev, A.; Artemov, V.; Di Ventra, M.; Kis, A.; Radenovic, A., Nanofluidic logic with mechano–ionic memristive switches. *Nat. Electron.* **2024,** *7* (4), 271–278.

(159) Yu, L.; Li, X.; Luo, C.; Lei, Z.; Wang, Y.; Hou, Y.; Wang, M.; Hou, X., Bioinspired

nanofluidic iontronics for brain-like computing. *Nano Research* **2023,** *17* (2), 503-514.

(160) Ismail, A.; Radha, B., Mechano-ionic memristors for nanofluidic logic. *Nat. Electron.* **2024,** *7* (4), 258-259.

(161) Wang, J.; Zhou, H.; Li, S.; Wang, L., Selective Ion Transport in Two-Dimensional Lamellar Nanochannel Membranes. *Angew. Chem. Int. Ed. Engl.* **2023,** *62* (19), e202218321.

(162) Emmerich, T.; Ronceray, N.; Agrawal, K. V.; Garaj, S.; Kumar, M.; Noy, A.; Radenovic, A., Nanofluidics. *Nat. Rev. Method. Prim.* **2024,** *4* (1) 69.

(163) Chen, B.; Jiang, H.; Liu, X.; Hu, X., Molecular Insight into Water Desalination across Multilayer Graphene Oxide Membranes. *ACS Appl. Mater. Interfaces* **2017,** *9* (27), 22826-22836.

(164) Mancinelli, R.; Botti, A.; Bruni, F.; Ricci, M. A.; Soper, A. K., Perturbation of water structure due to monovalent ions in solution. *Phys. Chem. Chem. Phys.* **2007,** *9* (23), 2959-2967.

(165) Esfandiar, A.; Radha, B.; Wang, F. C.; Yang, Q.; Hu, S.; Garaj, S.; Nair, R. R.; Geim, A. K.; Gopinadhan, K., Size effect in ion transport through angstrom-scale slits. *Science* **2017,** *358* (6362), 511-513.

(166) Hong, S.; Constans, C.; Surmani Martins, M. V.; Seow, Y. C.; Guevara Carrio, J. A.; Garaj, S., Scalable Graphene-Based Membranes for Ionic Sieving with Ultrahigh Charge Selectivity. *Nano Lett.* **2017,** *17* (2), 728-732.

(167) Abraham, J.; Vasu, K. S.; Williams, C. D.; Gopinadhan, K.; Su, Y.; Cherian, C. T.; Dix, J.; Prestat, E.; Haigh, S. J.; Grigorieva, I. V.; Carbone, P.; Geim, A. K.; Nair, R. R., Tunable sieving of ions using graphene oxide membranes. *Nat. Nanotechnol.* **2017,** *12* (6), 546-550.

(168) Goutham, S.; Keerthi, A.; Ismail, A.; Bhardwaj, A.; Jalali, H.; You, Y.; Li, Y.; Hassani, N.; Peng, H.; Martins, M. V. S.; Wang, F.; Neek-Amal, M.; Radha, B., Beyond steric selectivity of ions using angstrom-scale capillaries. *Nat. Nanotechnol.* **2023,** *18* (6), 596-601.

(169) Ding, L.; Li, L.; Liu, Y.; Wu, Y.; Lu, Z.; Deng, J.; Wei, Y.; Caro, J.; Wang, H., Effective ion sieving with $Ti_3C_2T_x$ MXene membranes for production of drinking water from seawater. *Nat. Sustain.* **2020,** *3* (4), 296-302.

(170) Xia, J.; Gao, H.; Pan, S.; Huang, T.; Zhang, L.; Sui, K.; Gao, J.; Liu, X.; Jiang, L.,

Light-Augmented Multi-ion Interaction in MXene Membrane for Simultaneous Water Treatment and Osmotic Power Generation. *ACS Nano* **2023,** *17* (24), 25269-25278.

(171) Su, S.; Zhang, Y.; Peng, S.; Guo, L.; Liu, Y.; Fu, E.; Yao, H.; Du, J.; Du, G.; Xue, J., Multifunctional graphene heterogeneous nanochannel with voltage-tunable ion selectivity. *Nat. Commun.* **2022,** *13* (1), 4894.

(172) Ma, X.; Neek-Amal, M.; Sun, C., Advances in Two-Dimensional Ion-Selective Membranes: Bridging Nanoscale Insights to Industrial-Scale Salinity Gradient Energy Harvesting. *ACS Nano* **2024,** *18* (20), 12610-12638.

(173) Tong, X.; Liu, S.; Crittenden, J.; Chen, Y., Nanofluidic Membranes to Address the Challenges of Salinity Gradient Power Harvesting. *ACS Nano* **2021,** *15* (4), 5838-5860.

(174) Liu, X.; Zhang, L.; Cui, X.; Zhang, Q.; Hu, W.; Du, J.; Zeng, H.; Xu, Q., 2D Material Nanofiltration Membranes: From Fundamental Understandings to Rational Design. *Adv. Sci.* **2021,** *8* (23), 2102493.

(175) Kim, D.-K.; Duan, C.; Chen, Y.-F.; Majumdar, A., Power generation from concentration gradient by reverse electrodialysis in ion-selective nanochannels. *Microfluid. Nanofluid.* **2010,** *9* (6), 1215-1224.

(176) Liu, Y.; Zhang, S.; Song, R.; Zeng, H.; Wang, L., Preanchoring Enabled Directional Modification of Atomically Thin Membrane for High-Performance Osmotic Energy Generation. *Nano Lett.* **2023,** *24* (1), 26-34.

(177) Lao, J. C.; Wu, S.; Gao, J.; Dong, A. P.; Li, G. J.; Luo, J. Y., Electricity generation based on a photothermally driven $Ti_3C_2T_x$ MXene nanofluidic water pump. *Nano Energy* **2020,** *70*, 104481.

(178) Koenig, S. P.; Wang, L. D.; Pellegrino, J.; Bunch, J. S., Selective molecular sieving through porous graphene. *Nat. Nanotechnol.* **2012,** *7* (11), 728-732.

(179) Sun, P. Z.; Yagmurcukardes, M.; Zhang, R.; Kuang, W. J.; Lozada-Hidalgo, M.; Liu, B. L.; Cheng, H. M.; Wang, F. C.; Peeters, F. M.; Grigorieva, I. V.; Geim, A. K., Exponentially selective molecular sieving through angstrom pores. *Nat. Commun.* **2021,** *12* ,7107.

(180) Celebi, K.; Buchheim, J.; Wyss, R. M.; Droudian, A.; Gasser, P.; Shorubalko, I.; Kye, J. I.; Lee, C.; Park, H. G., Ultimate Permeation Across Atomically Thin Porous Graphene.

Science **2014,** *344* (6181), 289-292.

(181) Yuan, Z.; Govind Rajan, A.; Misra, R. P.; Drahushuk, L. W.; Agrawal, K. V.; Strano, M. S.; Blankschtein, D., Mechanism and Prediction of Gas Permeation through Sub-Nanometer Graphene Pores: Comparison of Theory and Simulation. *ACS Nano* **2017,** *11* (8), 7974-7987.

(182) Schlichting, K.-P.; Poulikakos, D., Selective Etching of Graphene Membrane Nanopores: From Molecular Sieving to Extreme Permeance. *ACS Appl. Mater. Interfaces* **2020,** *12* (32), 36468-36477.

(183) Liu, J.; Jin, L.; Allen, F. I.; Gao, Y.; Ci, P.; Kang, F.; Wu, J., Selective Gas Permeation in Defect-Engineered Bilayer Graphene. *Nano Lett.* **2021,** *21* (5), 2183-2190.

(184) Hsu, K.-J.; Li, S.; Micari, M.; Chi, H.-Y.; Villalobos, L. F.; Huang, S.; Zhong, L.; Song, S.; Duan, X.; Züttel, A.; Agrawal, K. V., Graphene membranes with pyridinic nitrogen at pore edges for high-performance CO_2 capture. *Nat. Energy* **2024,** *9* (8), 964-974.

(185) Li, H.; Song, Z. N.; Zhang, X. J.; Huang, Y.; Li, S. G.; Mao, Y. T.; Ploehn, H. J.; Bao, Y.; Yu, M., Ultrathin, Molecular-Sieving Graphene Oxide Membranes for Selective Hydrogen Separation. *Science* **2013,** *342* (6154), 95-98.

(186) Ding, L.; Wei, Y.; Li, L.; Zhang, T.; Wang, H.; Xue, J.; Ding, L.-X.; Wang, S.; Caro, J.; Gogotsi, Y., MXene molecular sieving membranes for highly efficient gas separation. *Nat. Commun.* **2018,** *9*, 9155.

(187) Shen, J.; Liu, G.; Huang, K.; Chu, Z.; Jin, W.; Xu, N., Subnanometer Two-Dimensional Graphene Oxide Channels for Ultrafast Gas Sieving. *ACS Nano* **2016,** *10* (3), 3398-3409.

(188) Wang, R.; Qian, J.; Chen, X.; Low, Z.-X.; Chen, Y.; Ma, H.; Wu, H.-A.; Doherty, C. M.; Acharya, D.; Xie, Z.; Hill, M. R.; Shen, W.; Wang, F.; Wang, H., Pyro-layered heterostructured nanosheet membrane for hydrogen separation. *Nat. Commun.* **2023,** *14* (1), 2161.

(189) Thakur, M.; Macha, M.; Chernev, A.; Graf, M.; Lihter, M.; Deen, J.; Tripathi, M.; Kis, A.; Radenovic, A., Wafer-Scale Fabrication of Nanopore Devices for Single-Molecule DNA Biosensing using MoS_2. *Small Methods* **2020,** *4* (11), 2000072.

TOC Figure: